VELOCITY DISTRIBUTIONS IN BEAMS OF METASTABLE ATOMS EXCITED BY ELECTRON IMPACT

by

John Christopher Pearl

A dissertation submitted in partial fulfillment
of the requirements for the degree of
Doctor of Philosophy in
The University of Michigan
1970

Doctoral Committee:

Associate Professor Jens C. Zorn, Chairman
Lecturer George R. Carignan
Associate Professor Gordon L. Kane
Professor Gabriel Weinreich
Associate Professor William L. Williams

ACKNOWLEDGMENTS

I am deeply grateful to Professor Jens C. Zorn for proposing the present problem and for his generous advice and assistance.

I would also like to express my sincere appreciation to Mr. George R. Carignan, Director of the Space Physics Research Laboratory, for his unflagging support and encouragement.

I am indebted to Professor William L. Williams for useful discussions and for his support.

I also wish to thank Professor R. T. Robiscoe for discussions of the recoil problem and its bearing on measurements of the Lamb shift.

I am grateful to Richard A. Heppner for the design and construction of the vacuum system.

I thank also Dr. Denis P. Donnelly and David R. Crosby for development of the electronics used in the time-of-flight experiment.

I thank Martin Misakian for our many conversations about the molecular dissociation experiment and for providing me with helium velocity distributions from his machine.

I am also grateful to Mr. Leslie R. Thurston for his skillful execution of the illustrations contained in this thesis.

To my wife, Susan, an especially warm "thank you" for her cheerful forbearance, and for typing the manuscript.

I am grateful to the National Aeronautics and Space Administration for its financial support of this research.

TABLE OF CONTENTS

LIST OF TABLES

LIST OF FIGURES

ABSTRACT

This thesis is concerned with the velocity distribution in a beam of metastable atoms produced from ground state atoms by electron impact excitation. A relation between the velocity distribution functions in the ground state and metastable beams is derived, assuming that the electron beam is well collimated and monoenergetic, and that the scattering of the electrons by the atoms is isotropic.

In the case where the ground state beam is well collimated and has a Maxwellian velocity distribution, it is shown that a measured distribution in the resulting metastable beam should be distinctly non-Maxwellian. In general, it is characterized by two peaks and by the existence of sharp cutoff velocities which are themselves very sensitive functions of the alignment of the ground state and electron beams, the position of the metastable detector, and the energy of the incident electrons. Collimation of the ground state and of the metastable beams also strongly affects the distribution. A simple experiment is described which verifies these effects in a helium 2^3S beam.

For the case where the ground state gas enters the electron beam isotropically, the double peaked structure disappears. However, the metastable velocity distribution

may still deviate significantly from that of the ground state gas.

Extension of the calculations shows that non-isotropic electron scattering may affect the metastable velocity distribution strongly. A simple parametrization is derived to compare the distributions for different gases and/or different excited states.

Several experiments in which such distorted velocity distributions can introduce systematic errors are briefly discussed.

CHAPTER 1

INTRODUCTION

There are many atomic physics experiments utilizing beams of metastable atoms or molecules in which the metastables are produced by electron bombardment of ground state species, e.g., fine and hyperfine structure measurements on $2^2S_{\frac{1}{2}}$ hydrogen (Lamb, 1950; Heberle, 1956; Robiscoe, 1965, 1968; Shyn, 1969), measurements of electron impact excitation of n = 2 states in helium (Holt, 1966; Vriens, 1968), excitation of metastable H(2S) atoms by electron impact (Stebbings, 1960), time-of-flight studies of repulsive molecular states (Leventhal, 1967; Freund, 1967; Clampitt, 1969), analysis of the kinetic properties of single and multicomponent gases (French, 1967; Crosby, 1969), and measurements of lifetimes of excited molecular states (Freund, 1969). Frequently, the velocity distribution of the metastable particles enters explicitly into the analysis of such experiments. It is surprising, therefore, that very little has been reported on the actual form of the velocity distribution to be expected from the common experimental arrangement in which ground state particles in a collimated beam are excited by a transverse beam of electrons. It is the purpose

of this thesis to investigate theoretically and experimentally the relationship between the velocity distributions of the ground state and excited atoms in such an experiment, identifying the various parameters which must be controlled in order to produce a metastable beam with a predictable velocity distribution.

The thesis is organized as follows. First, the kinematics of the electron-atom collision process is discussed and the relation between the velocity distribution functions of the ground state and metastable atoms is determined; the results obtained are applied to several configurations which approximate common experimental arrangements. The use of the time-of-flight technique for measurement of velocity distributions is then considered and two systematic effects in such a measurement are discussed. Next, a simple crossed beam experiment is described which is designed to check various aspects of the calculations. The work is concluded with some remarks on the effects of various factors previously neglected in the analysis, and with a discussion of several actual experiments to which the present work is applicable.

CHAPTER 2

THE KINEMATICS OF THE PROBLEM

For purposes of this thesis, an "apparatus" shall be defined by the following:

i) a source of ground state atoms. The velocity distribution of these atoms may be isotropic, as within a Maxwellian gas in a large container, or may be highly directional, as in a collimated beam;

ii) a perfectly collimated monoenergetic beam of electrons;

iii) a detector for the metastable atoms. This will generally be assumed to subtend some given solid angle at the interaction region of the atoms and electrons. The solid angle may result from the physical size of the detector itself, or from collimation of the beam of metastable atoms after it leaves the electron beam.

For purposes of analysis, the three beams may be described in terms of the velocity distribution function $f(\bar{v}_o)$ of the ground state atoms, the collimation of the ground state beam, the velocity $\bar{u}_o$ of the incident electrons, the

velocity distribution function $g(\bar{v})$ of the metastable atoms, and the solid angle $\Omega_{det.}$ of the detector. The object of the analysis is to relate the distribution functions $f(\bar{v}_o)$ and $g(\bar{v})$, taking into account the effects of beam collimation.

2.1 The Elementary Contributing Event: The Collision of an Atom and an Electron

Fundamental to the entire analysis is a description of the inelastic collision of pairs of particles, as viewed in a laboratory frame of reference. Problems of this nature have been considered in detail by physical chemists for the purpose of analyzing reactive scattering experiments (Toennies, 1967; Warnock, 1968). The most extensive discussion to date of electron-atom collision kinematics is that of Rubin et al. (1969).

The principal features of the relationship between the velocities of a ground state atom and of the metastable atom produced from it can be obtained by applying the laws of conservation of momentum and energy for the two particle (electron-atom) collision. Consider the collision, as seen in a laboratory-based coordinate system, of a ground state atom (velocity $\bar{v}_o$) and an electron (velocity $\bar{u}_o$). Let the laboratory velocities of the two particles after the collision be $\bar{v}$ and $\bar{u}$, respectively, and denote their respective masses by M and m. For convenience, all masses will be normalized with respect to the mass of the atom. In these units

the atomic mass is unity; the normalized electron mass will be indicated by the quantity

$$\mu = \frac{m}{M} \tag{2.1}$$

This normalization makes the atomic velocity and momentum identical; for the atom, therefore, velocity and momentum diagrams are "equivalent".

In the above units, the total normalized momentum of the system is given by

$$\bar{v}_o + \mu \bar{u}_o = \bar{\mathcal{M}} \equiv (1+\mu)\bar{W} \tag{2.2}$$

where $\bar{W}$ represents the velocity of the center of mass of the two particle system in the laboratory frame of reference.

Denoting quantities in the center of mass (CM) system by upper case letters, the two particles have incoming velocities given by

$$\bar{V}_o = \bar{v}_o - \bar{W}$$

$$= \frac{\mu}{1+\mu}(\bar{v}_o - \bar{u}_o) \tag{2.3}$$

and

$$\bar{U}_o = \bar{u}_o - \bar{W}$$

$$= \frac{1}{1+\mu}(\bar{u}_o - \bar{v}_o) \tag{2.4}$$

Taking $\bar{v}_o$ and $\bar{u}_o$ as the particles' velocities at large separations, the energy available to excite the atom to a

metastable state is the kinetic energy in the CM frame

$$E_{CM}(\bar{u}_o,\bar{v}_o) = \tfrac{1}{2} M V_o^2 + \tfrac{1}{2} m U_o^2$$

$$= \frac{M}{2}\left[\frac{\mu^2}{(1+\mu)^2}(\bar{v}_o-\bar{u}_o)^2 + \frac{\mu}{(1+\mu)^2}(\bar{u}_o-\bar{v}_o)^2\right]$$

$$= \frac{1}{2}\cdot\frac{M\mu}{1+\mu}\cdot(\bar{u}_o-\bar{v}_o)^2 \qquad (2.5)$$

i.e., one half of the reduced mass times the square of the relative velocity.

Assume that the atom is excited directly to its metastable state by the electron, so that energy E^* equal to the excitation energy of the metastable level is "absorbed" by the atom. Then, after excitation, when the electron and the metastable are at large separations, the total kinetic energy in the CM frame is

$$\Delta E(\bar{u}_o,\bar{v}_o) = E_{CM}(\bar{u}_o,\bar{v}_o) - E^* \qquad (2.6)$$

To relate the velocities of the particles in the CM frame after the collision (quantities without subscripts), the laws of conservation of momentum

$$\bar{V} = -\mu\bar{U} \qquad (2.7)$$

and of energy

$$\Delta E(\bar{u}_o,\bar{v}_o) = \tfrac{1}{2} M V^2 + \tfrac{1}{2} m U^2$$

$$= \frac{M(1+\mu)}{2\mu} V^2 \qquad (2.8)$$

are again utilized. From this last relation, the speed of the outgoing metastable in the CM frame is given by

$$V = \sqrt{\frac{2\mu}{M(1+\mu)}\,\Delta E(\bar{u}_o, \bar{v}_o)} \qquad (2.9)$$

An alternative derivation of this result is given in Appendix I.

It is noted explicitly that the direction in which the outgoing metastable travels is not determined by the conservation laws; only the magnitude is fixed, so that, in velocity space, the vector $\bar{V}$ can terminate anywhere on a complete spherical surface of radius V (the center of the sphere is located at the tip of the center of mass velocity vector, $\bar{W}$). Statistically, the probability that the vector $\bar{V}$ will terminate within a given element of solid angle, $d\omega$, on the sphere is determined by the inelastic differential scattering cross section, $\frac{d\sigma^*}{d\omega}$, for the excitation process. Once the direction of $\bar{V}$ is specified, however, the velocity, $\bar{v}$, of the metastable in the laboratory system is found by the transformation

$$\bar{v} = \bar{V} + \bar{W} \qquad (2.10)$$

The relationship between the normalized variables for the excitation process is indicated in Figure 2.1.

The above results show that, in an experiment utilizing very narrow, perfectly collimated, monoenergetic electron and ground state atom beams, the velocity distribution of the metastables is not only spread over a range of speeds,

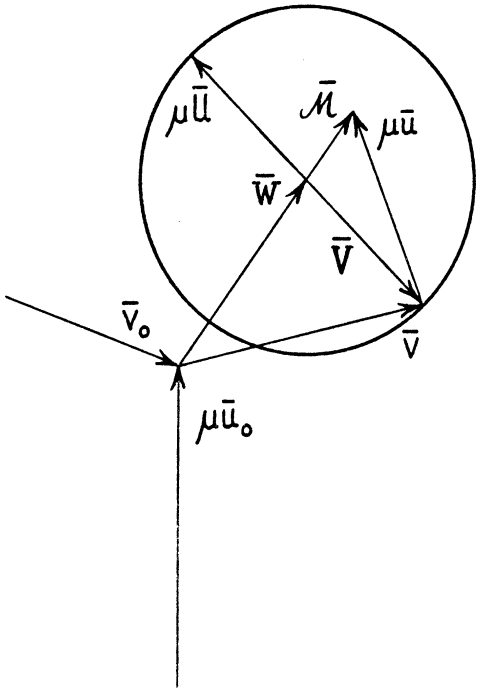

Figure 2.1 Normalized momenta used for discussion of electron-atom collision. In the laboratory system, the incoming atom and electron momenta are $\bar{v}_o$ and $\mu\bar{u}_o$, respectively. The same symbols without subscripts denote the momenta of the outgoing particles; the same quantities capitalized represent the momenta within the center of mass system. The motion of the center of mass itself is denoted by $\bar{W}$. The total momentum of the system is $\bar{\mathcal{M}}$.

but is also spread over a finite solid angle. Consequently, if any collimation is imposed on the beam after excitation, the distribution of metastable speeds which is observed at the detector will be altered, unlike, for example, the case of a beam formed by ideal effusion from a reservoir containing a Maxwellian gas. To assess the severity of such effects, it is useful to consider the observed distribution of particle speeds in two limiting cases.

Case I: no post-collimation

In this case, all of the metastables are assumed to be detected; the expected distribution of particle speeds can be easily ascertained with the help of Figure 2.2. If the metastables are uniformly distributed over the surface of the sphere (pure s-wave scattering), the fraction of metastables having speeds within dv of v is given by

$$P(v)\,dv = \frac{2\pi V \sin\xi\, d\ell}{4\pi V^2} \tag{2.11}$$

However

$$d\ell = V\, d\xi \tag{2.12}$$

$$dv = \sin\xi\, d\ell \tag{2.13}$$

and from the law of sines

$$\frac{W}{\sin\lambda} = \frac{v}{\sin\xi} \tag{2.14}$$

Combining these results leads to

$$P(v)\,dv = \frac{v}{2VW}\, dv \tag{2.15}$$

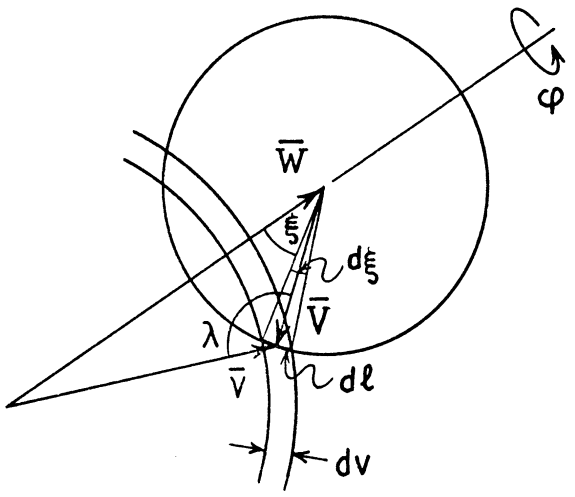

Figure 2.2 Vector diagram showing variables used in determining velocity distribution when all metastables are detected.

Thus the distribution of particle speeds P(v) is given by the linear relation

$$P(v) = \begin{cases} \dfrac{v}{2VW} & |W-V| \leq v \leq W+V \\ 0 & \text{all other values of } v \end{cases} \qquad (2.16)$$

This result is true regardless of the relative magnitudes of W and V; it can easily be shown that $W \gtrless V$ provided that

$$\bar{u}_o \cdot \bar{v}_o \gtrless -\frac{1}{2} \frac{\mu u_o}{v_o} \left\{ (1-\mu) \left(\frac{v_o}{\mu u_o} \right)^2 + \frac{E^*}{E} \right\} \qquad (2.17)$$

A value of $W < V$ merely states that the velocity vectors of the metastable particles are spread over 4π solid angle and that the speed is a single valued function of angle; $W > V$, on the other hand, implies that the vectors are spread over a solid angle less than 2π and that the speed is double valued.

Case II: very narrow post-collimation

In this case it is assumed that only metastables in a small element of solid angle $d\Omega_{det.}$ are observed. Referring to Figure 2.3, the only metastables which pass through the collimation system are those with velocities $\bar{v}_1$ and $\bar{v}_2$, corresponding to the two surface elements $d\sigma(\bar{v}_1)$ and $d\sigma(\bar{v}_2)$. Of the total number of metastables produced, the fraction which falls in such an element is given by

$$P(v)dv = \frac{d\Omega_{sph.}}{4\pi} = \frac{d\sigma(\bar{v})}{4\pi V^2} \qquad (2.18)$$

However, the surface element $d\sigma(\bar{v})$ is related to the element

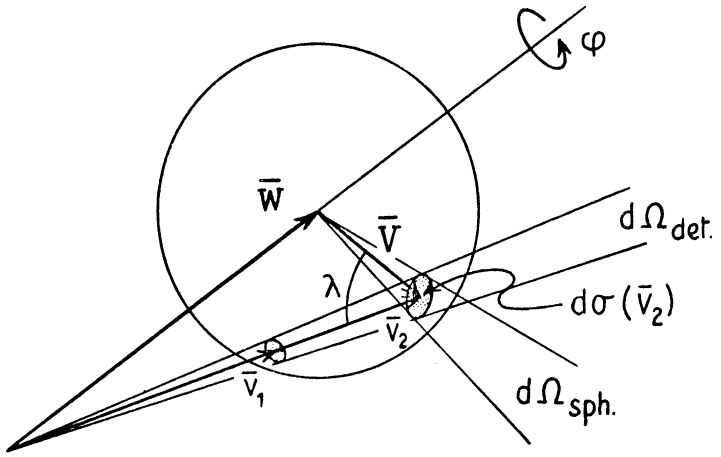

Figure 2.3 Vector diagram showing variables used in determining velocity distribution when only metastables within a small solid angle are detected.

of solid angle, $d\Omega_{det.}$ by

$$d\Omega_{det.} = \frac{d\sigma(\bar{v})\,|\cos\lambda|}{v^2} \qquad (2.19)$$

so that

$$P(v)dv = \frac{1}{4\pi\bar{V}^2} \cdot \frac{v^2}{|\cos\lambda|} \cdot d\Omega_{det.} \qquad (2.20)$$

Since it is difficult to relate $d\Omega_{det.}$ to $d\varphi dv$ in a simple manner, the above expression will not be reduced to these variables. The important point to notice is that, for $W > V$, the distribution in such an arrangement consists of metastables with just two velocities, the relative intensities being proportional to the square of the ratio of their speeds (if $W < V$, there will only be metastables of a single velocity contributing to the signal).

It is concluded, therefore, that the velocity distribution of metastable particles which arises from initially collimated and monoenergetic ground state and electron beams will vary from linear (no post collimation) to one or two delta functions (strong collimation).

2.2 Summation over Elementary Collisions: The General Velocity Distribution Function is Determined

It is convenient at this time to introduce the approximation that all terms of order of the electron-atom mass ratio, $\mu(< 10^{-3})$, and of order of the atom-electron speed ratio, v_o/u_o (normally $< 5 \times 10^{-3}$) are to be neglected relative to unity. The normalized momentum $\bar{\mathcal{M}}$ and the center of

mass velocity $\bar{W}$ then become equal:

$$\bar{v}_o + \mu\bar{u}_o \equiv \bar{\mathcal{M}} \approx \bar{W} \tag{2.21}$$

In addition, the radius, V, of the sphere becomes independent of $\bar{v}_o$ and may be expressed in the simple form

$$V \approx \mu u_o \sqrt{1 - \frac{E^*}{E}} \tag{2.22}$$

where E is the electron energy in the laboratory frame:

$$E = \frac{m}{2} u_o^2 \tag{2.23}$$

Henceforth these approximations will always be assumed.

The results of the previous section show that metastables arising from ground state atoms with a single velocity must have velocities which terminate on a sphere of radius V in velocity space. Since this sphere is centered at the tip of the center-of-mass velocity vector, $\bar{W}$, the simplest representation of the (normalized) resulting velocity distribution occurs in the center of mass system, where it may be expressed

$$g(\bar{v}) = \frac{1}{4\pi V^2}\, \delta(w - V) \tag{2.24}$$

Here w is the magnitude of the velocity of the metastable in the CM system, and s-wave scattering is assumed. The relation between CM variables ($\bar{w}$) and those in the laboratory system ($\bar{v}$) is

$$\bar{w} = \bar{v} - \bar{W}$$

$$\approx \bar{v} - \bar{v}_o - \mu\bar{u}_o \tag{2.25}$$

Suppose now that the ground state gas has an arbitrary velocity distribution function, $f(\bar{v}_o)$, defined so that

$$\int d^3\bar{v}_o \, f(\bar{v}_o) = 1 \qquad (2.26)$$

Upon excitation by electrons, atoms having velocities within $d^3\bar{v}_o$ of $\bar{v}_o$ will become metastables with the velocity distribution represented by the sphere of the previous section. In addition, the number of metastables produced will be proportional to the electron flux, $\frac{j}{e}$, to the density, $n_o f(\bar{v}_o) d^3\bar{v}_o$, of ground state atoms in the interaction region[1], and to the total metastable excitation cross section, σ^*. Consequently, the velocity distribution function of the metastable atoms, $g(\bar{v})$, is given to within geometrical factors by

$$g(\bar{v}) = \frac{j}{e} n_o \sigma^* \int d^3\bar{v}_o \, f(\bar{v}_o) \frac{1}{4\pi \bar{V}^2} \delta(w-V) \qquad (2.27)$$

where the integration is taken over the portion of ground state velocity space which contributes to metastables with velocity $\bar{v}$, and s-wave scattering has been assumed, as before.

To reduce this expression to usable form, it is necessary to convert the delta function from CM variables ($\bar{w}$) to laboratory variables ($\bar{v}_o$). This is accomplished using the

[1] Note that the density is the relevant quantity. Therefore, when discussing excitation of a ground state beam formed by effusion from a reservoir containing a Maxwellian gas, the quantity $n_o f(\bar{v}_o) d^3\bar{v}_o$ will be proportional to $n_o v_o^2 \exp(-v_o^2/\alpha^2)$ (where α is the most probable atomic velocity in the reservoir), rather than to $n_o v_o^3 \exp(-v_o^2/\alpha^2)$, which actually represents the flux of atoms in the beam.

relation

$$\delta(w-V) = \sum_i \frac{\delta(v_o - v_{oi})}{\left|\frac{dw}{dv_o}\right|} \tag{2.28}$$

where the quantities v_{oi} are the solutions of $w(v_{oi}) = V$.

To determine $w(v_o)$, it is convenient first to rearrange the vectors in Equation 2.25 to define a vector $\bar{B}$ which is constant for a given value of $\bar{v}$ (see Figure 2.4)

$$\bar{B} \triangleq \bar{v} - \mu\bar{u}_o = \bar{w} + \bar{v}_o \tag{2.29}$$

From this it immediately follows that

$$w^2 = B^2 + v_o^2 - 2Bv_o\cos\vartheta \tag{2.30}$$

The roots, $v_{o\pm}$, of the expression $w(v_o) = V$ are then

$$v_{o\pm} = B\cos\vartheta \pm \sqrt{V^2 - B^2\sin^2\vartheta} \tag{2.31}$$

If $B < V$, only v_{o+} is physically meaningful. In addition, it is found by differentiation of Equation 2.30 that

$$\left|\frac{dw}{dv_o}\right| = \left|\hat{v}_o \cdot \hat{V}\right| \tag{2.32}$$

where the carats indicate unit vectors.

After substituting these results in Equation 2.27, it is found that the velocity distribution function, $g(\bar{v})$, for metastables arising from a ground state gas with velocity distribution function $f(\bar{v}_o)$ is given by

$$g(\bar{v}) = \frac{j}{e}\frac{n_o\sigma^*}{4\pi V^2}\int d^3\bar{v}_o\, f(\bar{v}_o)\frac{\delta(v_o - v_{o+}) + \delta(v_o - v_{o-})}{|\hat{v}_o \cdot \hat{V}|} \tag{2.33}$$

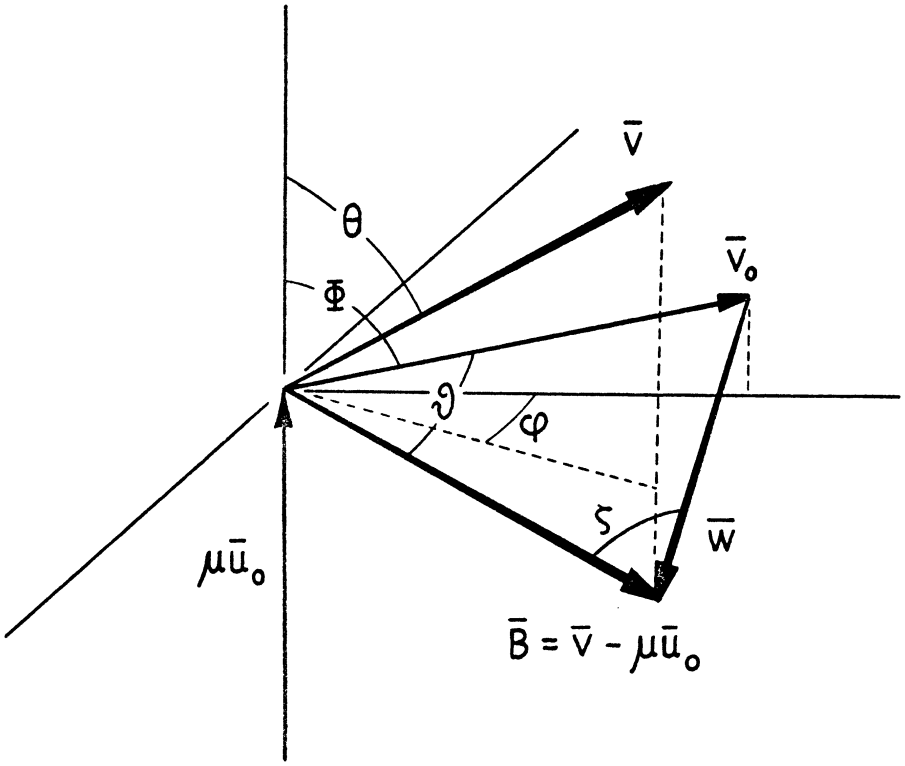

Figure 2.4 Diagram showing relationship between vector variables and an imposed coordinate system. The normalized momenta of the incoming atom and electron are $\bar{v}_o$ and $\mu\bar{u}_o$, respectively. The vectors $\bar{v}$ and $\bar{w}$ represent the total and center of mass contribution to the momentum of the outgoing metastable atom.

or

$$g(\bar{v}) = \frac{j}{e}\frac{n_o \sigma^*}{4\pi V^2}\int_{\Omega_o} d\omega_o \frac{v_{o+}^2 f(\bar{v}_{o+}) + v_{o-}^2 f(\bar{v}_{o-})}{|\hat{v}_o \cdot \hat{V}|} \qquad V<B \quad (2.34)$$

where the range of integration, Ω_o, is determined by the degree of collimation of the ground state gas beam. If B<V, only the first term in the integral appears. A geometric interpretation of the various factors occurring in the integrand of Equation 2.34 is given in Appendix II.

CHAPTER 3

METASTABLE VELOCITY DISTRIBUTIONS ARISING FROM MAXWELLIAN GROUND STATE GAS SOURCES

The relationship between the velocity distribution function $g(\bar{v})$ of metastable atoms and the velocity distribution function $f(\bar{v}_o)$ of the ground state atoms from which the metastables are produced is given by Equation 2.34. In the present chapter, the predictions of this result will be investigated for various degrees of collimation of the ground state gas beam.

In evaluating Equation 2.34 it will be assumed that the ground state beam is formed from a gas with a Maxwellian distribution of velocities. Taking account of the normalization condition of Equation 2.26, the appropriate form for $f(\bar{v}_o)$ is

$$f(\bar{v}_o) = \frac{1}{\pi^{3/2}\alpha^3} \; e^{-v_o^2/\alpha^2} \qquad (3.1)$$

where $\alpha = \sqrt{\frac{2kT}{M}}$ (k is Boltzmann's constant and T is the absolute temperature of the gas). In this case, the velocity distribution function for the metastables may be written

$$g(\bar{v}) = \frac{j}{e} \frac{n_o \sigma^*}{4\pi \bar{V}^2} \frac{1}{\pi^{3/2}\alpha^3} \int_{\Omega_o} d\omega_o \; \frac{v_{o+}^2 e^{-v_{o+}^2/\alpha^2} + v_{o-}^2 e^{-v_{o-}^2/\alpha^2}}{|\hat{v}_o \cdot \hat{V}|} \qquad V<B \quad (3.2)$$

The explicit form for this integral is given by Equations III.9 and III.10 of Appendix III.

3.1 Ground State Beam Well Collimated

Suppose that the ground state beam is confined to a small solid angle $d\omega_o$. The integral in Equation 3.2 then degenerates to the integrand itself. From the geometric arguments of Appendix II, the distribution function of the metastables, $g(\bar{v})$, is expected to have the following properties:

i) it is zero outside of two well defined cutoff speeds, $v_\pm$;

ii) within the cutoffs, $g(\bar{v})$ is generally nonzero; it becomes large near the limiting values of v;

iii) the magnitudes of the cutoffs are very sensitive functions of the observation angle Θ.

3.1.1 General Characteristics of the Metastable Velocity Distribution in the Plane of the Incident Beams

Consider now the excitation of the metastable 2^3S state of helium ($E^* = 19.8$ eV). Suppose that the detector is located in the plane of the incoming beams ($\varphi = 0^o$). Then, for reasonable conditions of beam orientation and detector position (see Section III.2 of Appendix III), the distribution function $g(\bar{v})$ takes the form

$$g(\bar{v}) = \begin{cases} \frac{j}{e}\frac{n_0\sigma^*}{4\pi V}\frac{1}{\pi^{3/2}\alpha^3}\dfrac{v_{o+}^2 e^{-v_{o+}^2/\alpha^2} + v_{o-}^2 e^{-v_{o-}^2/\alpha^2}}{\sqrt{V^2 - \left[\mu u_0 \sin\Phi - v\sin(\Phi-\theta)\right]^2}} & v_- < v < v_+ \\ 0 & \text{otherwise} \end{cases} \tag{3.3}$$

where

$$v_{o\pm} = v\cos(\Phi-\theta) - \mu u_0 \sin\Phi \pm \sqrt{V^2 - \left[\mu u_0 \sin\Phi - v\sin(\Phi-\theta)\right]^2} \tag{3.4}$$

and

$$v_\pm = \left[\mu u_0 \sin\Phi \pm V\right]\csc(\Phi-\theta) \tag{3.5}$$

(see Appendix III). It is emphasized here that Equation 3.3 assumes isotropic scattering of the electrons in the CM frame.

Figure 3.1 shows several distributions, taking the detector angle Θ as the parameter (the numerical scale on the ordinate represents the magnitude of $\left(\frac{v}{\alpha}\right)^2 g\left(\frac{v}{\alpha}\right)$ using the arbitrary normalization $\frac{j\, n_0\sigma^*}{4\pi^{5/2}\alpha e} = 10$. This same scaling is used consistently throughout the thesis). All of the previously mentioned properties are evident; the sensitivity of the cutoff positions is due to the cosecant factor in Equation 3.5. It is interesting to notice how the distributions "ride over" the Maxwellian distribution in the integrand (actually, there is an additional factor of v^2 since the ob-

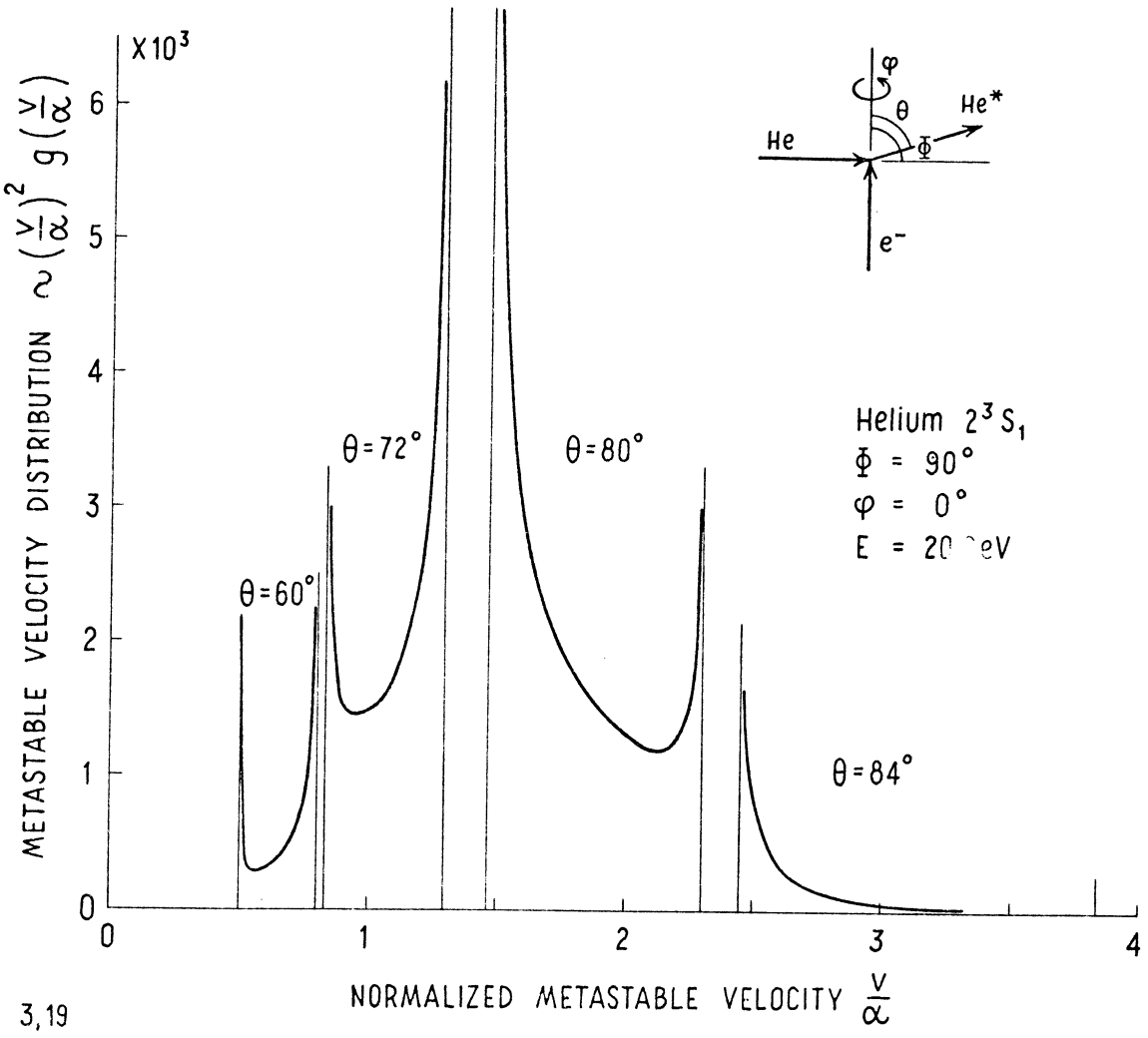

Figure 3.1 Metastable velocity distributions for 2^3S helium, with detector angle Θ as parameter. The ground state beam is assumed to be perfectly collimated and to have a Maxwellian velocity distribution.

servable quantity is proportional to $v^2 g(\bar{v})$; this is why the underlying "envelope" appears to peak closer to $v/\alpha = \sqrt{2}$ than to $v/\alpha = 1$).

Figure 3.2 indicates how the velocity distribution at a fixed angle Θ varies with electron energy. The widening of the distribution with increasing energy results from the corresponding increase in the radius V of the cylindrical envelope on which the metastable velocities terminate (see Appendix II). Figure 3.3 shows that if the energy of the electron is sufficiently large, the cutoffs may become separated by enough so that the Maxwellian-like envelope mentioned in conjunction with Figure 3.1 can appear as a bump within the distribution found for a single set of parameters. The way in which the width of the distribution (cutoff separation) depends on energy is shown in Figure 3.4 for various detector angles Θ.

3.1.2 The Integrated Metastable Intensity[1]

Figure 3.5 indicates the variation of the total metastable intensity (integral of the velocity distribution over all velocities) with detector position Θ; the electron energy excess ΔE (energy above threshold) is the parameter (see Section III.3 of Appendix III). These curves indicate a substantial nonuniform behavior for the metastable intensity pattern in the plane of the incoming beams, even though the scattering is isotropic. Qualitatively, this can be understood as follows.

[1]Intensities for $\varphi \neq 0$ are shown in the addendum, page 129.

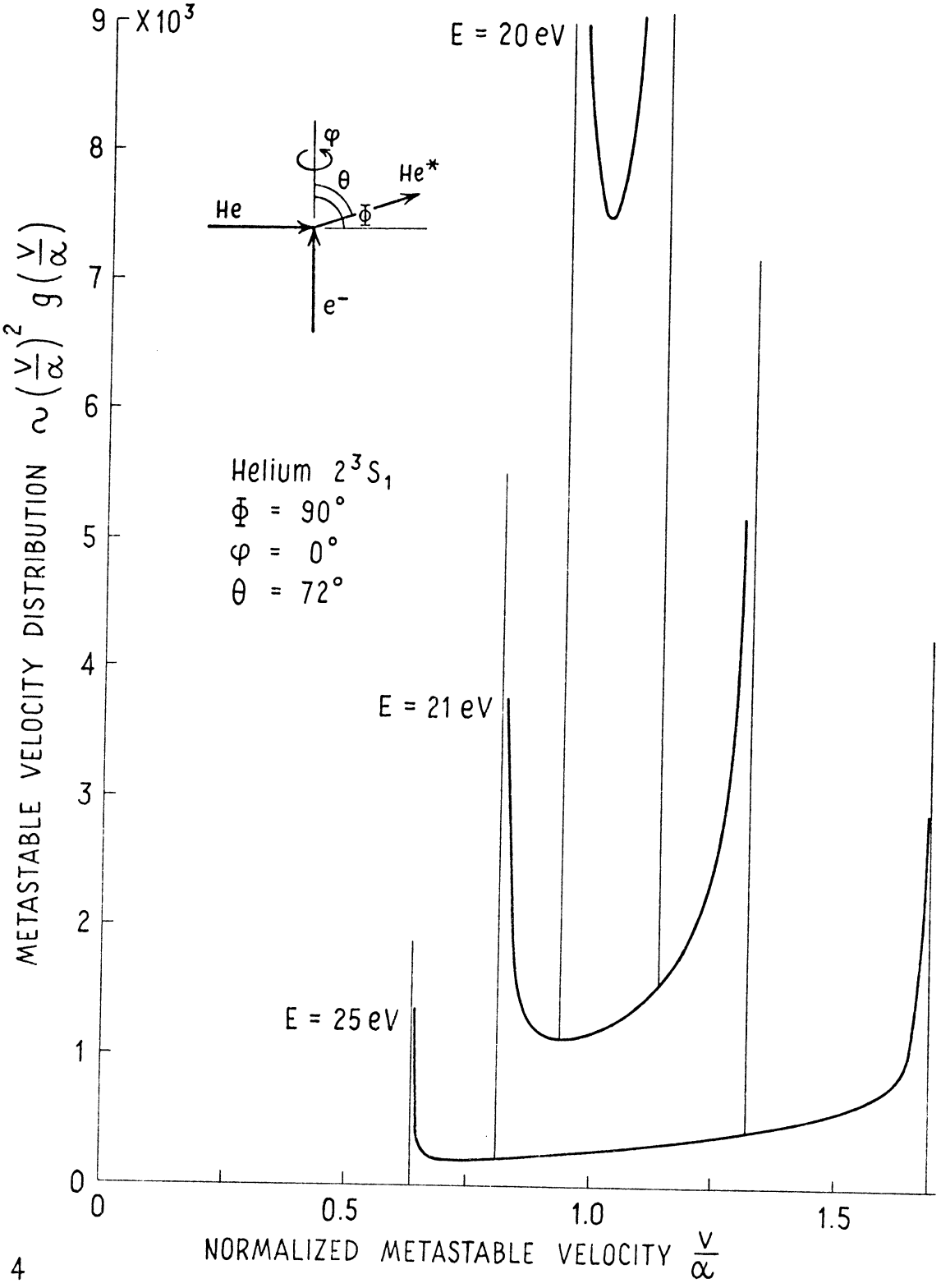

Figure 3.2 Metastable velocity distributions for 2^3S helium, with electron energy E as parameter. The ground state beam is assumed to be perfectly collimated and to have a Maxwellian velocity distribution.

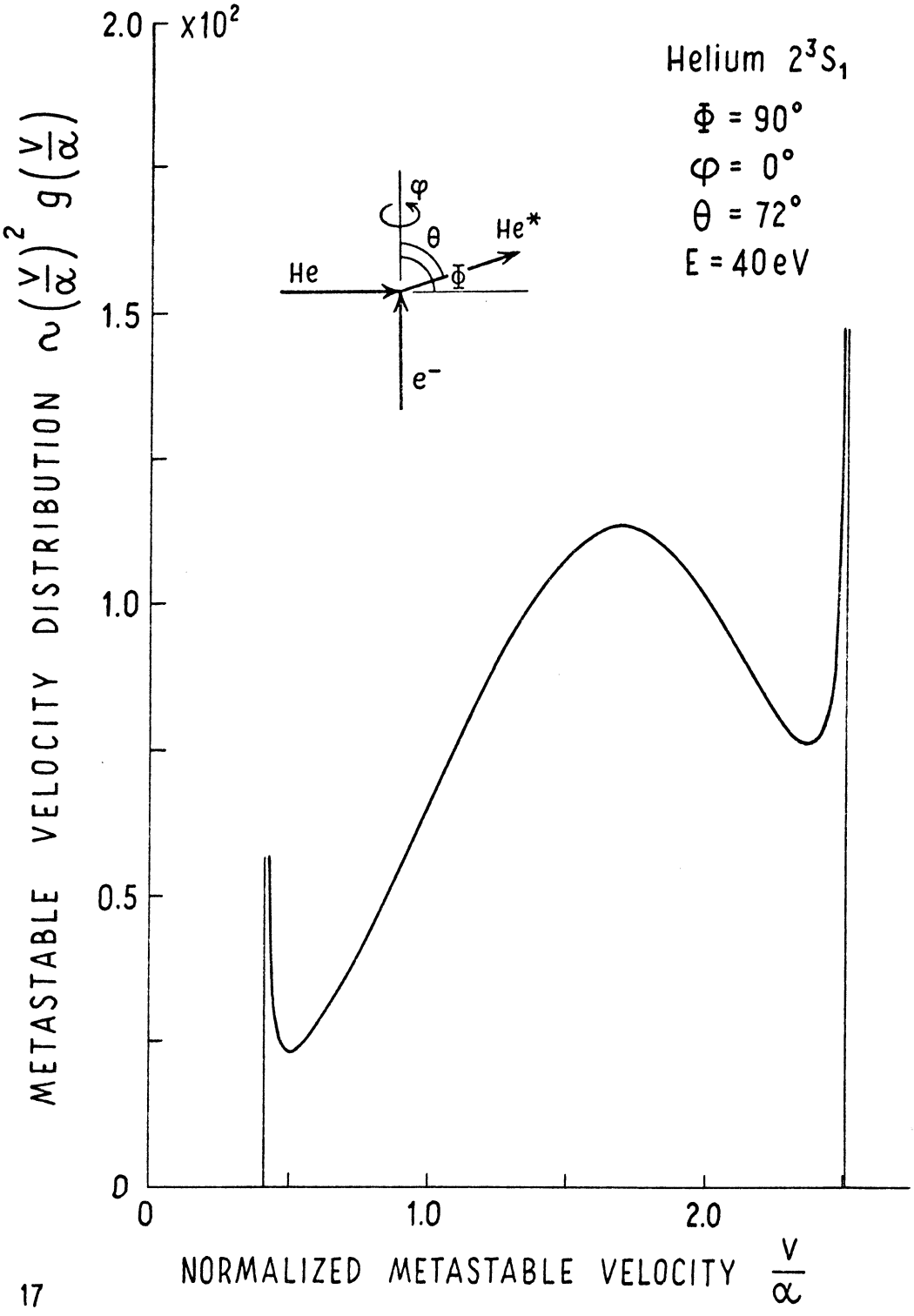

Figure 3.3 Metastable velocity distribution for 2^3S helium, showing structure due to Maxwellian velocity distribution in the (collimated) ground state beam. Note that ordinate scale differs from that of Figures 3.1 and 3.2.

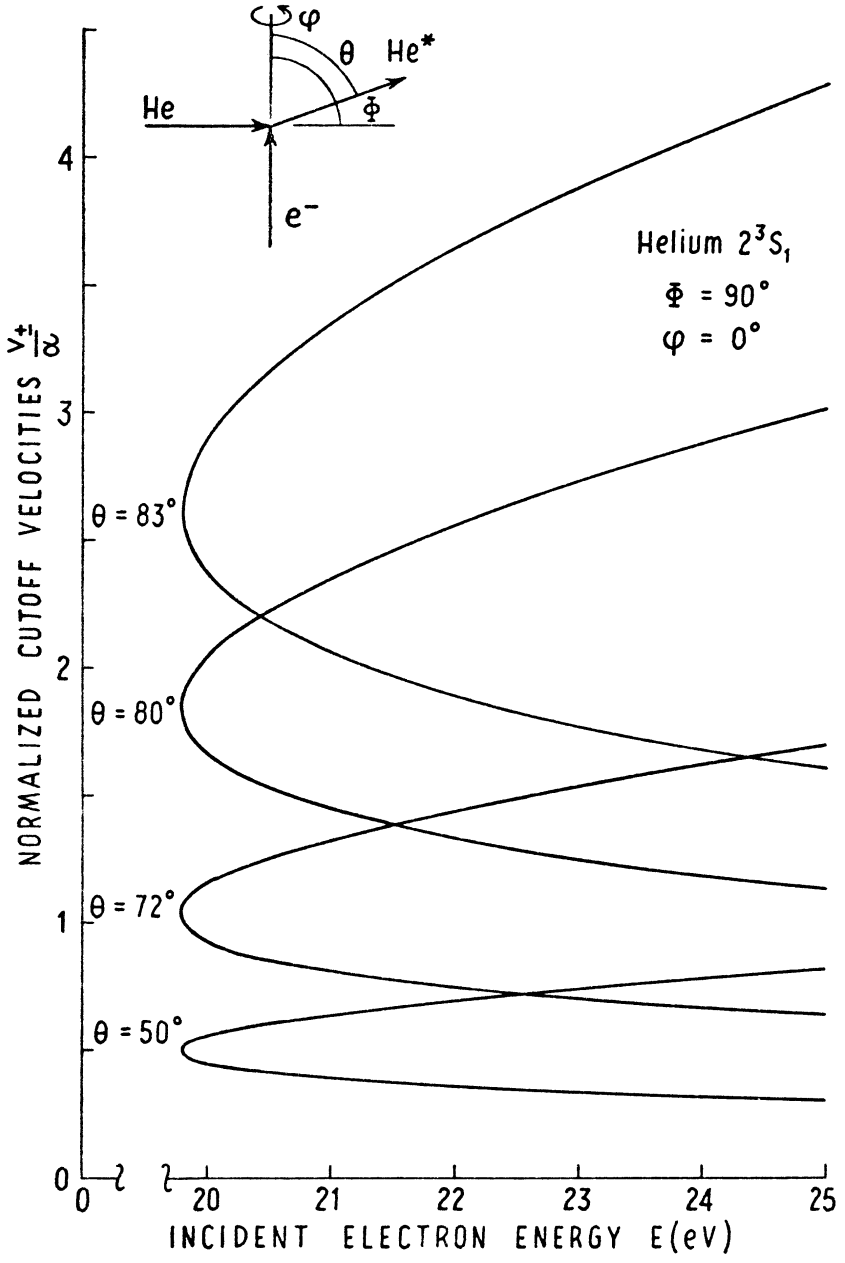

Figure 3.4 Variation of cutoff velocities with electron energy for 2^3S helium; detector angle Θ is the parameter. The ground state beam is assumed to be perfectly collimated and to have a Maxwellian velocity distribution.

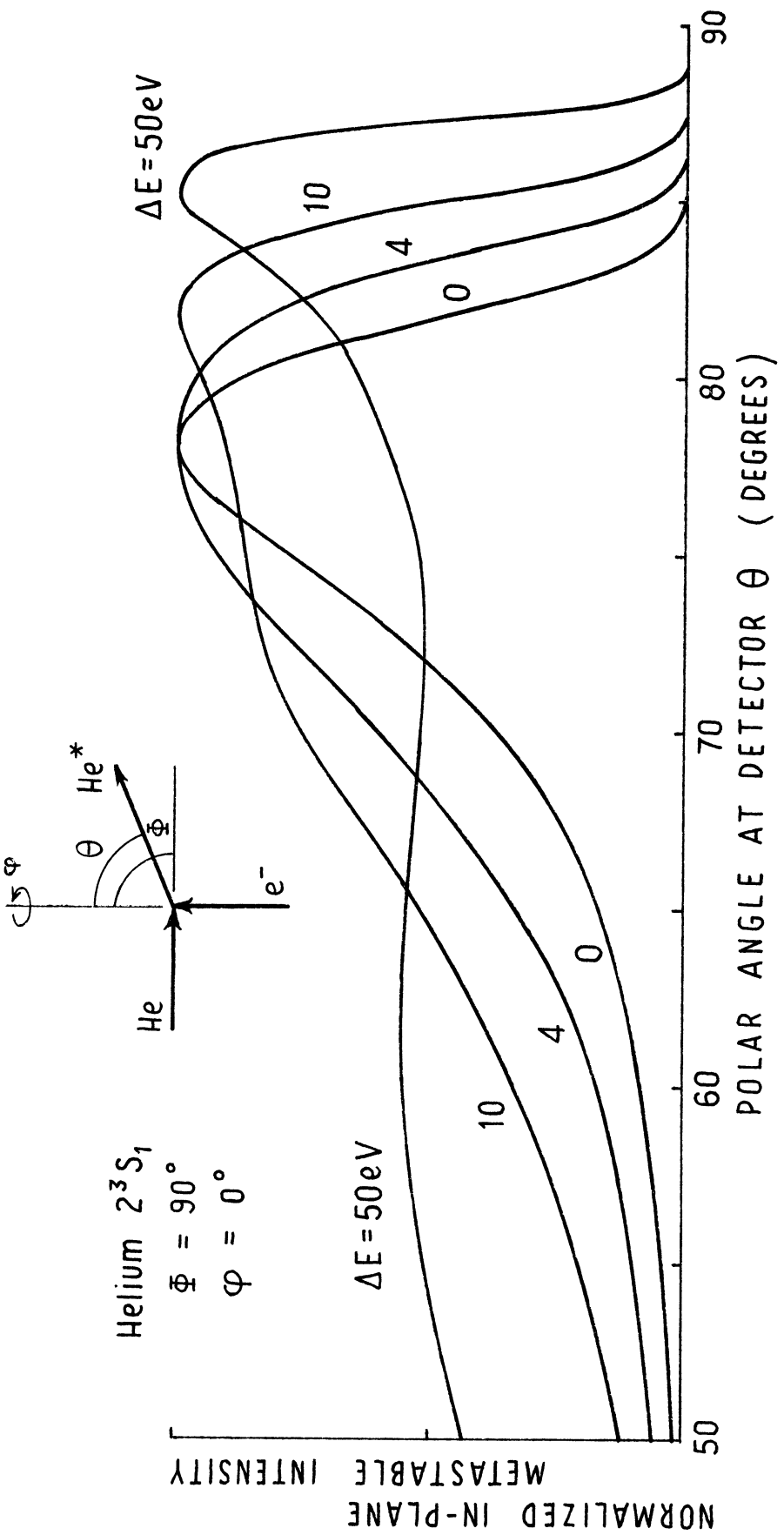

Figure 3.5 Total metastable intensity for 2^3S helium as a function of detector angle Θ. The electron energy increment above threshold, ΔE, is the parameter. The ground state beam is assumed to be perfectly collimated and to have a Maxwellian velocity distribution. It is emphasized that isotropic scattering of the electrons is also assumed.

The cylindrical portion of metastable velocity space which contains the allowed metastable velocities (see Figure II.1 of Appendix II) is composed of an infinity of spheres. Each sphere is weighted according to the ground state velocity distribution $f(\bar{v}_o)$; the most populated portion of $f(\bar{v}_o)$ is mapped into a densely populated sphere in the metastable space. For a given increment of metastable speeds, the greatest contributions to the metastable velocity distribution are made near the circumference of the cylinder. To lowest order, therefore, it is reasonable to expect that the total metastable intensity will exhibit maxima near angles Θ determined by the points at which the most densely populated sphere is tangent to the cylindrical envelope. In fact, this argument predicts the positions of the bumps in the curves of Figure 3.5 within 20%, provided that the extra factor v^2 is also included, giving the most weight to atoms with speeds roughly $\sqrt{2}$ times the most probable speed in the ground state beam.

Although the curves of Figure 3.5 are normalized to the same peak height, an estimate of the relative "average" amplitudes can be made using an approximation suggested by Equation III.28 of Appendix III. There, since $\lim_{V\to 0} VI(\Theta,\Phi;0,V)$ is finite, it appears reasonable to suppose that to lowest order in V the quantity $VI(\Theta,\Phi;0,V)/\sigma^*$ is a function of Θ and Φ only (the cross section is taken over from the right side since it is generally a strong function of the excess energy, and hence of V). This should be a good assumption

as long as V is resonably small, and as long as Θ (and Φ) is chosen in the range where the metastable intensity in the limit $V \to 0$ has a representative value, e.g., in the vicinity of the peak of the $\Delta E = 0$ curve. Since $V \propto \sqrt{\Delta E}$, the above condition reduces to the approximation

$$\sqrt{\Delta E}\left\langle I(\Theta,\Phi;0,\sqrt{\Delta E})\right\rangle / \sigma^*(\Delta E) \approx F(\Theta,\Phi) \qquad (3.6)$$

where $\langle I \rangle$ indicates a representative intensity.

This result may be given the following physical interpretation. The total metastable production is proportional to σ^*. These metastables are spread over a cylinder in velocity space which is characterized by a dihedral angle roughly proportional to the radius V of the cylinder (see Figure II.1 of Appendix II). If $\langle I \rangle$ is a representative intensity of the metastables over this angular range, then the total number of metastables is proportional to $V\langle I \rangle$. Dividing by σ^* for normalization gives Equation 3.6.

3.1.3 Sensitivity of the Velocity Distribution to Beam Misalignments

One important objective of the present work is to assess the effects of various misalignments on the velocity distribution of the metastable atoms. From Figure 3.1 it is seen that the velocity distribution is a very sensitive function of detector angle Θ; this has already been explained in terms of the cosecant factor in the equation for the cutoffs (Equation 3.5). Because this factor also contains the angle

Φ, the distribution should show about the same sensitivity to misalignment of the ground state beam. Thus, misalignment of either the ground state beam or of the detector will introduce strong shifts in the metastable velocity distribution.

Since the argument of the cosecant is $\Phi-\Theta$, it is to be expected that equal simultaneous errors in Θ and Φ should not produce a very large effect on the distribution (assuming that $\sin\Phi \approx 1$). Comparison of the velocity distributions in Figure 3.6a with each other and with the E = 25 eV curve of Figure 3.2 shows that this expectation is reasonwell substantiated for angular errors up to $\pm 10^{\circ}$ centered at $\Phi = 90^{\circ}$. For very large total angular deviations, however, the shape of the velocity distribution is more distorted (Figure 3.6b). Figure 3.7 shows that this distortion can become extreme if the energy of the incident electrons is sufficiently large.

It is worthy of note that equal simultaneous errors in Θ and Φ are equivalent to a misalignment of the <u>electron</u> beam in the plane of the ground state beam and the detector. It is therefore concluded that a small misalignment of the electron beam in that plane will not affect the metastable velocity distribution nearly as seriously as an equal misalignment of either the ground state beam or the detector alone.

The discussion so far has been concerned with velocity distributions in the plane of the incident beams ($\varphi = 0$);

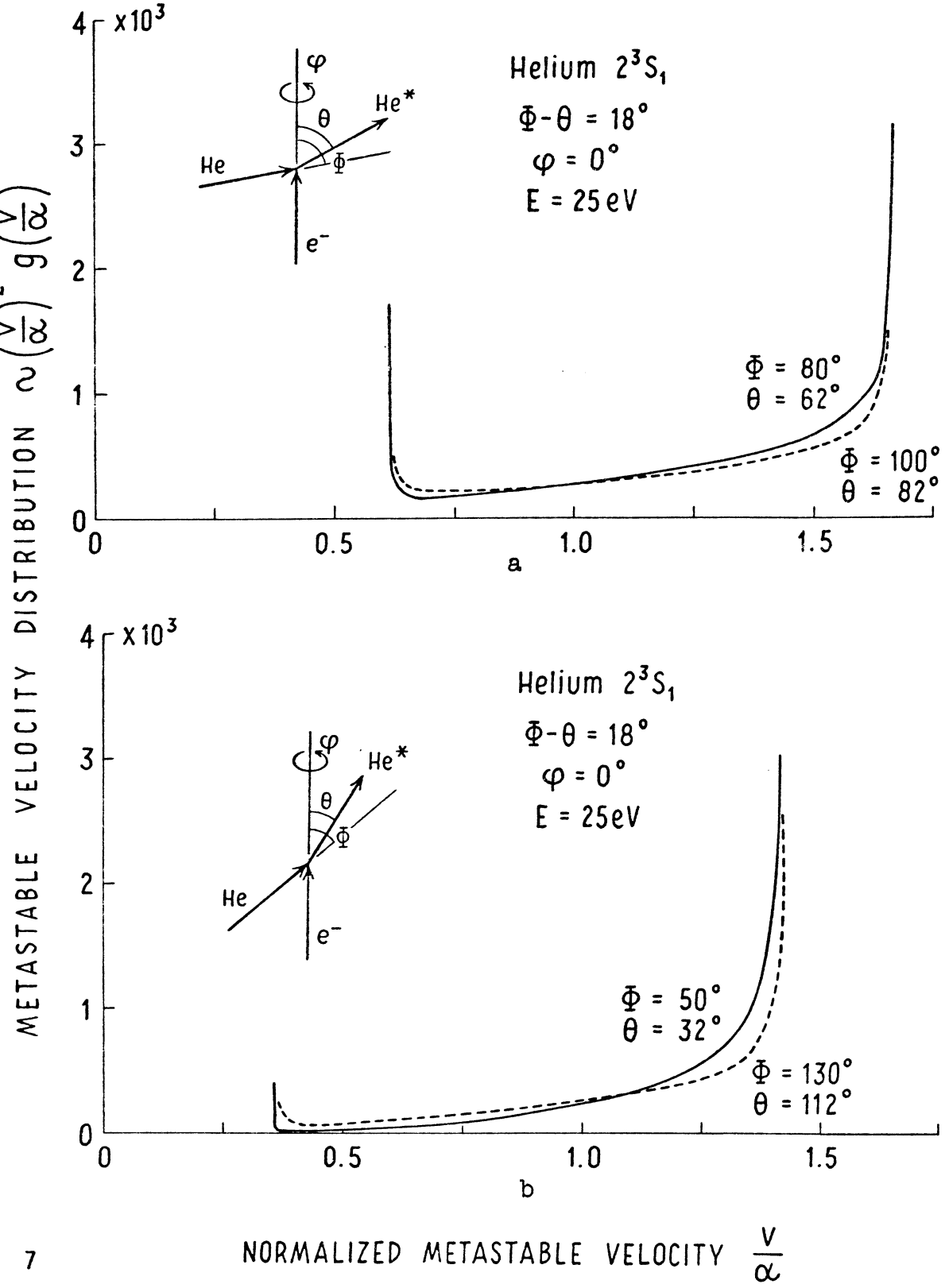

Figure 3.6 Metastable velocity distributions for 2^3S helium showing effect of simultaneous angular displacements of ground state beam and detector. The ground state beam is assumed to be perfectly collimated and to have a Maxwellian velocity distribution.

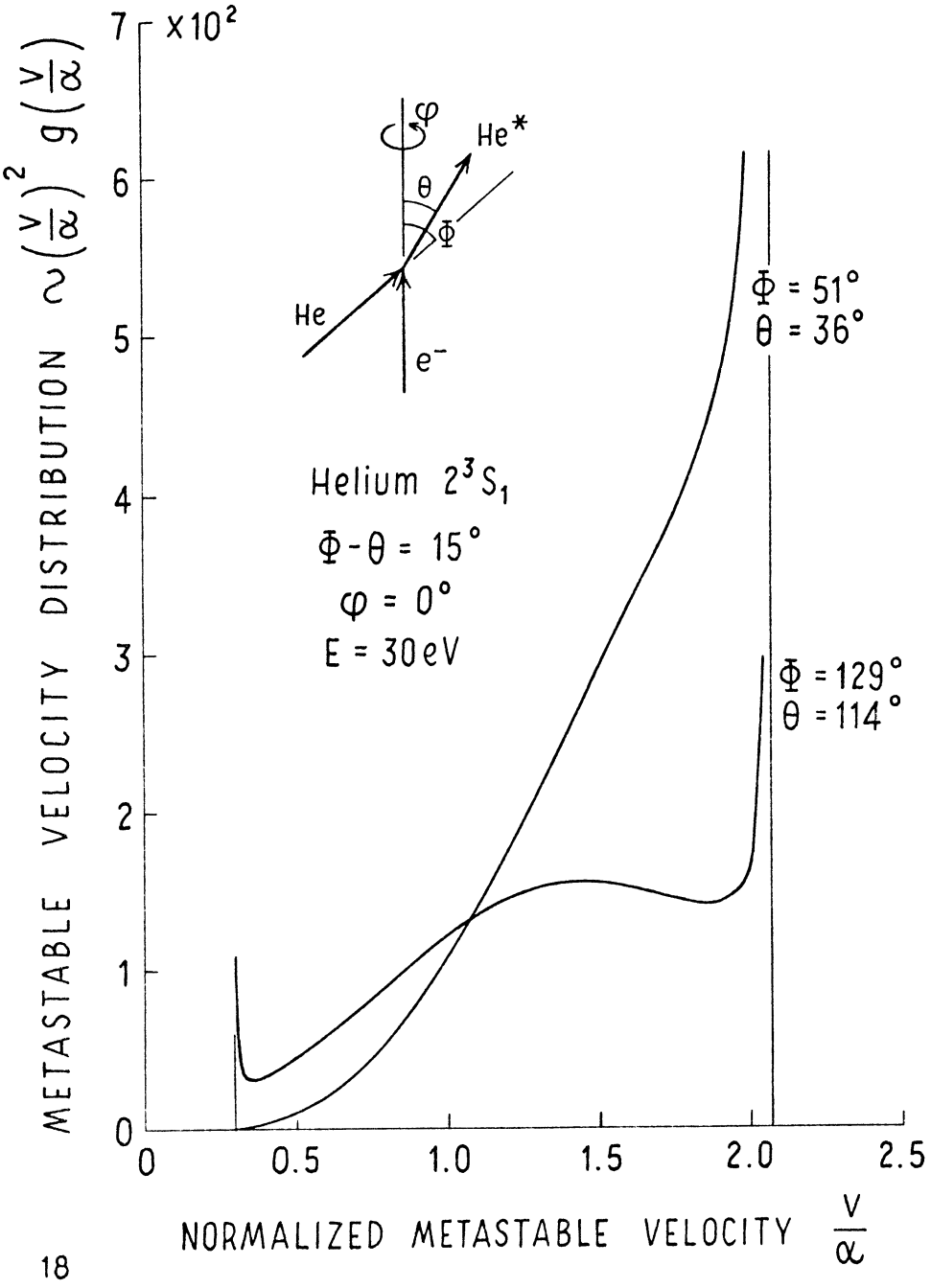

Figure 3.7 Metastable velocity distributions for 2^3S helium showing effect of simultaneous angular displacements of ground state beam and detector. The ground state beam is assumed to be perfectly collimated and to have a Maxwellian velocity distribution.

the effects of out-of-plane misalignment will now be considered. The cutoffs provide the most sensitive indicator of the distortions of the velocity distributions which result when $\varphi \neq 0$. The general expression for the cutoff velocities is given by Equation III.15. Figures 3.8a and 3.9a show how the cutoffs vary as a function of detector position, taking the azimuthal angle, φ, as parameter. The most striking feature of these results is that the cutoffs no longer move out to infinity with increasing Θ, but have a definite upper limit for a given φ. This merely reflects the fact that the plane described by $\varphi \neq 0$ cuts the cylindrical envelope obliquely, so that as the angular position Θ of the ray to the detector is increased, the ray eventually passes outside of the envelope. Thus, whereas distributions corresponding to $\varphi = 0$ always widen as Θ is increased (see Figure 3.1), the distributions will generally widen and then narrow again if $\varphi \neq 0$. This behavior is indicated by the plots of cutoff separations shown in Figures 3.8b and 3.9b, e.g., for $\varphi = 2^{o}$.

If the plane in which the detector moves is far enough out of plane, the resulting velocity distributions may show very little variation in width over a relatively large range of Θ. Figure 3.10 shows such a case (compare Figure 3.1).

If the detector is kept at a fixed angle Θ, and φ is slowly increased, a value $\varphi_{max.}$ will eventually be reached where the ray to the detector becomes tangent to the cylinder. This value of φ is given by Equation III.16. The ef-

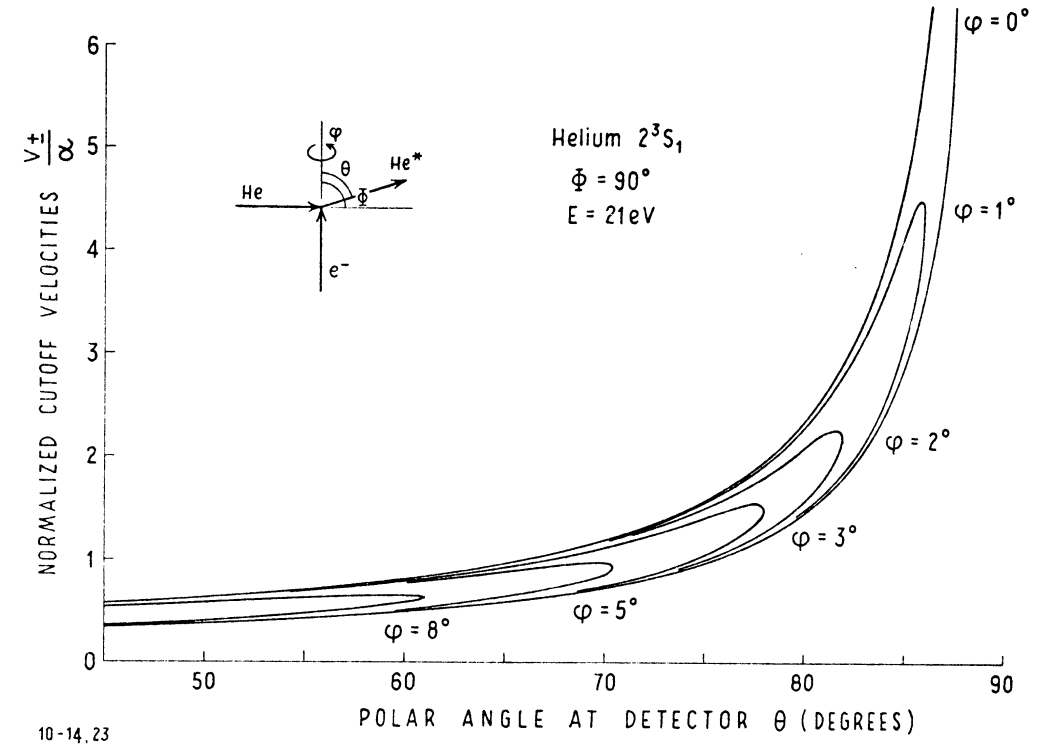

a

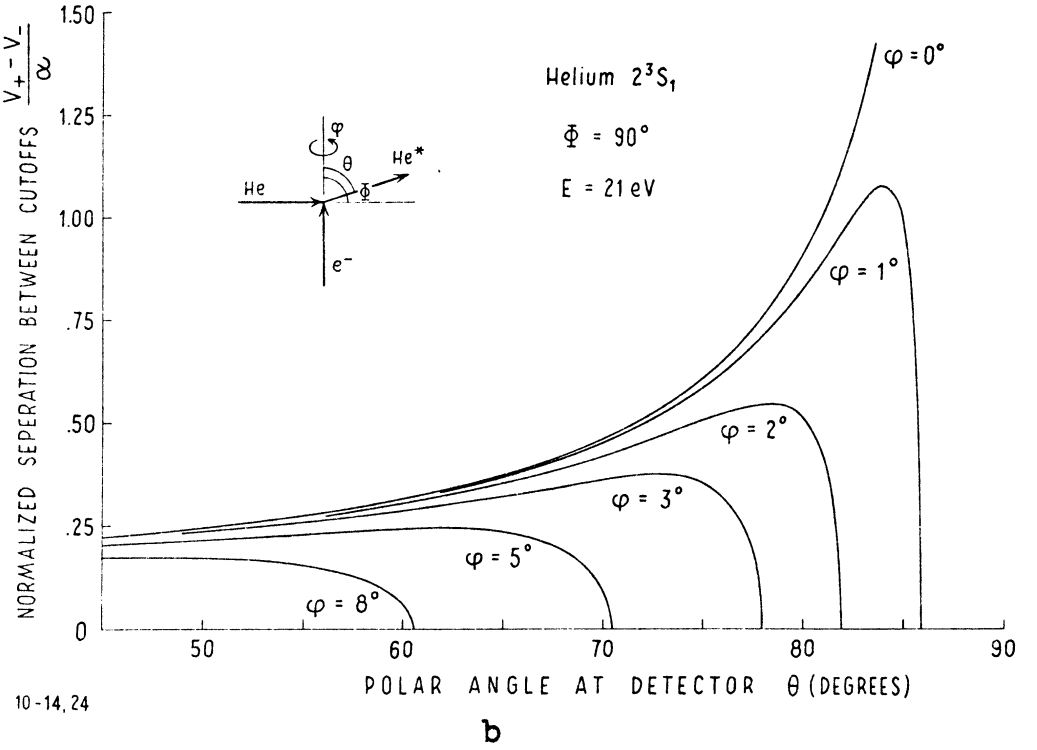

b

Figure 3.8 Behavior of cutoffs for 2^3S helium with azimuthal angle φ as parameter. Curves a: normalized cutoff velocities; curves b: normalized separation between cutoffs. Ground state beam assumed Maxwellian and perfectly collimated.

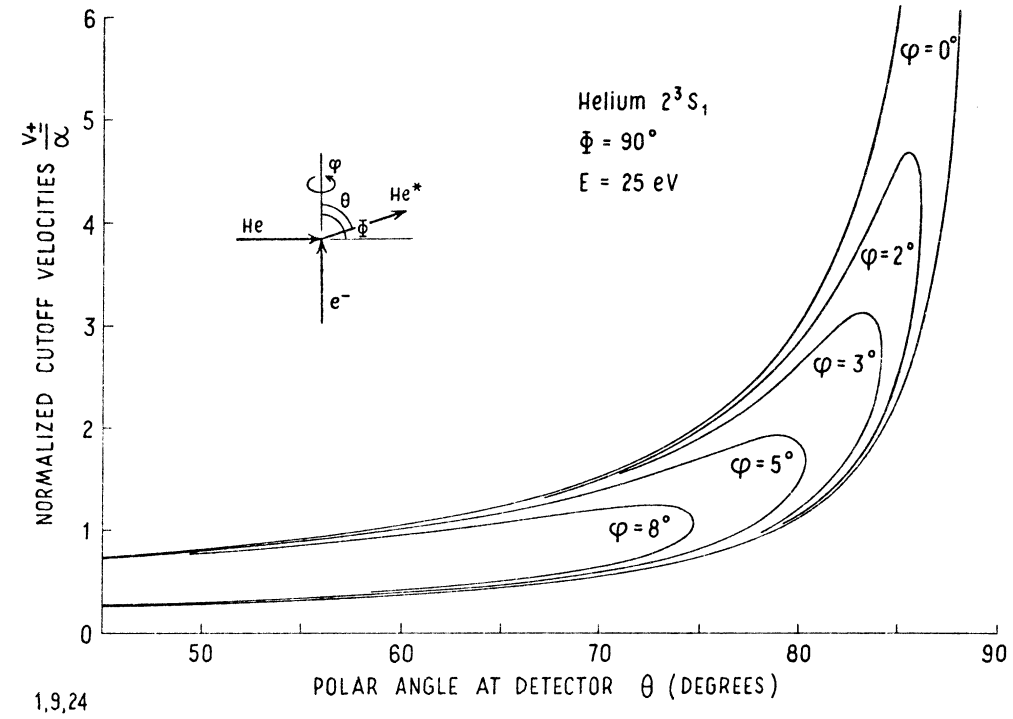

a

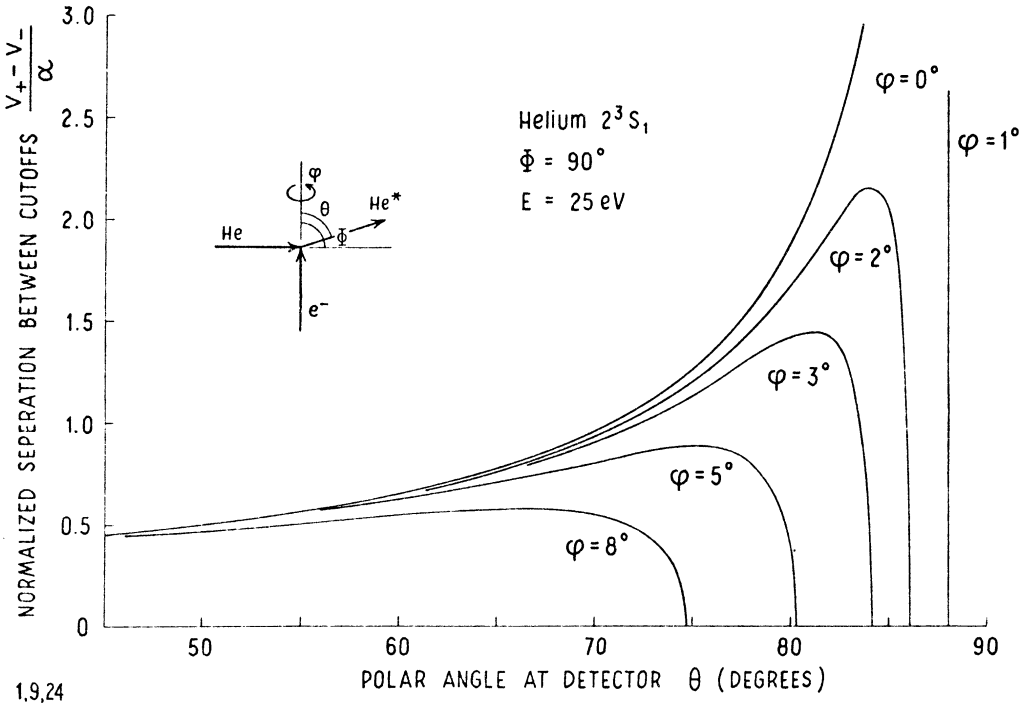

b

Figure 3.9 Behavior of cutoffs for 2^3S helium with azimuthal angle φ as parameter. Curves a: normalized cutoff velocities; curves b: normalized separation between cutoffs. Ground state beam assumed Maxwellian and perfectly collimated.

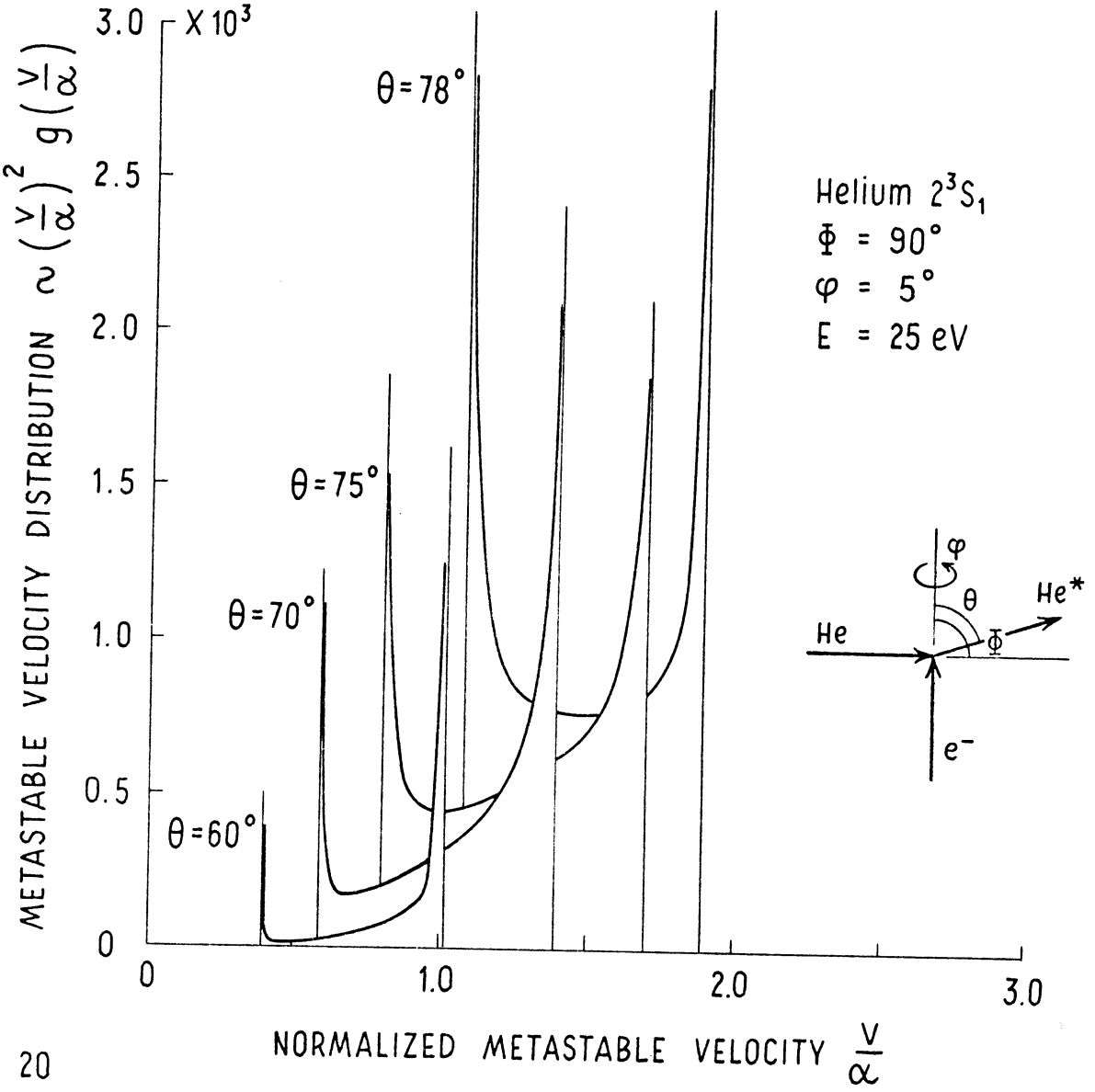

Figure 3.10 Metastable velocity distributions for 2^3S helium in plane defined by $\varphi = 5^0$; detector angle Θ is parameter. Ground state beam assumed Maxwellian and perfectly collimated.

fect on the velocity distribution is a gradual narrowing, as indicated by the curves in Figure 3.11; for this choice of Θ, Φ it is found that $\varphi_{max.} = 4.588^{o}$. This effect is qualitatively similar to decreasing the value of ΔE (compare Figure 3.2).

The behavior of the metastable velocity distribution arising from a well collimated ground state beam can be summarized as follows. The cutoffs (which determine the "position" of the distribution in the velocity coordinate v) are sensitive functions of Θ, Φ and φ. The width of the distribution is a sensitive function of φ and ΔE; it is also usually sensitive to Θ and Φ, except when in proper combination with φ. The distribution is relatively insensitive to misalignment of the electron beam in the plane of the ground state beam and the detector.

3.2 Divergent Ground State Beam

If the ground state beam is not perfectly collimated, then the integration indicated in Equation 3.2 must be performed. The resulting metastable velocity distribution will therefore tend to be smoother than the distributions discussed in Section 3.1.

Figure 3.12 shows the effect of finite detector width on the metastable velocity distribution[1] (since the effects

[1] I would like to thank Dr. E. S. Fry for the use of his computer program (which is included as Appendix IV) to evaluate these integrals; numerical results from this program were also used in Figures 3.5, 5.3 and 7.1.

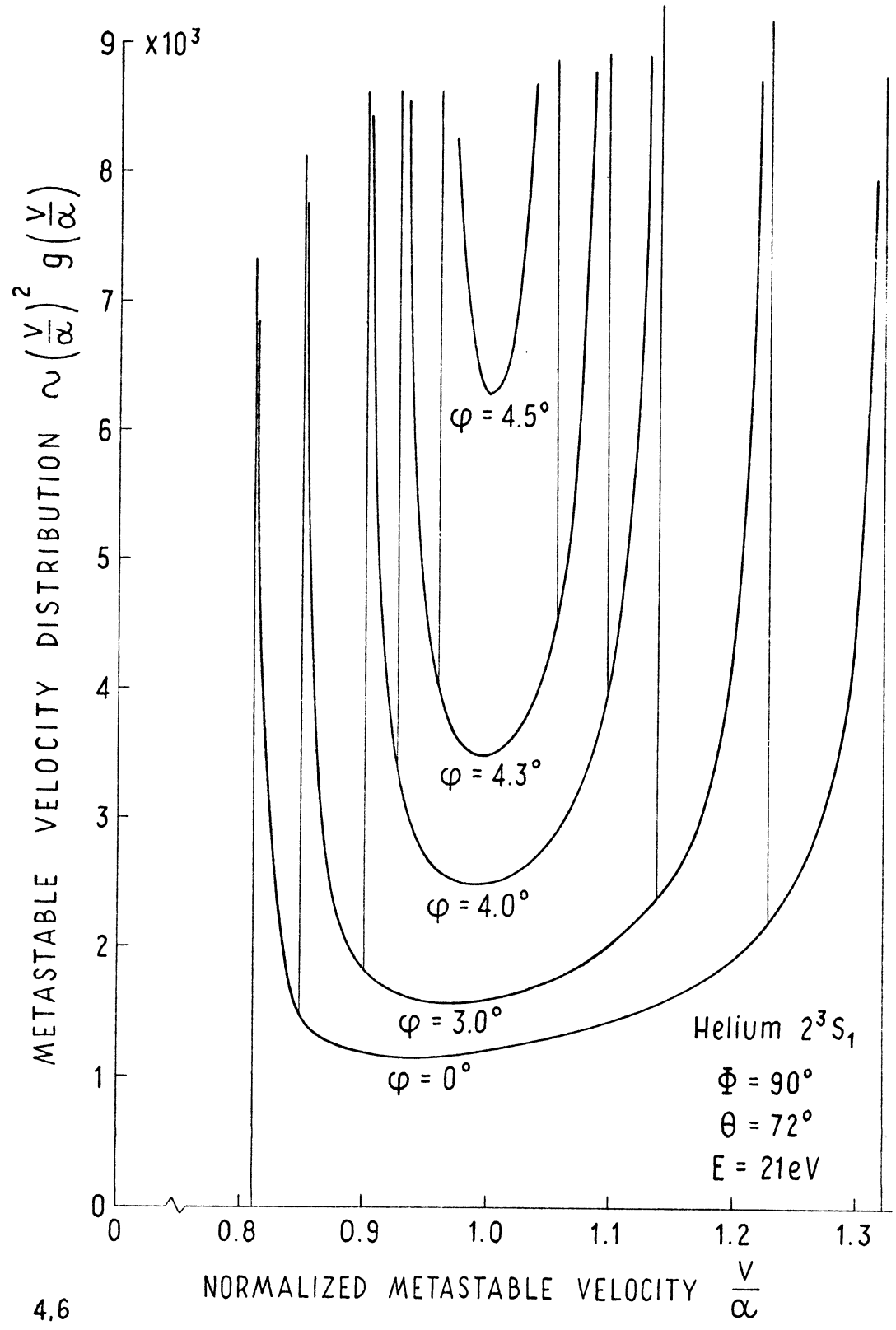

4.6

Figure 3.11 Metastable velocity distributions for 2^3S helium at fixed detector angle Θ; azimuthal angle Φ is parameter. Ground state beam assumed Maxwellian and perfectly collimated.

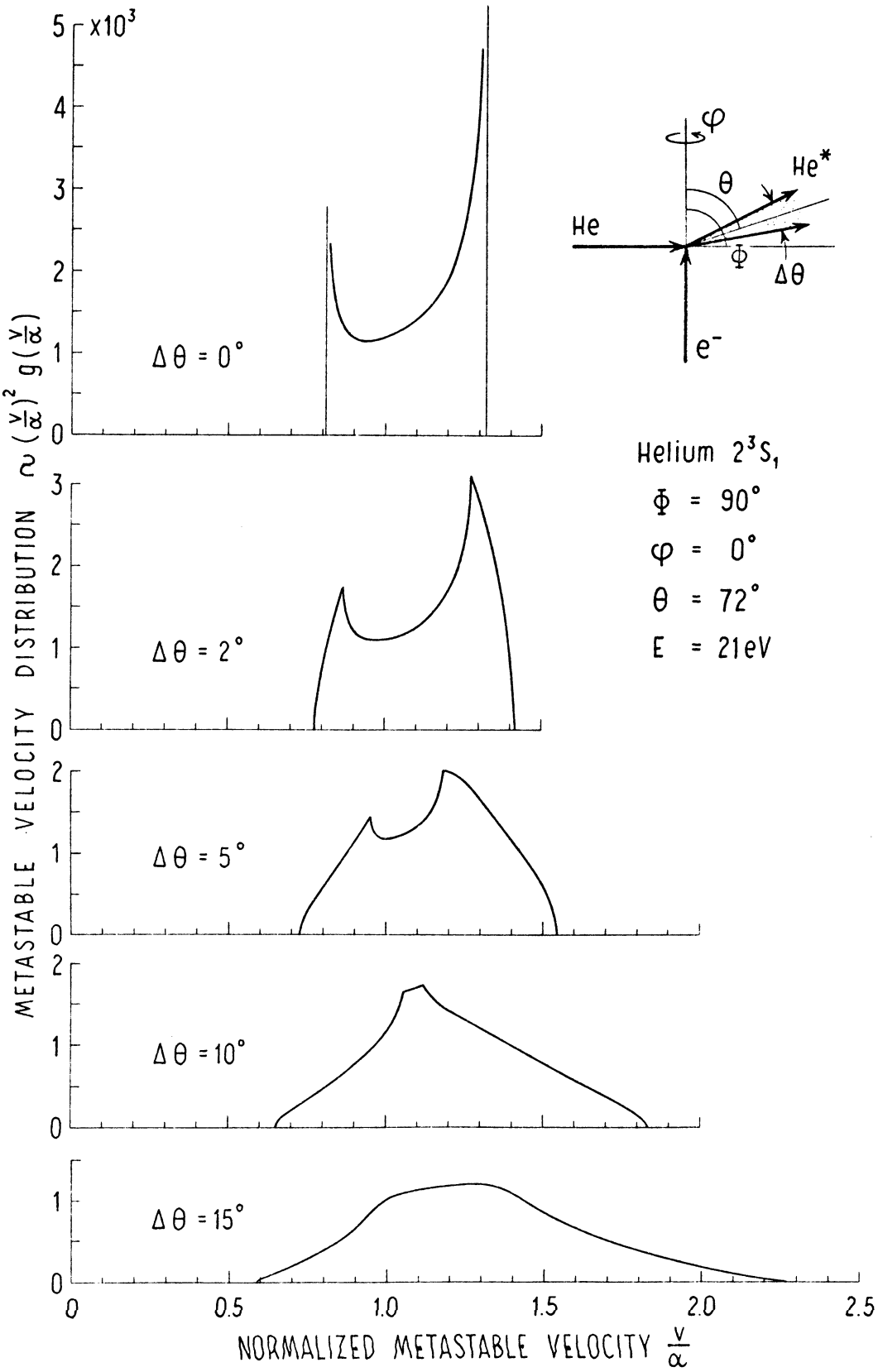

Figure 3.12 Metastable velocity distributions for 2^3S helium at fixed detector angle Θ; angular width of detector $\Delta\Theta$ is parameter. Ground state beam assumed Maxwellian and perfectly collimated.

of an error in Φ are roughly the same as those of an error in Θ - see Equation 3.5 and Figure 3.6a - this is approximately equivalent to the distribution arising from a ground state beam of angular divergence $\Delta\Phi=\Delta\Theta$, assuming the detector width to be negligible). The curves are normalized to represent intensity per degree of detector width.

Qualitatively, the effects are as expected. The peaks are gradually smoothed out, and the width of the distribution increases. For sufficiently wide collimation, the distribution takes on a relatively smooth, single-humped character. Other similarly integrated distributions are shown in Figures 5.3 and 7.1.

3.3 Isotropic Ground State Gas Source

The ultimate in divergent ground state beams is a completely isotropic gas source; such a situation exists for an electron gun in a gas filled container. Interestingly enough, in this case the integral in Equation 3.2 can be evaluated analytically, as will now be shown.

The integration is most easily performed in a coordinate system with origin at the center of the contributing sphere (see Appendix II), i.e., centered at the tip of the vector $\bar{B}$. Defining a polar coordinate ς which is related to the variable ϑ(Figure 2.4) by the law of sines, the solid angle element $d\omega_o$ can be transformed to a corresponding element in the new coordinate system. Making this transforma-

tion, Equation 2.34 takes the simple form

$$g(\bar{v}) = \frac{j}{e}\,\frac{n_o \sigma^*}{4\pi}\int_{\tilde{\Omega}_o} d\tilde{\omega}_o\; f(\bar{v}_o) \tag{3.7}$$

where $d\tilde{\omega}_o$ is the solid angle element in the system with origin at the tip of the vector B, and the integral is taken over the entire sphere ($\tilde{\Omega}_o = 4\pi$).

From Equation 2.29 with $\bar{w} = \bar{V}$ it follows that

$$v_o^2 = B^2 + V^2 - 2BV\cos\varsigma \tag{3.8}$$

With the Maxwellian form of $f(\bar{v}_o)$ (Equation 3.1), Equation 3.7 becomes

$$g(\bar{v}) = \frac{j}{e}\,\frac{n_o \sigma^*}{\pi^{3/2}\alpha^3}\,\frac{1}{4\pi}\int_0^{2\pi} dv \int_0^{\pi} d\varsigma\, \sin\varsigma\; e^{-\frac{B^2+V^2-2BV\cos\varsigma}{\alpha^2}}$$

$$= \frac{j}{e}\,\frac{n_o \sigma^*}{\pi^{3/2}\alpha^3}\; e^{-\frac{B^2+V^2}{\alpha^2}}\; \frac{\sinh\frac{2BV}{\alpha^2}}{\frac{2BV}{\alpha^2}} \tag{3.9}$$

The dependence of the result on $\bar{v}$ is of course hidden in the quantity B which is obtained from

$$\bar{B} = \bar{v} - \mu\bar{u}_o \tag{3.10}$$

One remarkable prediction of Equation 3.9 concerns the behavior of $g(\bar{v})$ at threshold ($V = 0$). In this case the quotient involving the hyperbolic sine becomes equal to unity. If the vectors $\bar{v}$ and $\mu\bar{u}_o$ are perpendicular ($\Theta = \frac{\pi}{2}$) then it follows that

$$\lim_{\substack{V\to 0\\ \Theta\to\frac{\pi}{2}}} g(\bar{v}) = \frac{j}{e}\,\frac{n_0\sigma^*}{\pi^{3/2}\alpha^3}\, e^{-\frac{\mu^2 u_0^2}{\alpha^2}} \cdot e^{-\frac{v^2}{\alpha^2}} \qquad (3.11)$$

i.e., the distribution function $g(\bar{v})$ is Maxwellian once again.

The velocity distribution which results from Equation 3.9 at threshold is plotted for several values of Θ in Figure 3.13; the curves have been normalized to identical peak values. As the angle of observation Θ shifts from zero to 180°, it is seen that the distribution shifts from "wide and fast", through Maxwellian to "narrow and slow". Figures 3.14 and 3.15 show, respectively, the behavior of the peak position and of the peak intensity (assuming σ^* is constant) of the velocity distributions obtained from Equation 3.9. Over the full range of Θ, the shift in peak position and the variation in peak intensity are seen to be substantial.

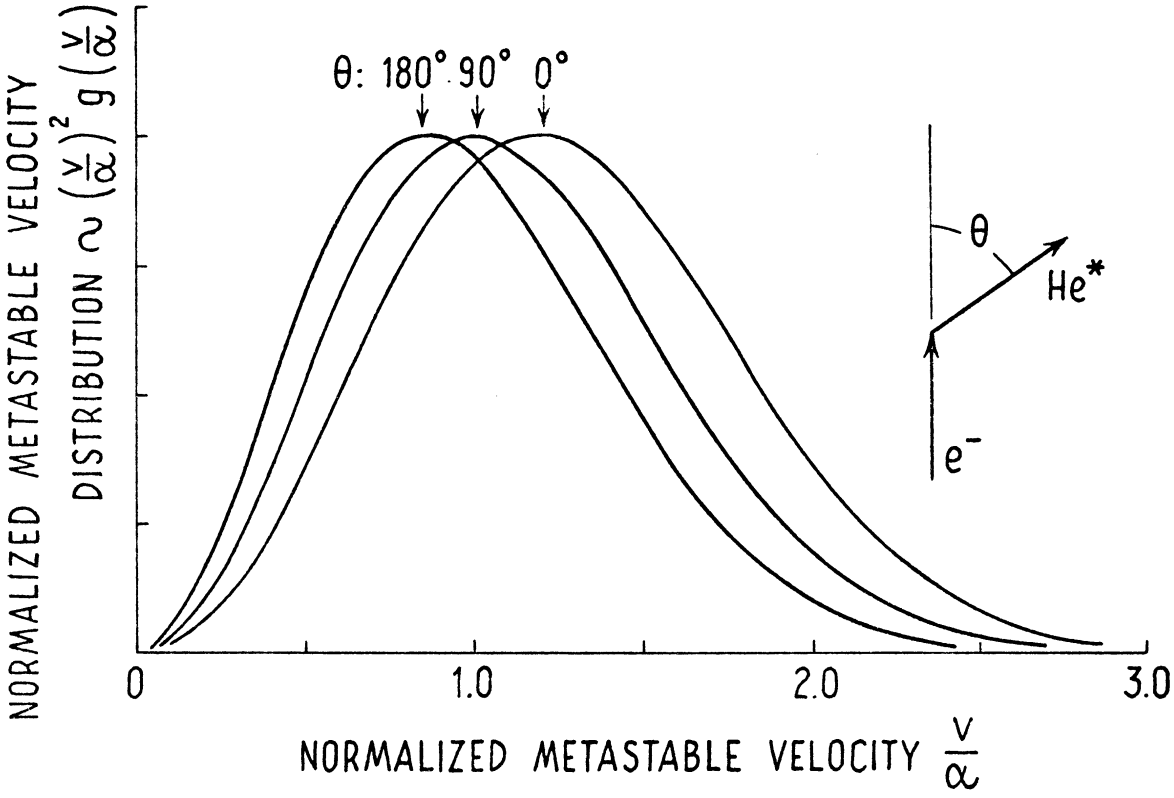

Figure 3.13 Normalized velocity distributions for 2^3S helium; detector angle Θ is parameter. Arrows indicate peak positions. The Maxwellian ground state gas is assumed to enter the electron beam diffusely; the electrons are assumed to have threshold energy.

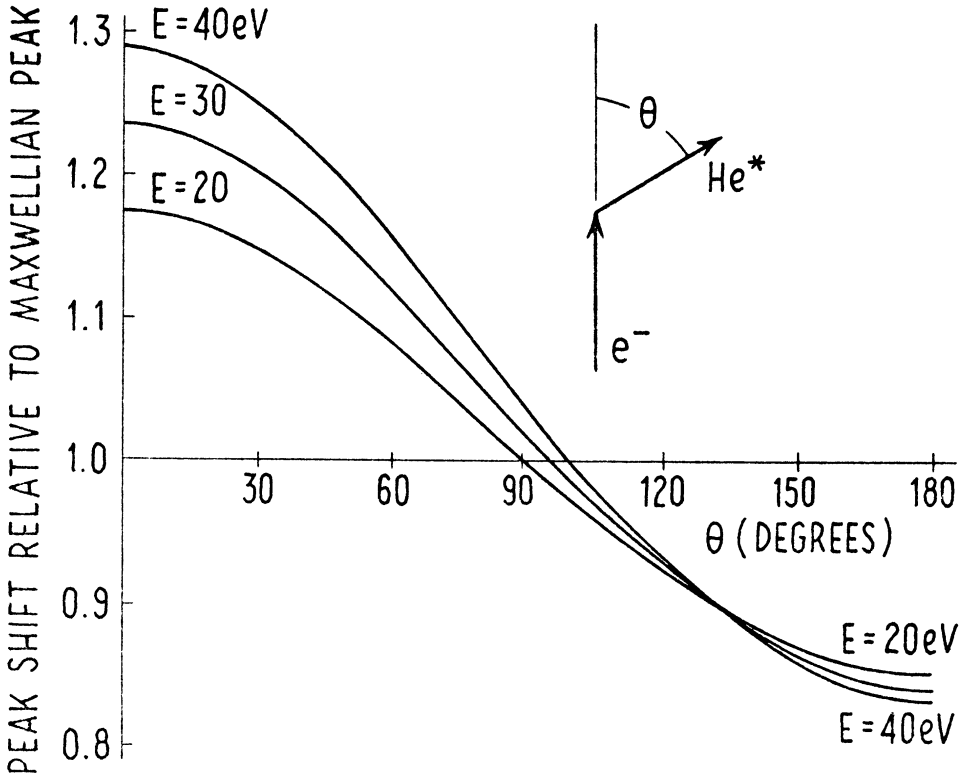

Figure 3.14 Peak shift of 2^3S helium velocity distributions relative to peak of Maxwellian distribution; electron energy E is parameter. The Maxwellian ground state gas is assumed to enter the electron beam diffusely.

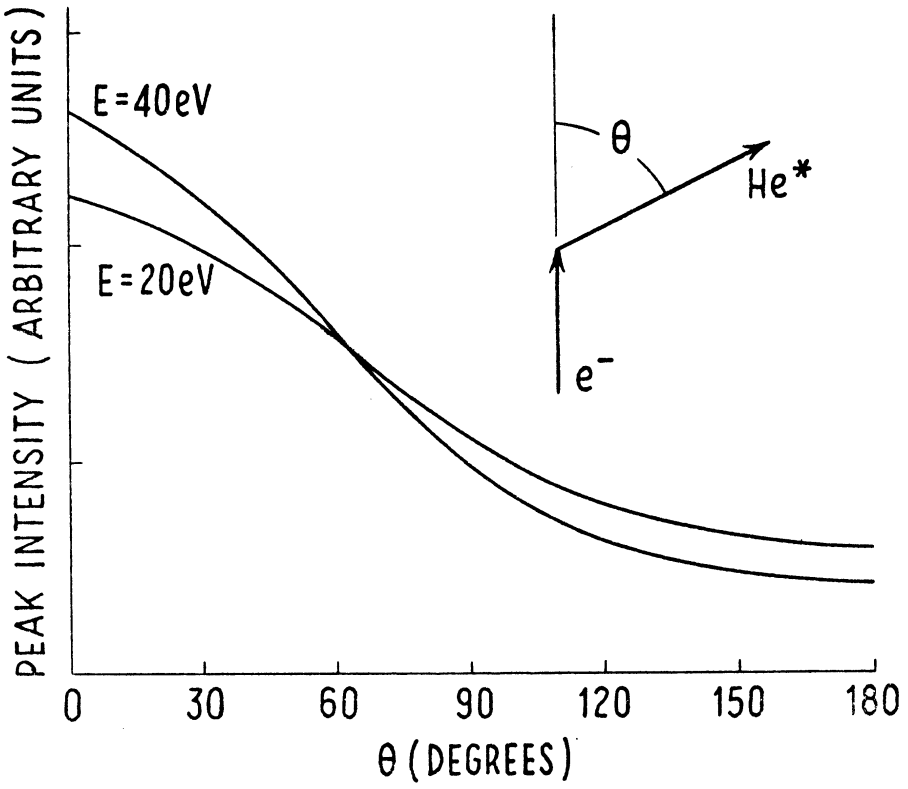

Figure 3.15 Variation of peak intensity of 2^{3}S helium velocity distributions with detector angle Θ; electron energy E is parameter. The Maxwellian ground state gas *is assumed to enter* the electron beam diffusely.

CHAPTER 4

THE RELATIONSHIP BETWEEN VELOCITY DISTRIBUTIONS AND TIME-OF-FLIGHT SPECTRA

Frequently in atomic physics, and in the measurements made for the present work in particular, velocity distributions are measured by means of time-of-flight techniques. However, it is known that systematic effects in time-of-flight systems can complicate the analysis of such data (Zorn, 1967; Alcalay, 1969). Consequently, a simplified analysis of the relation between velocity distributions and their corresponding time-of-flight spectra is presented below.

Given a beam of neutral atoms with arbitrary velocity distribution function and a burst of electrons for excitation, the present problem is to determine the flux of metastable atoms at a downstream detector as a function of time. The assessment of effects due to the duration of the electron pulse and to the finite extent of the excitation region is of particular interest here.

The problem stated above can be broken into two parts: the determination of the metastable velocity distribution function given the distribution function of the ground state

beam; and the determination of the metastable flux at the detector given the metastable velocity distribution function. The first of these problems has been treated in Chapter 3; the second will be discussed below.

The analysis is based on the following assumptions:

i) The metastable lifetime is infinite (no metastables decay while travelling from the electron gun to the detector);

ii) The fraction of the neutral beam which is metastabilized is negligible (the neutral particle density is constant over the region of excitation);

iii) The electron density is uniform over the cross-section of the electron beam;

iv) The electron pulse is rectangular in time (zero rise and fall times; constant intensity over an interval T).

These assumptions, along with certain reasonable physical requirements, lead to a simple relation between the detected metastable flux and the velocity distribution of the metastable atoms. The geometry to be considered for the analysis is shown in Figure 4.1.

If the metastable atoms were all produced instantaneously in a volume of negligible dimensions, then the resulting time-of-flight distribution could be determined from the dispersion of the "packet" of metastable atoms as follows. Let the detector be located a distance L from the ex-

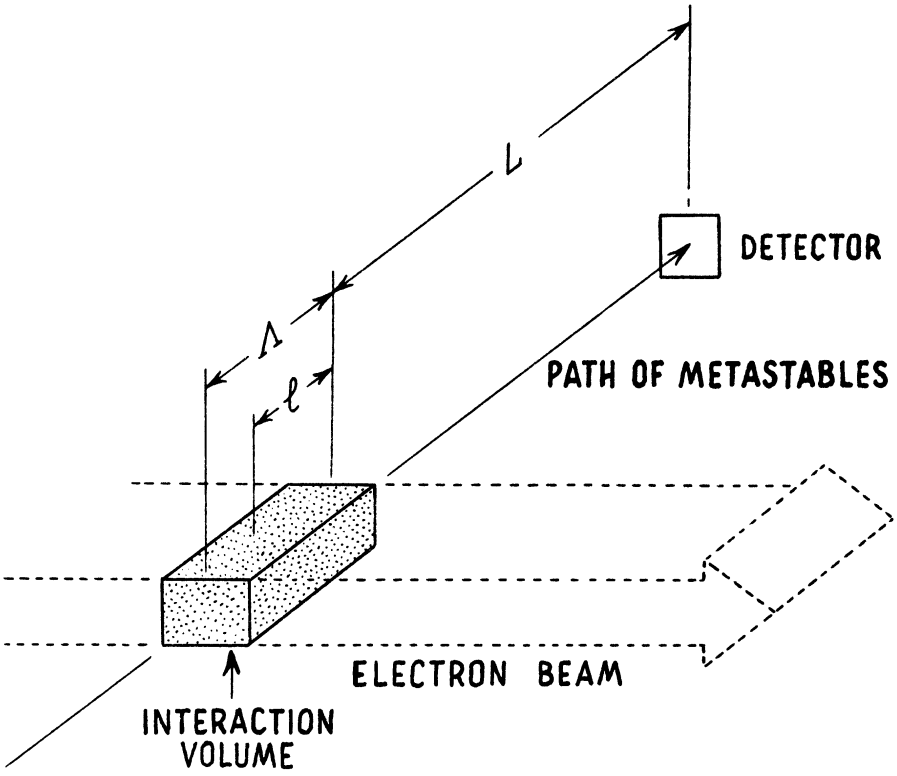

Figure 4.1 Simplified beam geometry for time-of-flight calculations.

citation region; the transit time t to the detector for a metastable with speed v is then

$$t = \frac{L}{v} \tag{4.1}$$

Due to spatial dispersion, metastables having speeds within dv of v will strike the detector over a time increment of magnitude

$$dt = \frac{L}{v^2}\, dv \tag{4.2}$$

so that

$$dv = \frac{L}{t^2}\, dt \tag{4.3}$$

Let the velocity distribution of the metastables be $v^2 g(v)$. Then $v^2 g(v) dv$ metastables will strike the detector within the indicated time interval; using Equation 4.3 this can be written

$$v^2 g(v) dv = \frac{L^3}{t^4}\, g\left(\frac{L}{t}\right) dt \tag{4.4}$$

The coefficient of the time increment dt on the right side of this expression represents the rate at which metastables strike the detector at time t

$$R^*(L,t) = \frac{L^3}{t^4}\, g\left(\frac{L}{t}\right) \tag{4.5}$$

This states that, in the limit of small interaction volume and short pulse duration, the metastable flux at the detector differs from g only by a factor proportional to t^{-4}.

Transforming the metastable velocity distributions of Figure 3.1 as indicated in Equation 4.5 yields the time-of-flight distributions shown in Figure 4.2.

In an actual experiment, the interaction volume is of finite size (characterized by the electron beam width Λ), and the electron gun pulse is of finite duration (T). While these effects do not alter the form of $g(\bar{v})$, (see Section 6.1), they do change the time-of-flight distribution because the metastables are no longer all created at the same instant and because different metastables must travel different distances to the detector. To account for these effects, Equation 4.5 for the metastable flux must be integrated over both the width, Λ, of the electron beam and over the duration, T, of the electron pulse. Before carrying out this general program it is of interest to see what effect each of these factors has on time-of-flight distributions individually.

First consider an electron beam of width Λ which is pulsed instantaneously. Let the coordinate describing a lateral position in the electron beam be ℓ (see Figure 4.1), and suppose that this is measured from the edge of the beam at which the metastables leave; let ℓ be taken in a positive sense if it is measured opposite to the motion of the metastables. Then the distance a metastable created at ℓ must travel to reach the detector is $L+\ell$, where $0 < \ell < \Lambda$. Introducing this path length into Equation 4.5, normalizing with respect to the beam width, and integrating over the width of

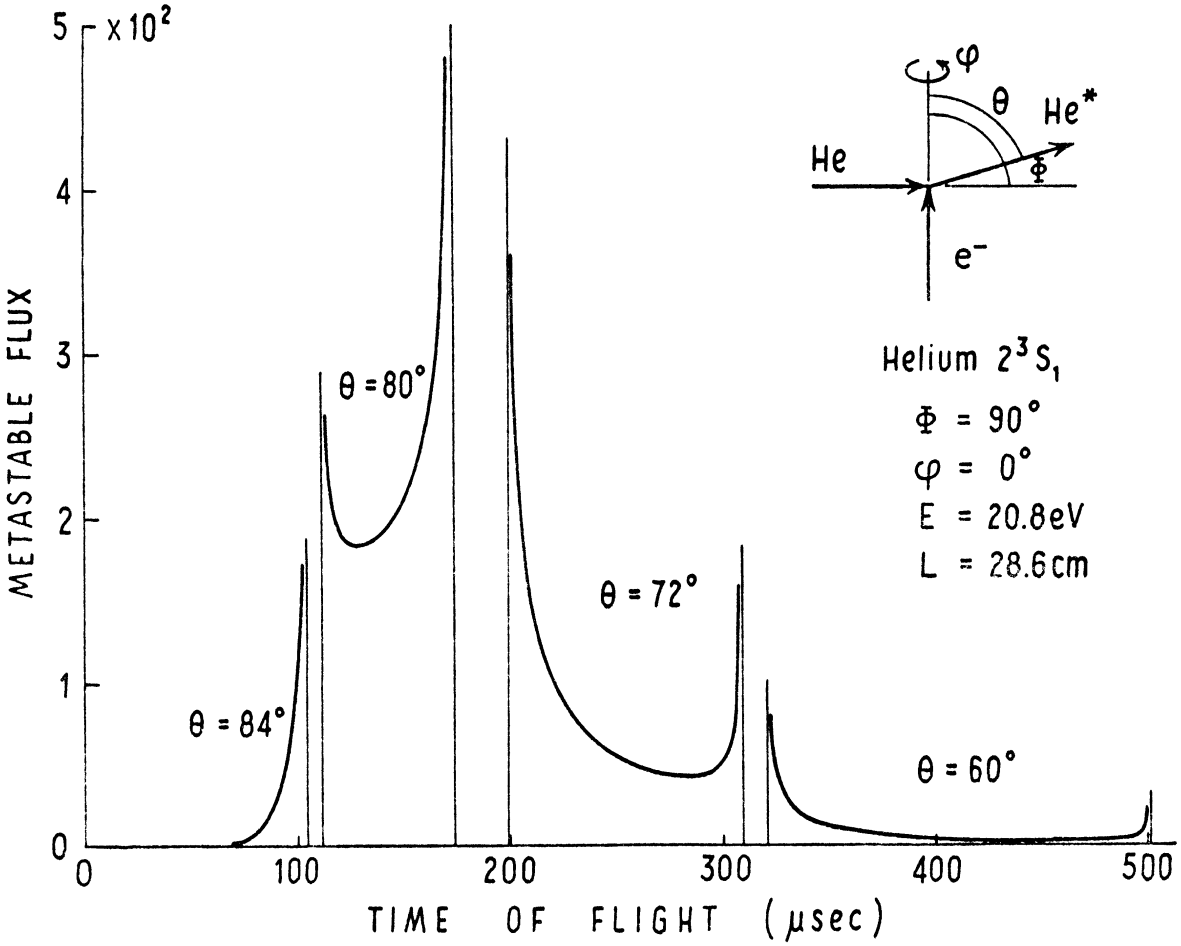

Figure 4.2 Time-of-flight spectra corresponding to the velocity distributions of Figure 3.1. It is assumed that the electron beam is of zero thickness and that the pulse is instantaneous. The ground state beam is assumed to be perfectly collimated and to have a Maxwellian velocity distribution.

the beam gives

$$R^*(L,t;\Lambda,0) = \int_0^{\Lambda} \frac{dl}{\Lambda} \frac{(L+l)^3}{t^4} g\left(\frac{L+l}{t}\right) \tag{4.6}$$

where the zero in the argument of R^* indicates that $T = 0$. Introducing a new variable of integration defined by

$$v = \frac{L+l}{t} \tag{4.7}$$

allows Equation 4.6 to be reduced to

$$R^*(L,t;\Lambda,0) = \frac{1}{\Lambda} \int_{\frac{L}{t}}^{\frac{L+l}{t}} dv\, v^3 g(v) \tag{4.8}$$

This expression can be used to determine the effect that finite Λ will have on time-of-flight spectra corresponding to velocity distributions such as those in Figure 3.1.

The salient features of the actual distributions are the sharp cutoffs and the singularities. The quantity responsible for the singularities is the radical in the denominator of $g(\bar{v})$ (see Equation 3.3 or III.9); to within a factor which is inessential for the present discussion, this radical can be written in the simple form $\sqrt{v_\Delta^2-(v-v_c)^2}$, where v_c and v_Δ are respectively the average speed and the halfwidth of the distribution

$$\left.\begin{aligned} v_c &= \frac{v_+ + v_-}{2} \\ v_\Delta &= \frac{v_+ - v_-}{2} \end{aligned}\right\} \tag{4.9}$$

The function in the numerator of Equation 3.3 (or III. 9) is relatively smoothly varying, and does not affect the character of the distribution drastically if the energy of the incident electrons is near threshold. For this reason, and because it greatly simplifies the integration of Equation 4.8 without losing any of the essential features of $g(\bar{v})$, it is convenient to replace the numerator of the actual distribution by the function $\frac{1}{v^2}$; this leads to the following qualitatively accurate but simple model of the metastable distribution function

$$g(v) = \begin{cases} \dfrac{1}{v^2\sqrt{v_\Delta^2 - (v-v_c)^2}} & v_c - v_\Delta < v < v_c + v_\Delta \\ 0 & \text{otherwise} \end{cases} \qquad (4.10)$$

Integrating Equation Equation 4.8 using this distribution leads to an expression of the form

$$R^*(L,t;\Lambda,0) = \frac{1}{\Lambda}\left[v_c \sin^{-1}\left(\frac{v-v_c}{v_\Delta}\right) - \sqrt{v_\Delta^2-(v-v_c)^2}\right]_{v^-(L,t;\Lambda)}^{v^+(L,t;\Lambda)} \qquad (4.11)$$

Here the limits $v^\pm$ are the boundaries of the interval common to the intervals $\frac{L}{t} < v < \frac{L+\Lambda}{t}$ and $v_c - v_\Delta < v < v_c + v_\Delta$ (the six possible cases which result are illustrated in Figure 4.3).

To study the behavior of Equation 4.11 for conditions similar to those of the experiment to be discussed in Chapter 5, the following parameters are chosen

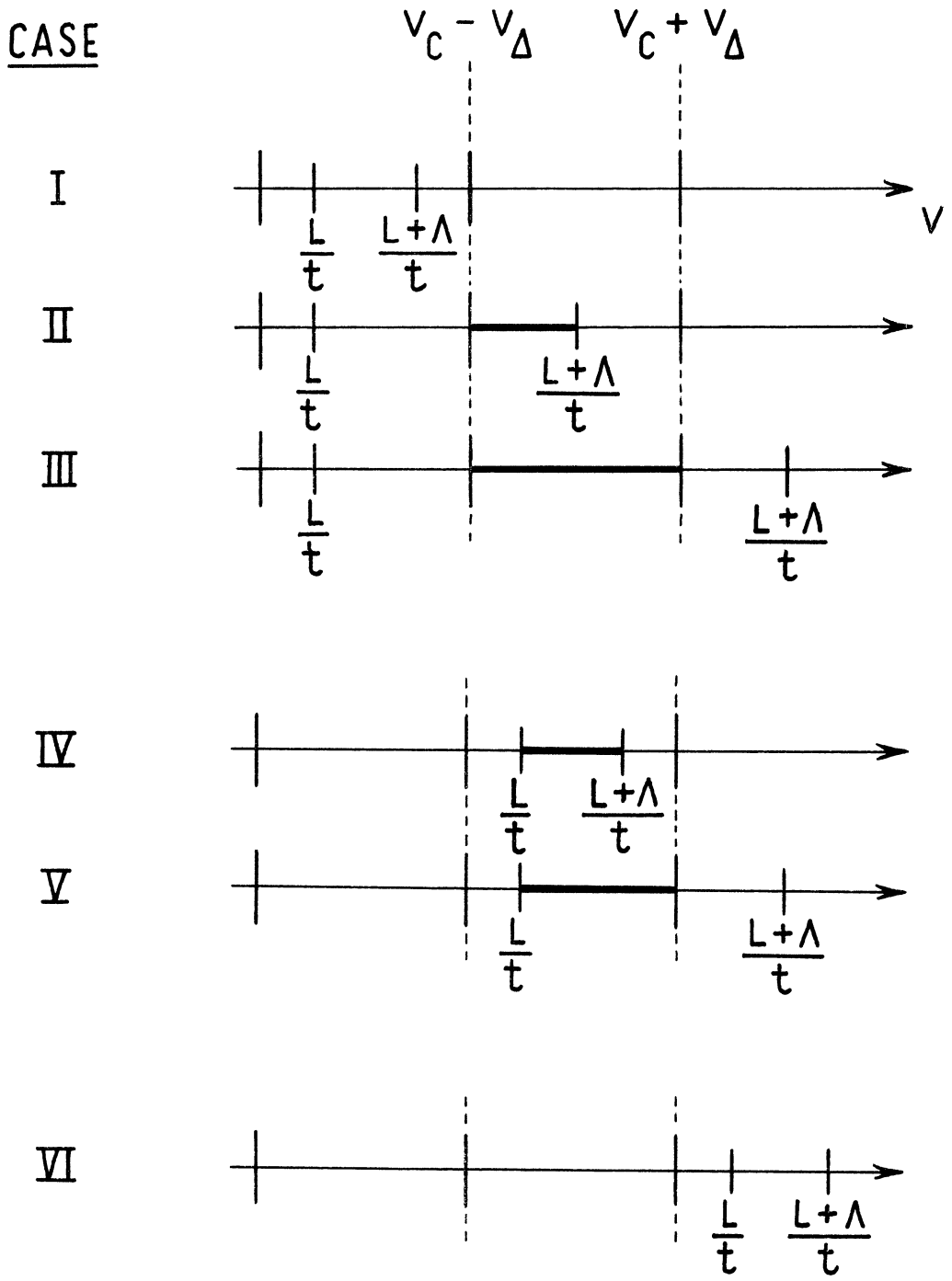

Figure 4.3 Range of integration for time-of-flight integral, accounting for finite beam width, Λ. The appropriate range, indicated by the heavily shaded portion of the axis, is the interval common to the intervals $\frac{L}{t} < v < \frac{L+\Lambda}{t}$ and $v_c - v_\Delta < v < v_c + v_\Delta$.

$$\left.\begin{aligned} v_c &= 1.359 \times 10^5 \text{ cm/sec} \\ v_\Delta &= .620 \times 10^5 \text{ cm/sec} \\ L &= 28.6 \text{ cm} \end{aligned}\right\} \qquad (4.12)$$

The quantities v_c and v_Δ correspond to the predicted parameters for a 2^3S helium beam described by $\Phi = 90^\circ$, $\varphi = 0^\circ$, $\Theta = 72^\circ$, E = 25 eV and a gas temperature of 300° K. The distortion of the model helium time-of-flight distribution due to finite electron beam width Λ (assuming the electron pulse duration to be negligible: T = 0) is illustrated in Figure 4.4.

Consider next the other limiting case of vanishing beam width ($\Lambda = 0$) and finite pulse duration T. Let the time τ at which a metastable is created be measured from the instant the electron beam is turned on; then the time it takes a metastable created at τ to reach the detector is $t - \tau$, where $0 < \tau < T$. Inclusion of this effect in Equation 4.5 leads to the following expression for the metastable flux at the detector

$$R^*(L,t;0,T) = \int_0^T \frac{d\tau}{T} \frac{L^3}{(t-\tau)^4} g\left(\frac{L}{t-\tau}\right) \qquad t > T$$

$$= \frac{1}{T} \int_{\frac{L}{t}}^{\frac{L}{t-T}} dv\, v^2 g(v) \qquad t > T \qquad (4.13)$$

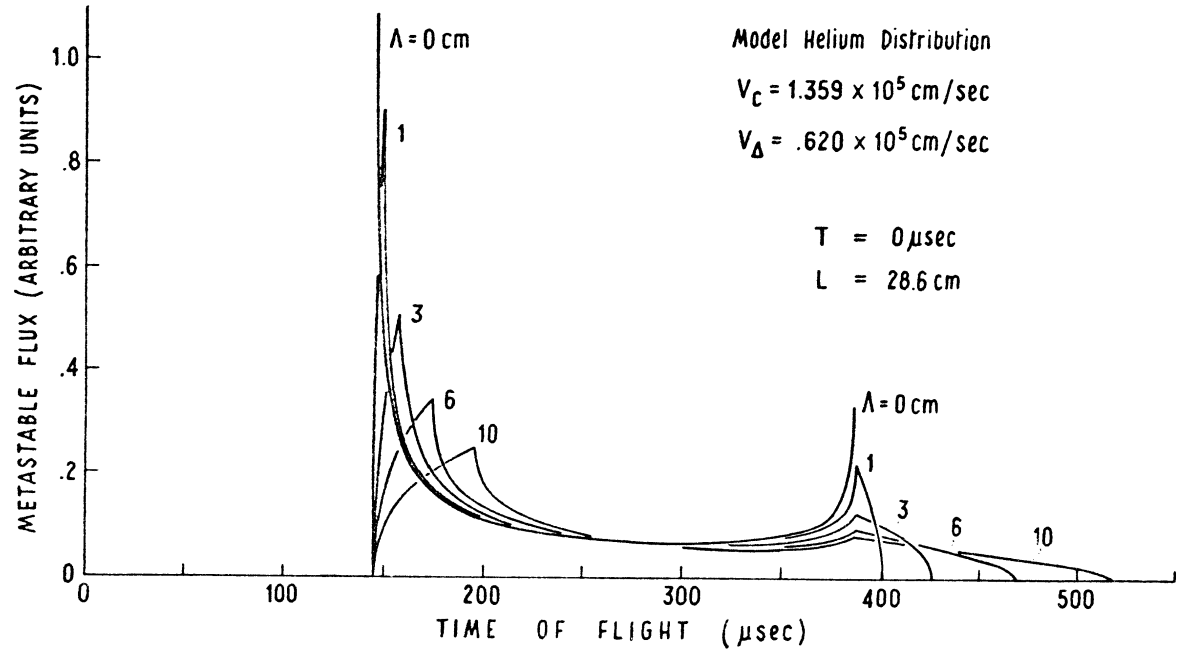

Figure 4.4 Time-of-flight spectra for model metastable helium velocity distribution, showing effects of finite electron beam width, Λ.

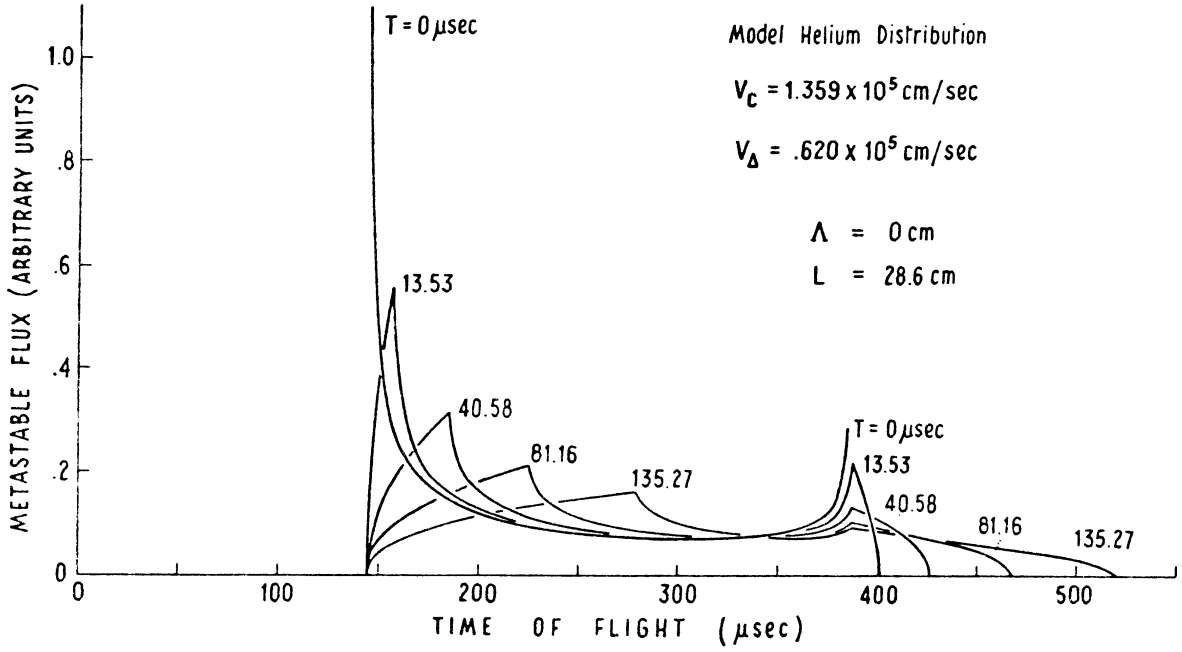

Figure 4.5 Time-of-flight spectra for model metastable helium velocity distribution, showing effects of finite duration, T, of electron pulse. Values of T are related to the values of Λ in Figure 4.4 in accordance with Equation 4.15.

which differs in form from Equation 4.8 only in the exponent of v in the integrand.

Inserting the model distribution 4.10 and carrying out the integration leads to the expression

$$R^*(L,t;0,T) = \frac{1}{T} \sin^{-1}\left(\frac{v-v_c}{v_\Delta}\right)\Bigg|_{v^-(L,t;T)}^{v^+(L,t;T)} \qquad t>T \qquad (4.14)$$

The indicated limits, $v^\pm$, are the boundaries of the interval which is common to the intervals $\frac{L}{t} < v < \frac{L}{t-T}$ and $v_c - v_\Delta < v < v_c + v_\Delta$ (the resulting six cases are qualitatively the same as those of Figure 4.3; however, $(L+\Lambda)/t$ is replaced by $L/(t-T)$.

For purposes of illustrating the behavior of Equation 4.14, the parameters given in Equations 4.12 are again used. Time-of-flight distributions for several values of the pulse duration T are shown in Figure 4.5.

Each T of Figure 4.5 is related to one of the Λ's of Figure 4.4 by the expression

$$T = \frac{\Lambda}{v_c - v_\Delta} \qquad (4.15)$$

In this sense, a beam width Λ=1cm in Figure 4.4 is equivalent to a pulse duration T = 13.53 μsec in Figure 4.5. Distributions in the two figures which are related in this way have identical widths. Comparing such related distributions, it is seen that the peak corresponding to the fast side of the velocity distribution is displaced more in the curve

parametrized by T than it is in the curve parametrized by Λ. This is to be expected, since a temporal displacement (the pulse duration, T) is uniform on a time-of-flight scale for all particles, while a spatial displacement (the beam width, Λ) translates into a time-of-flight interval which varies inversely with the velocity of the particles, and is therefore least for the fastest atoms.

The generalization of Equation 4.5 to include both finite Λ and finite T is given by

$$R^*(L,t;\Lambda,T) = \int_0^{\Lambda} \frac{d\ell}{\Lambda} \int_0^{T} \frac{d\tau}{T} \frac{(L+\ell)^3}{(t-\tau)^4} g\left(\frac{L+\ell}{t-\tau}\right) \qquad t>T \qquad (4.16)$$

Introducing the variable

$$v = \frac{L+\ell}{t-\tau} \qquad (4.17)$$

in place of τ, and performing the integration over ℓ leads to the expression

$$\Lambda T R^*(L,t;\Lambda,T) = t\left\{F\left(\frac{L}{t}\right) - F\left(\frac{L+\Lambda}{t}\right)\right\} - (t-T)\left\{F\left(\frac{L}{t-T}\right) - F\left(\frac{L+\Lambda}{t-T}\right)\right\} \qquad t>T \qquad (4.18)$$

where

$$F(x) = \int_x^{\infty} dv\, v^2 (v-x)\, g(v) \qquad (4.19)$$

Here it has been assumed that $g(v)$ has no cutoffs, so that the limits are not dependent on such quantities as $v_c \pm v_\Delta$. Calculated time-of-flight spectra assuming $g(v)$ is Maxwellian (as might occur in the case of a diffuse ground state gas

at $\Theta = 90^{o}$; see Equation 3.11) are shown in Figures 4.6 and 4.7 (note differences in scales on the abscissas of the two figures). Perhaps the most remarkable aspect of these curves is the absence of flattening at the peaks even when the beam width, Λ, or the pulse duration, T, become comparable respectively to the flight path, L, or to the most probable flight time.

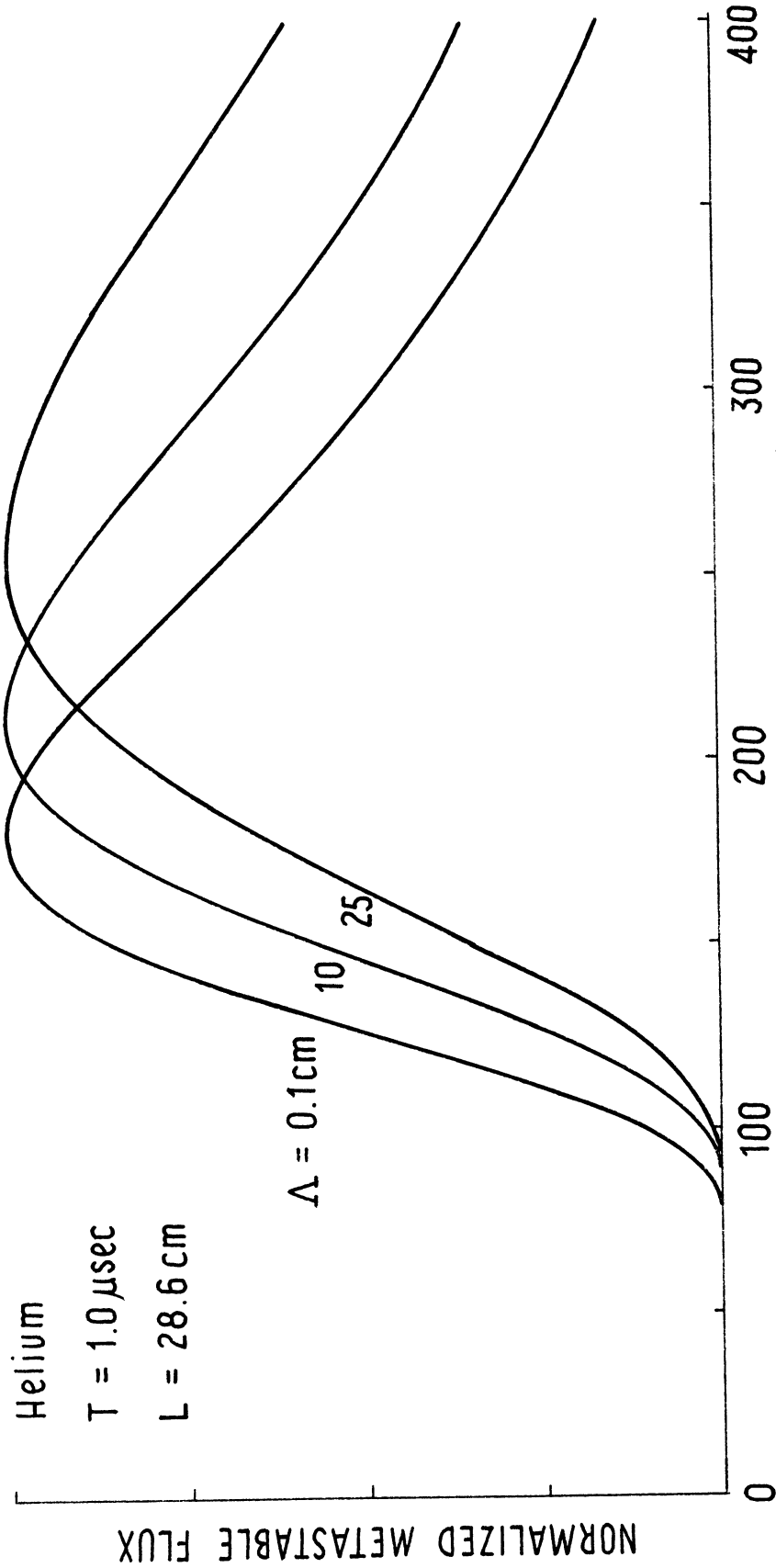

Figure 4.6 Time-of-flight spectra for a Maxwellian metastable beam, showing effect of finite electron beam width, Λ.

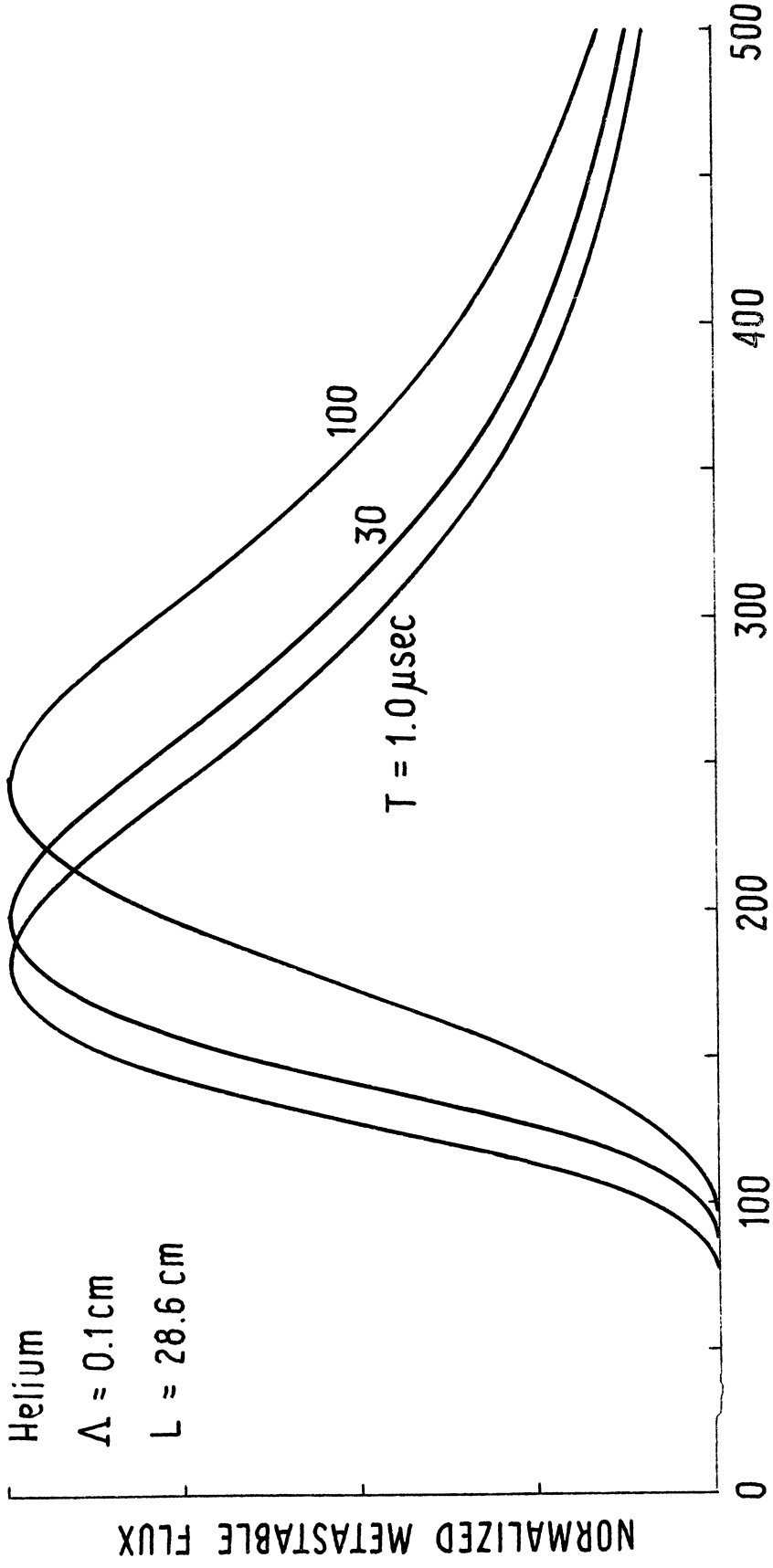

Figure 4.7 Time-of-flight spectra for a Maxwellian metastable beam, showing effect of finite duration, T, of electron pulse.

CHAPTER 5

EXPERIMENTAL INVESTIGATION OF METASTABLE VELOCITY DISTRIBUTIONS

Because the predicted forms for the metastable velocity distributions produced from collimated ground state beams are rather striking, experimental verification of their principal features should not be difficult. A simple time-of-flight experiment suffices for this purpose. Basically, the experiment utilizes a resonably monoenergetic pulsed electron beam to excite ground state atoms to metastable states by electron impact; the rate at which metastables arrive at a detector is recorded, providing time-of-flight spectra which can be compared with theoretical predictions.

5.1 Apparatus

The experiment is conducted within two identical 70 liter chambers. The chambers share a common flange, enabling the system to be differentially pumped. Each chamber contains a liquid nitrogen cold trap and is connected to a 4 inch oil diffusion pump; these pumps exhaust into a common foreline which is connected to a rotary forepump. Base

pressure in the system with liquid nitrogen in the traps is typically 1 x 10^{-7} torr.

The first chamber is used in forming the ground state beam. The gas effuses into the chamber from a copper pipe of 1.6 mm inside diameter, and is collimated by an adjustable slit system in the flange between the two chambers. The path length and slits are typically adjusted to give a divergence of about 3^{o} in the ground state beam (see Figures 5.1 and 5.2); typically, the density in the resulting beam is $\sim 10^{11}$ atoms/cm^3. The gas flow is controlled by a Nupro very fine metering valve which is fed from a glass storage bulb.

The second vacuum chamber contains the electron gun and the detector (see Figure 5.1). The electron gun is a simple three element device, utilizing a directly heated thoriated tungsten ribbon cathode, an accelerating grid of tungsten mesh, and a stainless steel anode. The cathode is heated by a direct current of 4 to 6 amperes at about as many volts. With 20 volts applied to the grid-plate combination, the electron current through the interaction volume defined by the electron and ground state atom beams is about 100 microamperes; it is estimated that the electron energy spread over this region is between 0.5 and 1.0 eV.

The detector is a Bendix "Channeltron" continuous dynode electron multiplier (Donnelly, 1969; see Appendix V). Ultraviolet photons or metastable atoms striking the cathode eject electrons by photoelectric and Auger processes, re-

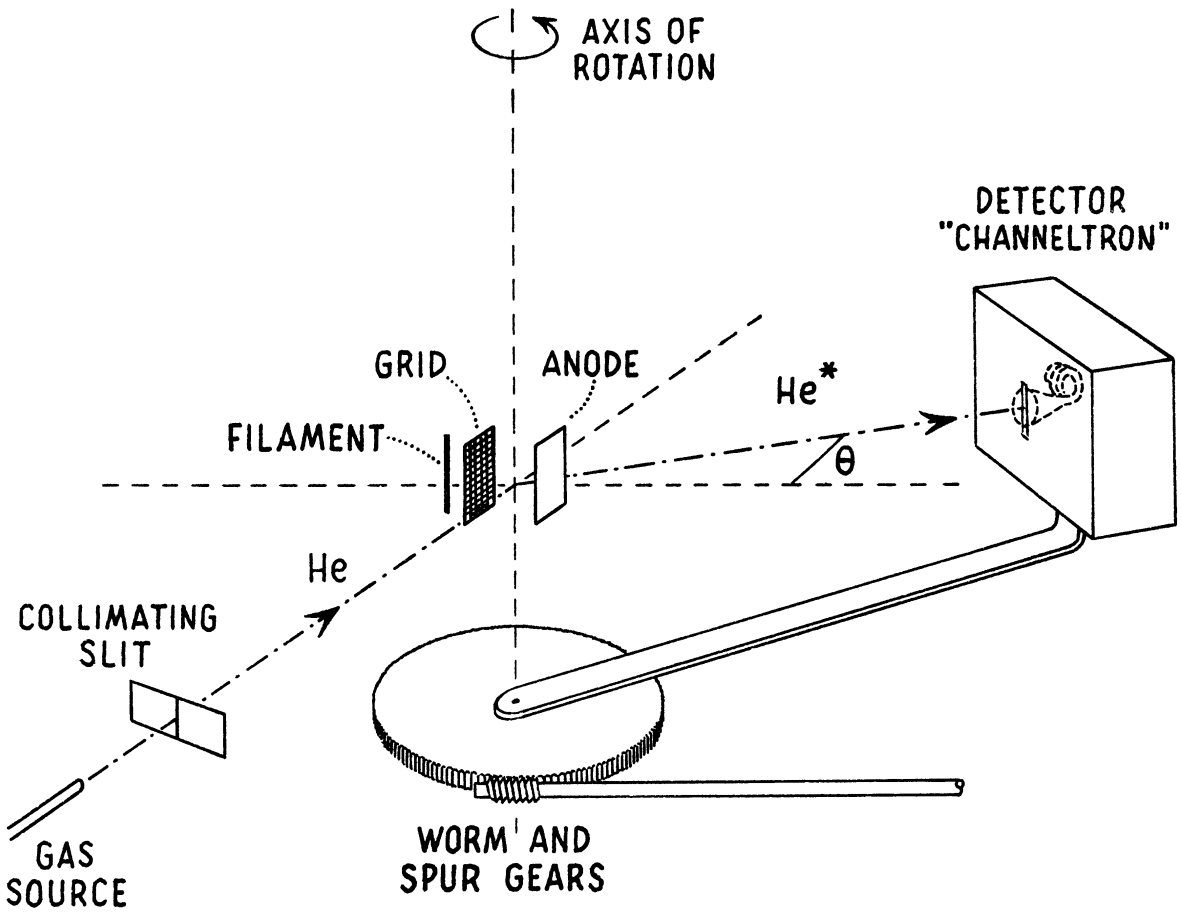

Figure 5.1 Pictorial representation of experiment for measurement of metastable velocity distributions.

spectively, with an efficiency of a few per cent. To reduce background counts arising from free electrons or ions produced in the electron gun, the detector is enclosed in an aluminun box composed of three electrically isolated sections. The first section is positively biased to repel ions; the second, located between the first section and the cathode of the electron multiplier, is biased negatively to repel electrons; the remainder of the box is grounded. The biased portions of the box have aligned 6.3 mm slits, which in combination with the beam-detector separation of 28.6 cm, give a detector width of approximately 8 minutes of arc. The entire detector assembly is mounted on a radial arm, enabling it to be rotated about the interaction region in the plane defined by the incident electron and atom beams; the rotation is controlled by a worm and spur gear combination with a 100-1 turns ratio, the worm being turned by a shaft which passes through the chamber wall via an O-ring seal.

The pulsing of the electron gun and the conditioning of data for storage are performed by the electronics system indicated schematically in Figure 5.2. Data conditioning involves the sorting of pulses from the electron multiplier according to their times of occurrence after initiation of the electron gun pulse; this is accomplished by time-to-pulse-height conversion, as follows. The entire system is controlled by a recurrent pulse generator. The raw data

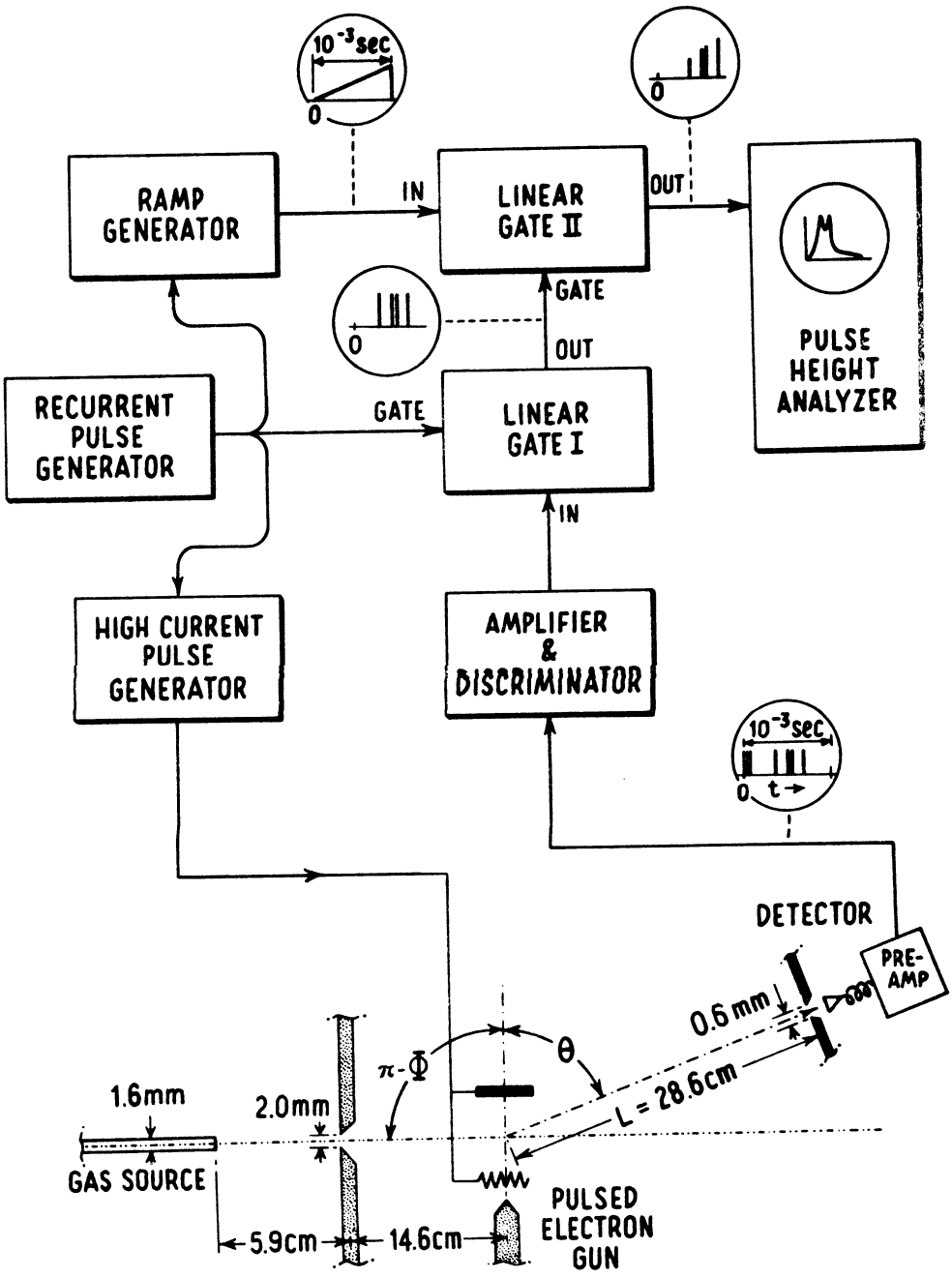

Figure 5.2 Functional diagram of the apparatus used for time-of-flight measurements.

pulses pass through a preamplifier, an amplifier and a discriminator to the input of a linear gate (I). The linear gate is operated in the anticoincidence mode, the gate input being a pulse which is synchronized with the electron gun current pulse. This gate eliminates pulses from the spectrum which correspond to the arrival of ultraviolet photons at the detector (these photons arise from the rapid decay of non-metastable states excited by the electron bombardment). The remaining pulses are used to gate the second linear gate (II). This is operated in a coincidence mode, the input being a linear ramp voltage which is initiated by the start of the electron gun pulse. The output of the second linear gate is then a series of pulses, each having an amplitude proportional to the time interval between the firing of the electron gun and the arrival of the corresponding metastable at the detector. After further shaping, these pulses are stored in a Nuclear Data series 1100 multichannel analyzer.

5.2 Results

Helium was chosen as the test gas because its small mass and high excitation energy lead to a relatively large angular spreading of the metastable "beam" (see Sections 3.1 and 3.2). The experiment outlined in Section 5.1 was performed using the following parameters:

Electron pulse duration	$T = 3\,\mu$sec
Width of electron beam	$\Lambda = 0.5$ cm

Path length from interaction region to detector	$L = 28.6$ cm
Pulse repetition rate	1600/sec
Number of analyzer channels	128
Nominal angle between ground state and electron beams	$\Phi = 90^\circ$
Divergence of ground state beam	$\Delta\Phi = 3^\circ$
Angular width of detector	$\Delta\Theta = 0^\circ 8'$

The background pressure during the experiment was generally less than 2×10^{-7} torr.

Sample time-of-flight data for the 2^3S metastable state of helium are shown as points in Figure 5.3 (these results have been published: see Pearl (1969), included as Appendix VI). The solid curves represent theoretical predictions based on the results of Chapters 3 and 4. Curves a assume perfect collimation of the ground state beam; curves b allow for a 3° divergence in the beam. Curve c shows how the distribution would appear if the metastable velocity distribution were the same as the assumed Maxwellian velocity distribution in the ground state beam.

Although the fits are by no means perfect, the salient features of the predictions are experimentally established. These include

i) the narrowness of the distributions

ii) the double peak structure

iii) the sensitivity of the "position" of the distributions to the detector angle Θ.

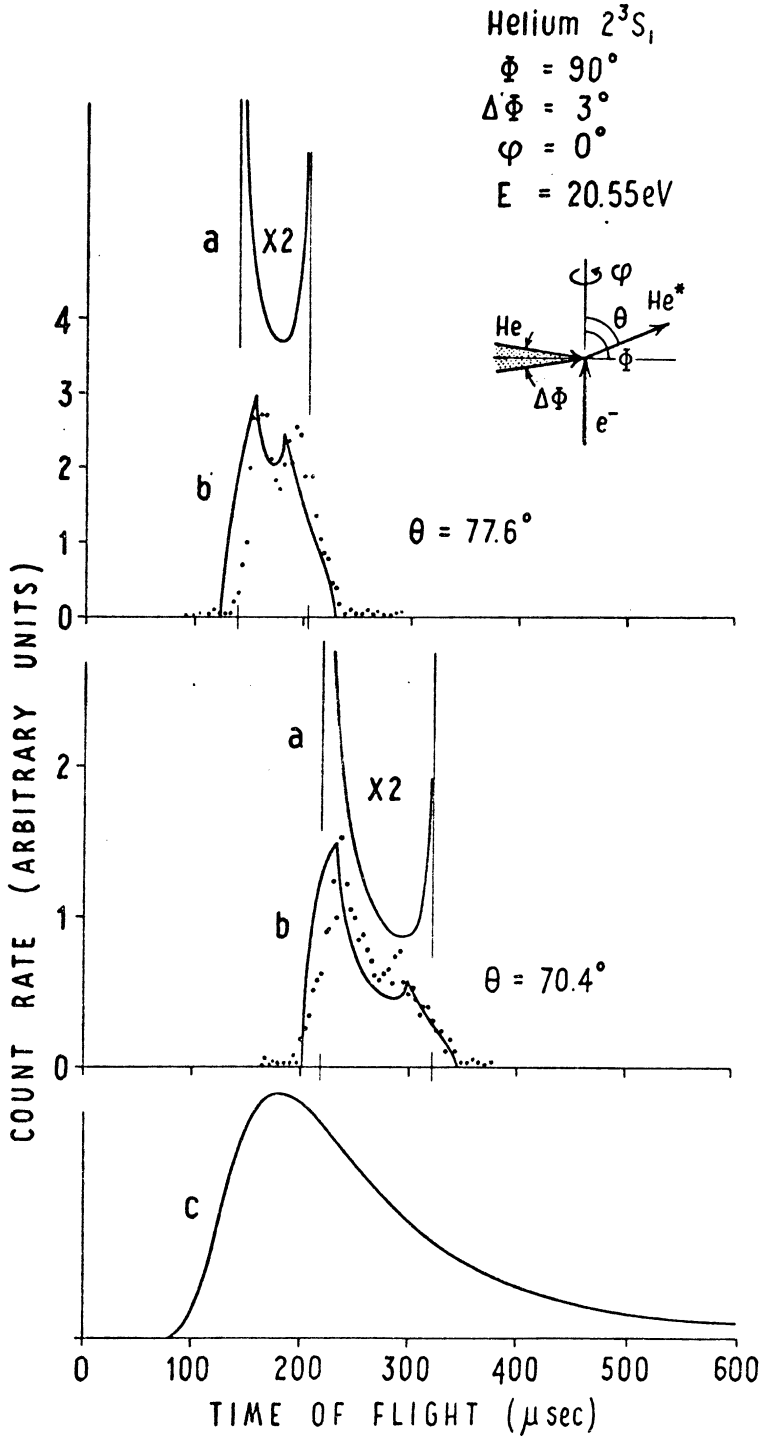

Figure 5.3 Time-of-flight spectra for metastable 2^3S helium. Points represent experimental data. Curves a are theoretical for perfect collimation; curves b are theoretical, accounting for 3° angular divergence in the incoming, ground state beam. Curves a and b are calculated assuming that the electron energy is 0.75 eV above threshold. Curve c is theoretical if recoil effects are neglected, i.e., it represents the spectrum of the full Maxwellian velocity distribution in the ground state beam.

The discrepancies between the data and theoretical curves b in Figure 5.3 are probably due in large part to the following factors. First, the actual energy distribution of the electrons in the electron beam is unknown. A reasonable estimate of the energy spread is ± 0.5 eV; this would tend to widen the distributions. Second, it was not possible to determine, except at $\Theta = 90^{\circ}$, that $\varphi = 0^{\circ}$, i.e., that the detector tracked perfectly in the plane of the incident beams. As indicated in Figures 3.8 and 3.11, non-zero values of φ tend to narrow the distributions. Finally, the resonance structure in the excitation function of 2^3S helium (see Section 6.4) can greatly affect the shape of the velocity distribution.

CHAPTER 6

FURTHER FACTORS AFFECTING METASTABLE VELOCITY DISTRIBUTIONS

The analysis of metastable velocity distributions presented in Chapters 2 and 3 is based on the simplest possible model of an experiment employing a metastable beam. The purpose of this chapter is to discuss the influence on the velocity distribution of several other effects which would play a part in a real experiment.

6.1 Geometrical Effects

Principal among factors to be discussed under this heading are the effects associated with a finite interaction volume. Consider the case of perfectly collimated beams. It is emphasized that if the interaction volume becomes finite, but the unidirectional character of the beams is preserved, there is no alteration in $g(\bar{v})$, a fact which remains true even if the spatial distribution of particles (atoms and electrons) in the beams is nonuniform over the beam cross sections. This is because the metastables produced in each differential volume element are all created under identical kinematic conditions. A measured time-of-

flight spectrum of such metastables, however, may be strongly affected (see, for example, Figure 4.4). This is due to the fact that different metastables travel along different paths (both in length and in direction) to reach the detector. The spatial integration implied to account for this effect will lead to variations in the observed velocity distribution which are qualitatively similar to those indicated in Figures 3.12 and 4.4.

An error in positioning the center of rotation of a movable detector relative to the point of intersection of the electron and ground state beams will result in apparent shifts of the velocity distributions due to transit time effects, and in shifts and distortions due to accompanying errors in angular measurements.

Divergence of the electron beam (or shearing or cyclotron motion, if it is magnetically confined) requires another angular integration. The principal corrections due to such effects will occur for the electrons with the greatest out-of-plane motions, since these have the largest azimuthal angles, φ (compare Figures 3.6 and 3.11).

In the case of diffuse ground state "beams", the interaction region is determined by the shape of the electron beam, e.g., a cylinder. A detector with a fixed viewing angle will therefore see an intensity pattern as a function of Θ which is increased by a factor of $\csc\Theta$ over that shown in Figure 3.16.

6.2 Complications Due to Several Excited States

It is obvious that if two or more (long lived) metastable states of a given atom are excited by electron impact, then the observed total velocity distribution will be a superposition of the distributions due to each state individually. However, it should also be noted that any optical levels which are excited and which can cascade into a given metastable state must also be considered. The treatment of each such state is identical to that for the directly excited metastable levels, since the same kinematic arguments apply; the only change is that the excitation energy of the level in question must be used in the calculations. The influence of recoil due to the photon emitted in the cascade process is negligible.

Figure 6.1 shows two velocity distributions. The solid curve is the distribution which would result from excitation of the helium 2s $^3S_1$ state alone by electrons of energy E = 25 eV (5.2 eV above threshold); the dashed curve represents the distribution which would result from excitation of the 3p $^3P_1^\circ$ state alone (assuming subsequent cascading into the 2s $^3S_1$ level) by electrons of energy E = 28.2 eV (5.2 eV above threshold). The widths of the distributions are identical; the principal difference between them is a slight shift, which is proportional to the square root of the energy of the incident electron (these results follow from the sum and difference of Equations 3.5). Excluding this shift, and assuming the s-wave scattering approximation,

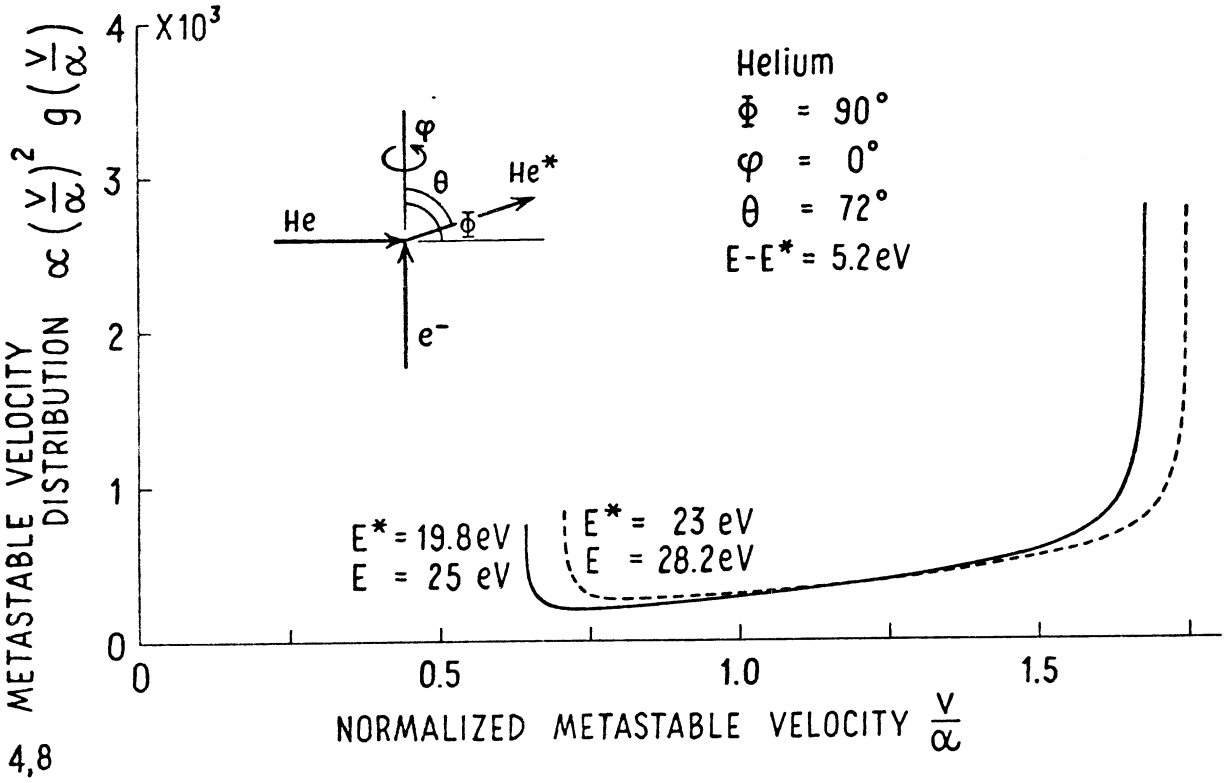

Figure 6.1 Metastable velocity distributions for 2^3S helium. The solid curve is the distribution for direct excitation of the 2s $^3S_1$ level by 25 eV electrons; the dashed curve is the distribution arising from direct excitation of the 3p $^3P_1^\circ$ level followed by cascade to the 2s $^3S_1$ metastable state. The electron energy increment above the respective thresholds is constant. A perfectly collimated Maxwellian ground state beam is assumed.

velocity distributions for two states are qualitatively the same if excited by electrons of a fixed energy above the thresholds of the states (see also Appendix VII).

A converse relation is also useful: if two states are excited by electrons of a single energy, the resulting velocity distributions will be qualitatively the same as distributions arising from the excitation of a single state by electrons of two energies, provided that the energy increments above threshold are made to correspond. The three distributions in Figure 3.2 for the excitation of the helium 2^3S state by electrons of energies 0.2, 1.2, and 5.2 eV above threshold, can therefore be reinterpreted: they are qualitatively the same as the total distribution which would result from the excitation of three states, A, B and C, by electrons of a single energy, provided that the energies of the states are related by $E_B - E_A = 1.0$ eV, $E_C - E_A = 5.0$ eV, and that the incident electrons have energy $E_C + 0.2$ eV (energies taken as positive from the ground state). Consequently, Figure 3.2 qualitatively represents a metastable distribution, considering the lowest level to be metastable, and allowing for cascades from the two higher levels. The effect of cascades, therefore, is to fill up the central region of the distribution arising from the lowest state with the narrower distributions corresponding to the higher levels.

6.3 Spread in Electron Energy

Since the width of the velocity distributions is a strong function of electron energy (see Figure 3.2), a spread of energies in the electron beam should have a marked effect on the observed metastable velocity distribution. Qualitatively, the principal effect should be of washing out the peak structure (see Rubin, 1969).

6.4 Anisotropic Scattering of the Electrons

Throughout this thesis, it has been assumed that the scattering of the electrons in the center of mass system is isotropic. It is known, however, that even for helium s-wave scattering does not occur for more than a few tenths of an electron volt above threshold; in fact, the excitation function for the 2^3S state exhibits s-, p-, and d-wave resonances at 19.95 ± .05, 20.45 ± .05, and 21.00 ± .05 eV respectively, as shown in Figure 6.2 (Ehrhardt, 1967; 1968; Andrick, 1968). The inclusion of such variations in the determination of the metastable velocity distribution function requires that the factor $\frac{d\sigma^*}{d\omega}$ be included in the scattering distribution, Equation 2.24. The same factor evaluated at the appropriate value of $\bar{v}_o$ therefore appears before each of the terms in the integrand of Equation 2.34.

The effects that such terms can have on helium metastable velocity distributions are shown in Figure 6.3. Figure 6.3a shows how the velocity distributions would appear at the energies of the resonances if the scattering were

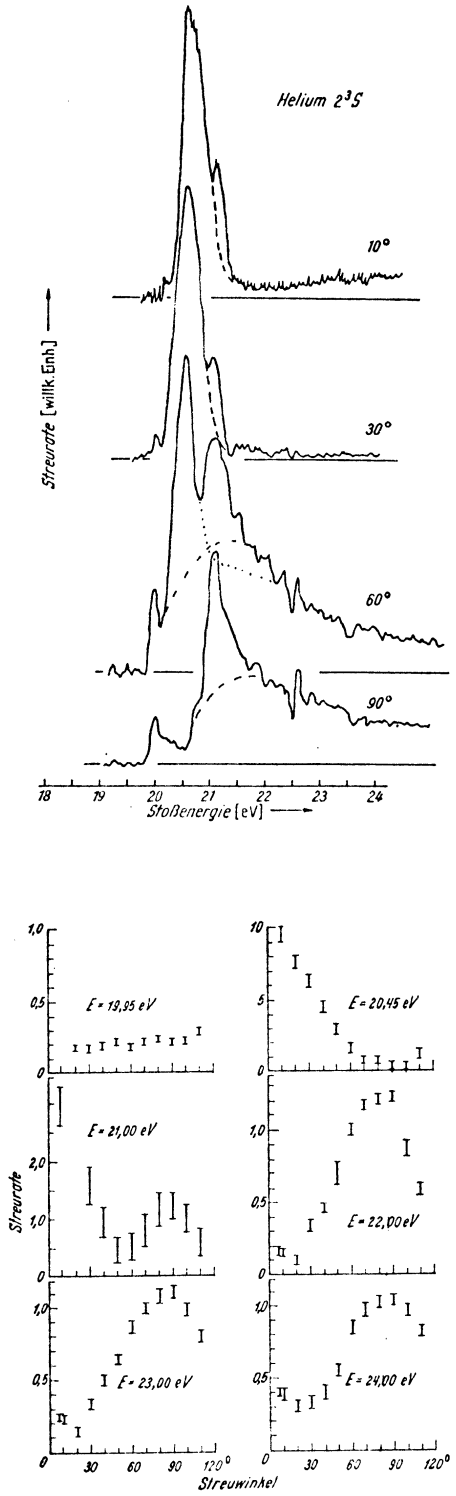

From H. Ehrhardt and K. Willmann, Z. Physik 203, 1 (1967)

Figure 6.2 Energy and angle dependences of 2^3S helium excitation function.

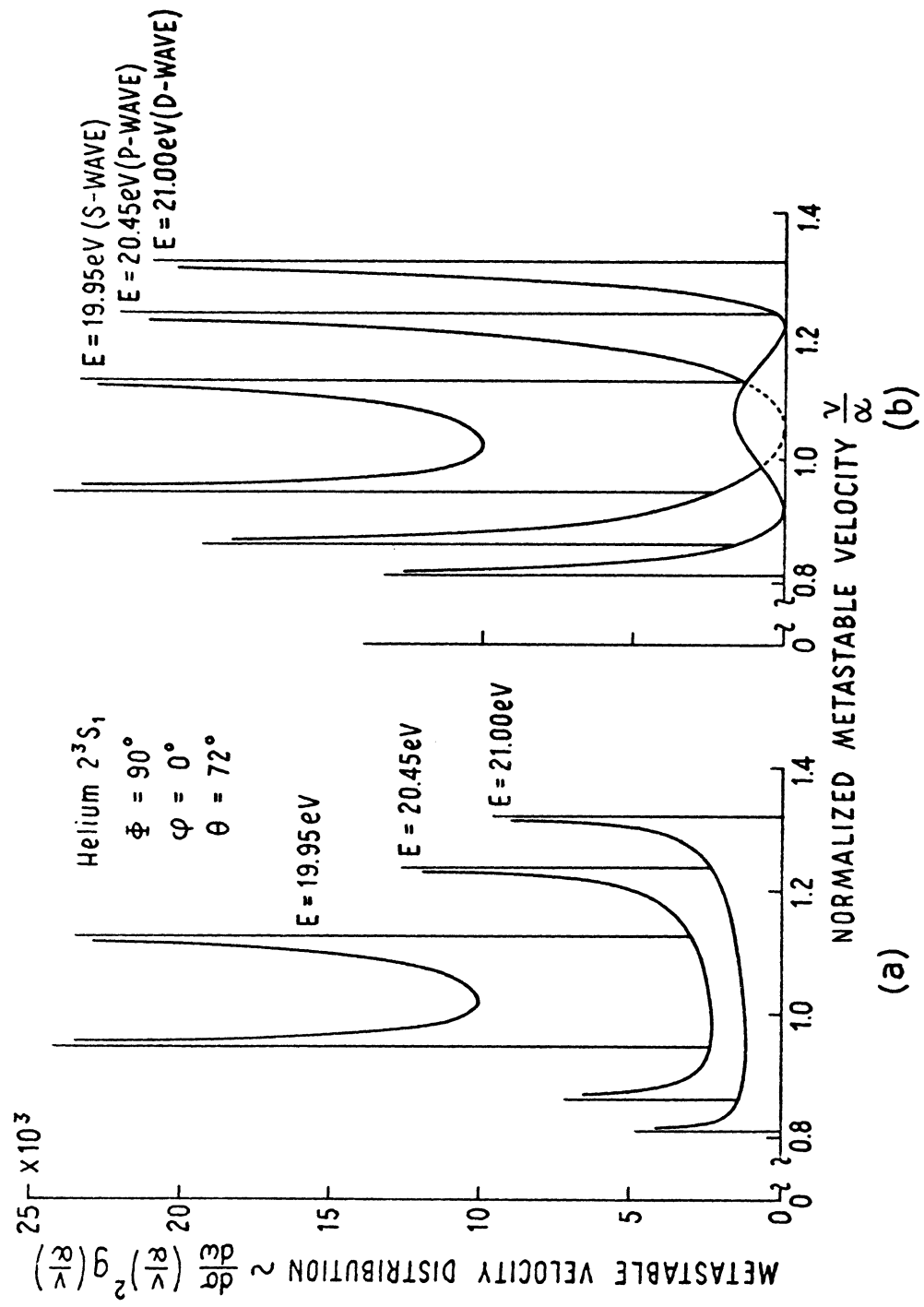

Figure 6.3 Velocity distributions at the 2^3S helium resonances. a: distributions assuming isotropic scattering at all electron energies; b: distributions assuming pure s-, p- and d-wave scattering at the 19.95, 20.45 and 21.00 eV resonances respectively. Perfectly collimated Maxwellian ground state beam assumed.

isotropic in the center-of-mass system; Figure 6.3b shows a more realistic evaluation, assuming that the resonances involve completely pure s-, p- and d-wave scattering of the electrons. Comparison of the resulting p- and d-wave distributions with the corresponding s-wave results shows that the former are characterized by relatively few metastables in the middle of the distributions, and by an excess of them at the extremes.

At very high electron energies, strong forward scattering of the electrons occurs in the center-of-mass system; the first Born approximation provides a description of this behavior. Applying the Born approximation to the forbidden $1s \rightarrow 2s$ transition in hydrogen leads to a very simple expression for the differential scattering cross section. Figure 6.4 shows several calculated velocity distributions for atomic hydrogen, assuming direct excitation to the 2s $^2S_{\frac{1}{2}}$ state. The curves of Figure 6.4a assume isotropic electron scattering; those of Figure 6.4b assume the scattering is described by the first Born approximation. The strong forward scattering of the electrons, with the concomitant small deflections of the metastables, results in a pronounced shift of the metastable velocity distributions to low velocities.

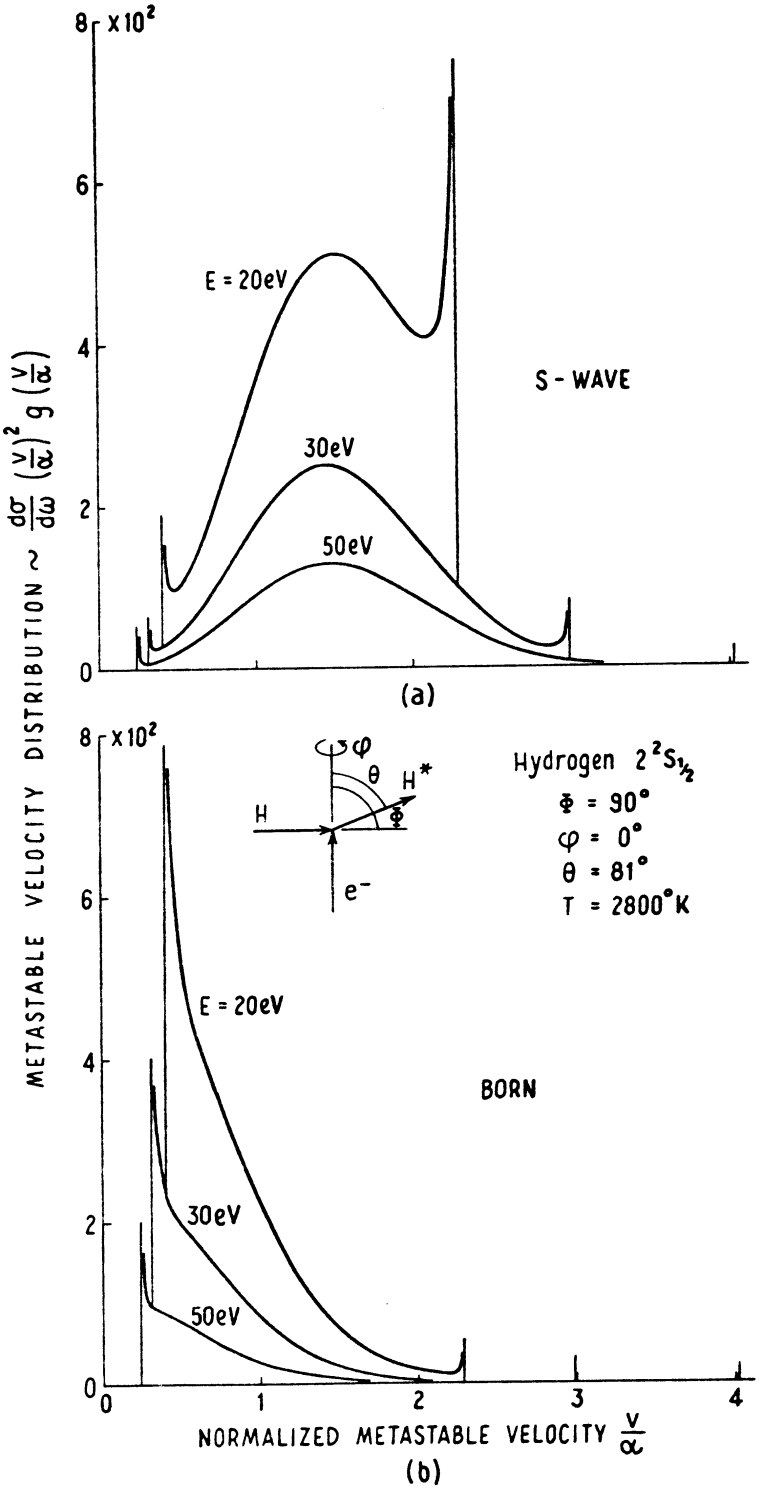

Figure 6.4 Velocity distributions for 2 $^2S_{\frac{1}{2}}$ hydrogen. Ground state beam assumed perfectly collimated and Maxwellian. a: s-wave scattering of electrons assumed; b: scattering assumed to be described by the Born approximation.

CHAPTER 7

APPLICATIONS AND CONCLUSIONS

7.1 Application to Measurements of the Lamb Shift

It has been emphasized by Robiscoe and Shyn (1970) that departures from a Maxwellian velocity distribution in metastable hydrogen beams provide a source of systematic error in several determinations of the Lamb shift. The above authors present results of a measurement of the velocity distribution of metastable hydrogen atoms in the apparatus used for a recent determination of ΔE-S (Shyn, 1969). The deviation from Maxwellian is substantial. Using $U^4 \exp(-U^2)$ as a convenient analytical approximation to the data, Robiscoe and Shyn determined that an upward shift of about 0.04 MHz was indicated in the value of the Lamb shift (1057.86 ± 0.10 MHz (2σ)) previously determined in a level crossing experiment by Robiscoe (1968). The current status of the theory and experiments on the Lamb shift has been summarized by Appelquist and Brodsky (1970).

The theory of Chapters 2 and 3 can be applied to the velocity distribution data of Robiscoe and Shyn. A fit using the program of Appendix IV is shown in Figure 7.1. A comparison of the parameters used for this fit with those quoted by Robiscoe and Shyn is presented in Table 7.I. The

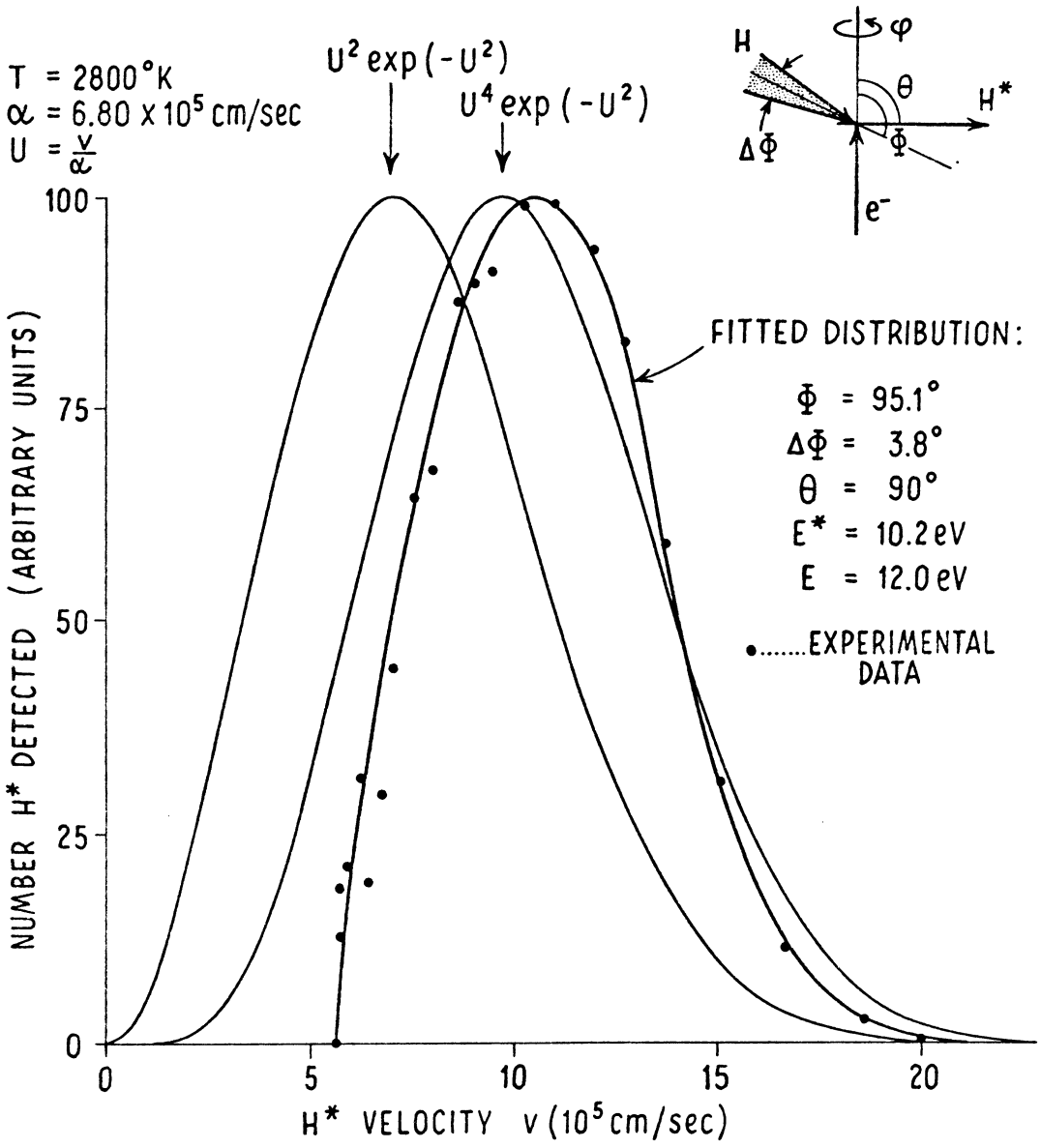

ADAPTED FROM ROBISCOE AND SHYN (1970)

Figure 7.1 Measured velocity distribution and theoretical fit for H(2S) beam. The $U^2\exp(-U^2)$ and $U^4\exp(-U^2)$ distributions are included for comparative purposes.

TABLE 7.I

Comparison of experimentally determined and fitted parameters for the metastable hydrogen velocity distribution from Robiscoe and Shyn (1970)

	E	ΔE	Θ	$\Delta\Theta$	$\Delta\Phi$	Φ
Experimental parameters (Robiscoe, 1970)	11.4 eV	2.9 ± 0.5 eV	90°	0.764°	not measured[1]	$96.3 \pm 0.3^\circ$
Fitted parameters (this work)	10.2 eV	1.8 eV	90°	$\Delta\Theta + \Delta\Phi = 3.8^\circ$		95.1°

[1] T. W. Shyn (private communication) estimates this to be several degrees.

fit is very sensitive to the parameters $\Delta E, \Phi-\Theta$, and $\Delta\Phi+\Delta\Theta$ (see Figures 3.2, 3.1 and 3.12 respectively); the values stated for the fit could only be varied within narrow limits without producing noticeable deviations from the measured velocity distribution. The parameter $\Delta\Phi$ is not included in the data of Robiscoe and Shyn; however, Shyn (private communication) estimates it to be several degrees, which is in qualitative agreement with the measurements made by Rebane (1970) on the same apparatus.

Although the assumptions used for calculating metastable velocity distributions in this thesis differ from those suggested by Robiscoe and Shyn, both works are in agreement that atomic recoil will have a substantial effect on velocity distributions in beams of light metastable atoms.

7.2 Application to H_2 Dissociation Experiment

Leventhal et al. (1967) have investigated the electron impact induced dissociation of molecular hydrogen:

$$H_2 + e^- \rightarrow H(2S) + H + e^- \qquad (7.1)$$

It is possible to learn about the relevant dissociating state of the molecule by studying the intensity and energy distribution of the metastable atoms. It is found that there are two groups of metastables which result from this reaction: one centered at an energy of 0.32 ± 0.05 eV and the other with an energy of 4.7 ± 0.7 eV. In an extension of this experiment, M. Misakian (private communication) has

found that the angular distribution of the "slow" metastables is probably influenced strongly by the kinematics of the electron-molecule collision itself. Using a diffuse source of helium for calibrating the experiment, Misakian has found a strong angular dependence in the scattered intensity of helium metastables. Comparison with the predictions shown in Figure 3.16 shows good agreement only if the factor sin (see Section 6.1) is <u>not</u> included when reducing the data. However, it is possible that the ground state gas distribution is not perfectly isotropic in the electron bombardment region and this may be the cause of the discrepancy.

7.3 Measurement of Differential Excitation Cross Sections

As is well known (Stebbings, 1960; Vriens, 1968; Bederson, 1968), it is possible in principle to use electron-atom recoil kinematics to study the differential cross section for electron impact excitation of metastable states. However, due to various complications, such as the inability to distinguish cascade contributions from those due to direct excitation, the energy analysis of the incoming and outgoing electrons is generally more suitable for this work (Ehrhardt, 1968). Nonetheless, the work of Stebbings et al., in which total intensities of metastable hydrogen atoms were measured as a function of detector angle and electron energy, shows nicely the effects mentioned in Section 3.1.2, as modified by the gradual onset of strong forward scattering of the electrons. Considering their data in the light of Figure

3.5 shows an initial broadening of the maximum (along with a curious shift to lower values of Θ), followed by a strong shift to large Θ accompanied by a decrease in intensity at small angles, in agreement with qualitative expectations of the effect of strong forward scattering.

7.4 Other Possible Applications

It would be both of intrinsic interest and a good check on the calculations to be able to resolve the helium 2^3S resonances (Figure 6.2) by observation of the changes in metastable helium velocity distributions (Figure 6.3). To observe the d-wave resonance, it would be necessary to quench the singlet metastables (Fry, 1969), allowing the triplet metastable to be observed for electron energies above 21 eV (the excitation function for the 2^3P state is a very shallow function of energy near threshold; see Ehrhardt, 1968).

A very useful application of the kinematic effects discussed in this thesis might be as a diagnostic tool for studying ground state gas conditions (French, 1967; Zorn, 1967; Pichlik, 1970). The simple velocity distribution given by Equation 3.9 (or more generally by Equation 3.7) indicates that excitation of gases by electrons of controlled energies might be useful as a temperature probe. Analysis of velocity distributions in streaming gases might also be accomplished. In order to minimize uncertainties in the metastable distributions due to imperfectly known differ-

ential cross section behavior, it might be best to operate at high electron energies where the Born approximation applies; this would have the advantage of increasing counting rates due to cascade contributions, while minimizing the effect of different excitation thresholds. The decrease in total cross section with increasing energy would be detrimental, but simple high current electron guns could be employed to compensate for this.

7.5 Summary and Conclusions

This thesis has been concerned with the determination of the velocity distribution of metastable atoms produced from ground state atoms by electron impact excitation. The analysis, which is based on the transformation of the collision kinematics from a center of mass coordinate system to a laboratory coordinate system, yields the following interesting results.

The velocity distribution of metastable atoms resulting from crossed electron and Maxwellian ground state atom beams is either void or is distinctly non-Maxwellian with the following features:

i) it has two peaks;

ii) it has upper and lower cutoff speeds;

iii) the magnitudes of the cutoff speeds are very sensitive to such factors as beam alignment, detector position, and electron energy;

iv) it is very sensitive to the form of the differential cross section for impact excitation.

Consideration of a diffuse Maxwellian ground state gas which contains an electron beam shows that the velocity distribution of the resulting metastables is still generally non-Maxwellian, although the double humped property is absent. The form of the distribution which is observed is still a fairly sensitive function of detector orientation, but the sensitivity to electron energy is relatively less than in the case of collimated beams.

In many experiments utilizing beams of metastable atoms, the present results are relevant as a possible source of systematic error. In addition, the sensitivity of the velocity distributions to various parameters of the beams of ground state atoms and electrons suggests that metastablization by electron impact can be used to monitor kinetic properties of the ground state gas.

APPENDIX I

ELEMENTARY KINEMATICS OF AN ELECTRON-ATOM COLLISION

The object of this appendix is to show by straightforward algebra that the velocities, $\bar{v}$, of metastables formed from ground state atoms with a single velocity, $\bar{v}_o$, must terminate on a sphere in velocity space and conversely, i.e., that metastables with a given velocity are produced from ground state atoms with velocities terminating on a sphere. Considering the former case, the normalized laws of conservation of momentum and energy may be written respectively as:

$$\bar{v} + \mu\bar{u} = \bar{v}_o + \mu\bar{u}_o \triangleq \bar{B}_o \qquad (I.1)$$

$$v^2 + \mu u^2 = v_o^2 + \mu u_o^2 - \frac{2E}{M} \triangleq A_o \qquad (I.2)$$

By assumption $\bar{v}_o$ and $\bar{u}_o$ are known, so that the quantities on the right are known also. Solving Equation I.1 for $\mu\bar{u}$ and squaring yields

$$\mu^2 u^2 = (\bar{B}_o - \bar{v})^2 \qquad (I.3)$$

Multiplying Equation I.2 by μ and substituting Equation I.3 gives

$$(1+\mu)v^2 - 2\bar{B}_o \cdot \bar{v} + B_o^2 - \mu A_o = 0 \qquad (I.4)$$

Taking $\bar{B}_0$ as the polar axis of a spherical coordinate system, so that $\bar{B}_0 \cdot \bar{v} = B_0 v_z$ allows Equation I.4 to be reduced to

$$v_x^2 + v_y^2 + \left(v_z - \frac{B_0}{1+\mu}\right)^2 = \frac{\mu}{(1+\mu)^2}\left[(1+\mu)A_0 - B_0^2\right] \qquad (I.5)$$

This equation, involving the components of the velocity, $\bar{v}$, of the metastable, is that of a sphere. Furthermore, since $\bar{B}_0 = (1+\mu)\bar{W}$, this sphere is centered at the tip of the vector $\bar{W}$, representing the velocity of the center of mass of the electron-atom system. Manipulation of the quantities in the right side of Equation I.5 shows that the radius of the sphere is given by

$$V = \sqrt{\frac{2\mu}{M(1+\mu)}\left\{\frac{1}{2}\frac{Mm}{M+m}(\bar{u}_0 - \bar{v}_0)^2 - E^*\right\}} \qquad (I.6)$$

in agreement with Equation 2.9.

Turning to the converse problem, it is convenient to rearrange the conservation laws as follows

$$\bar{v}_0 - \mu\bar{u} = \bar{v} - \mu\bar{u}_0 \triangleq \bar{B} \qquad (I.7)$$

$$v_0^2 - \mu u^2 = v^2 - \mu u_0^2 + \frac{2E^*}{M} \triangleq A \qquad (I.8)$$

where it is now assumed that $\bar{v}$ and $\bar{u}_0$ are known. Proceeding as above leads to the expression

$$v_{0x}^2 + v_{0y}^2 + \left(v_{0z} - \frac{B}{1+\mu}\right)^2 = \frac{-\mu}{(1+\mu)^2}\left[(1-\mu)A - B^2\right] \qquad (I.9)$$

showing that metastables with velocity $\bar{v}$ arise from ground state atoms with velocities $\bar{v}_0$ terminating on a sphere which is centered at the tip of the vector $\frac{1}{1-\mu}\bar{B}$. The radius of

this sphere is found to be given by

$$R = \sqrt{\frac{2\mu}{M(1-\mu)}\left\{\frac{1}{2}\frac{Mm}{M+m}(\bar{u}_o-\bar{v})^2 - E^*\right\}} \qquad (I.10)$$

Expanding Equation I.6 in powers of μ and v_o/u_o, and expanding Equation I.10 in powers of μ and v/u_o, it is found that to lowest order

$$V = R = \mu u_o \sqrt{1 - \frac{E^*}{E}} \qquad (I.11)$$

where $E = \frac{mu_o^2}{2}$ is the kinetic energy of the electron in the laboratory frame.

APPENDIX II

A GEOMETRIC VIEW OF THE METASTABLE VELOCITY DISTRIBUTION FUNCTION, $g(\bar{v})$

The representations of Figures 2.1, 2.2 and 2.3 provide a convenient means for visualizing the properties of the distribution function of metastables which arise from a monoenergetic beam of ground state particles. It is informative to extend this geometrical point of view to the case where the speeds of particles in the ground state beam are distributed over a range of values.

Returning to Figure 2.1, it is recalled that the position of the center of the sphere is determined by the vector sum of $\bar{v}_o$ and $\mu\bar{u}_o$. If, now, the magnitude of $\bar{v}_o$ is changed, but its direction remains unaltered, then the new sphere which results will be centered on a line passing through the center of the original sphere and parallel to $\hat{v}_o$. Consequently, if the gas in the ground state beam has a range of speeds but a fixed direction of motion, then the corresponding family of spheres will be strung along this line. Because V is constant, the envelope of these spheres is a right circular cylinder with axis parallel to $\hat{v}_o$. Thus, where the velocity distribution of metastables corresponding

to a single sphere and $V < W$ is spread over a cone in velocity space, the distribution corresponding to an entire cylinder (if $V < \mu u_o \sin\Phi$) is spread over roughly half of a lune with axis $\hat{v}_o$ (see Figure II.1). Consequently, a properly placed detector of infinitesimal solid angle will observe metastables with just two speeds v if the ground state beam contains atoms with a single speed, but will observe a continuous range of speeds (between well defined cutoffs) if the distribution of speeds in the ground state beam is continuous.

The above discussion has emphasized the determination of the range of velocities, $\bar{v}$, available to metastables produced from ground state atoms with known velocities, $\bar{v}_o$. However, a better insight into the form of $g(\bar{v})$ (Equation 2.34) can be gained if this point of view is reversed, i.e., if the range of velocities, $\bar{v}_o$, of ground state particles which contributes to a single known metastable velocity, $\bar{v}$, is determined.

As has already been mentioned, a monoenergetic, collimated ground state beam gives rise to metastables with velocity vectors which may terminate anywhere on a well defined spherical surface in velocity (or normalized momentum) space; for purposes of identification, this sphere will be referred to as the "outgoing" sphere. It is shown in Appendix I that a similar relation holds if the roles of the velocities $\bar{v}_o$ and $\bar{v}$ are interchanged, i.e., that metastables having a given velocity $\bar{v}$ can only be produced from ground

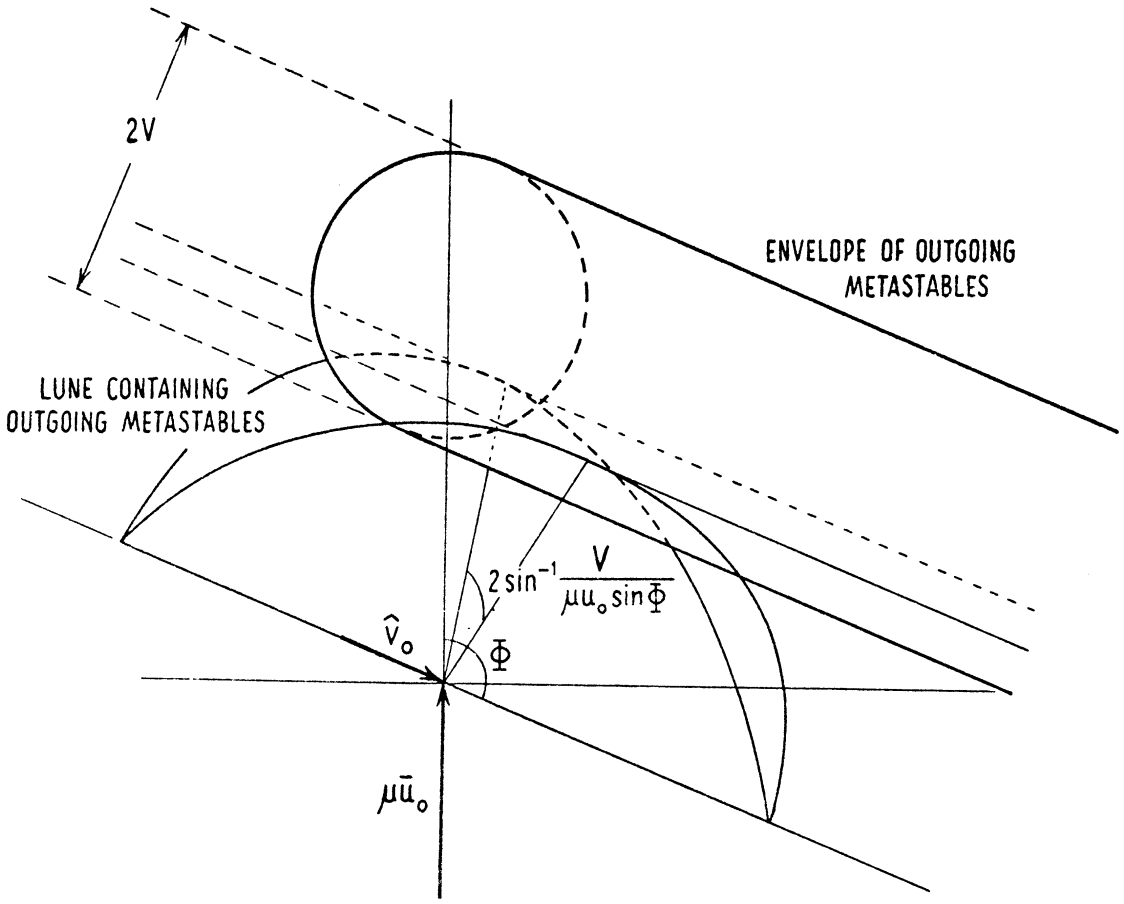

Figure II.1 Cylindrical envelope of metastable velocities which arise from a collimated ground state beam

state particles having velocities $\bar{v}_o$ which terminate on an altogether different sphere; this sphere will be referred to as the "contributing" sphere. To the present order of approximation, the outgoing sphere is centered at the tip of the center of mass velocity vector $\bar{W}$, while the contributing sphere is centered at the tip of the vector $\bar{B}$; in addition, the radii of the two spheres are equal (see Figure II.2).

Thinking now in terms of the contributing sphere, it is possible to glean a good deal of qualitative information about $g(\bar{v})$ from the geometric representation. For concreteness, consider the ground state beam to be collimated within a solid angle $d\omega_o$; let the atoms in the beam have a distribution function $f(\bar{v}_o)$, and suppose that this beam passes at right angles through an electron beam. Consider only metastables which leave the interaction region in some given direction defined by the unit vector $\hat{v}$; suppose, for simplicity, that $\hat{v}$ lies in the plane of the incoming beams and that it makes an angle Θ with the electron beam. Then salient features of $g(\bar{v})$ can be obtained by considering three different cases for the magnitude of $\bar{v}$ (see Figure II.2).

Case I: very small (very large) values of v.

If v is sufficiently small (large), then the vector $\bar{B} = \bar{v} - \mu\bar{u}_o$ will be such that the contributing sphere does not intersect the ground state beam at all. Consequently, there are no ground state particles available to contribute metastables with speed v; the distribution function $g(\bar{v})$ is

$$g(\bar{v}) = \frac{j}{e}\,\frac{n_o \sigma^*}{4\pi V^2}\int_{\Omega_o} d\omega_o\;\frac{V_{o+}^2 f(\bar{V}_{o+}) + V_{o-}^2 f(\bar{V}_{o-})}{|\hat{V}_o \cdot \hat{V}|}$$

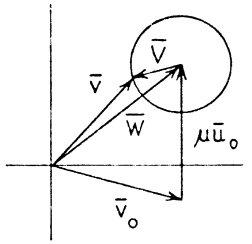

$\bar{W} = \bar{v}_{o+} + \mu\bar{u}_o$

$\bar{v} = \bar{W} + \bar{V}$

given a value of $\bar{v}_o$,
what values of $\bar{v}$ may occur?

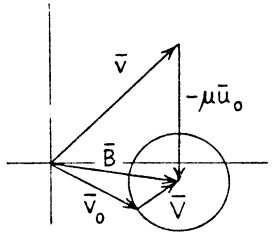

$\bar{B} = \bar{v} - \mu\bar{u}_o$

$\bar{V}_o = \bar{B} - \bar{V}$

given a value of $\bar{v}$,
what values of $\bar{v}_o$ contribute?

Now consider a beam of ground state atoms having an arbitrary distribution of speeds $f(\bar{v}_o)$
Then, for a given value of $\hat{v}$, there are three possibilities for contributing values of v_o.

Case I

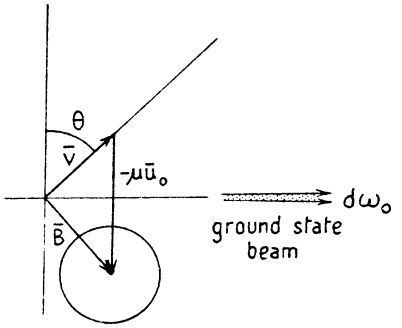

Sphere does not intersect beam; thus no metastables with speed v.

Case II

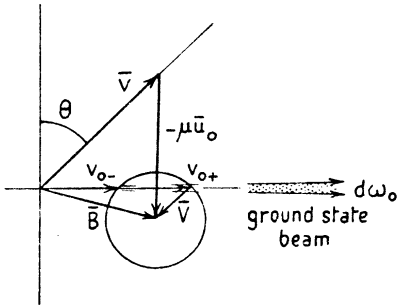

Sphere intersects beam twice; thus two values of v_o (v_{o-} and v_{o+}) contribute to metastables with speed v. Contribution proportional to area of sphere intersected by $d\omega_o$, i.e., to $v_o^2/|\hat{v}_o \cdot \hat{V}|$

Case III

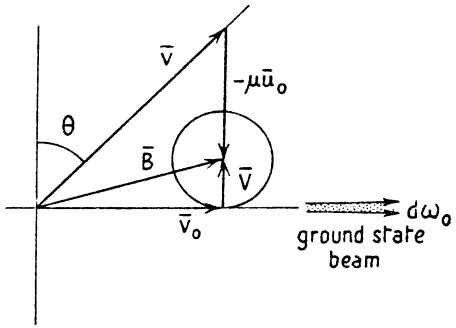

Sphere and beam tangent; thus one value of v_o contributes, and value of v is maximum possible, call it v_+. From geometry -

$v_+ = [\mu u_o + V]\sec\theta$

Figure II.2 Geometrical interpretation of metastable velocity distribution function $g(\bar{v})$.

therefore zero for all such values of v.

Case II: intermediate values of v.

For a range of values of v between those mentioned above, the vector $\bar{B}$ will be such that the contributing sphere intersects the ground state beam. Normally there will be <u>two</u> such intersections, corresponding to ground state velocities v_{o+} and v_{o-}.

In addition, the contribution to the metastable signal will be proportional to $f(\bar{v}_{o\pm})$, and to the portion of the sphere, $d\sigma_\pm$, intersected by the solid angle element $d\omega_o$. Expressing $d\sigma_\pm$ in terms of $d\omega_o$ leads at once to

$$d\sigma_\pm = \frac{v_{o\pm}^2}{|\hat{v}_o \cdot \hat{V}|} d\omega_o \qquad \text{(II.1)}$$

Case III: cutoffs

The limiting values of v between Cases I and II occur when the vector $\bar{B}$ is such that the contributing sphere just touches the ground state beam. Under these conditions $\bar{v}_o$ is perpendicular to $\bar{V}$ and the corresponding values of v (cutoffs) are found from simple trigonometry (Figure II.2) to be

$$v_\pm = \left[\mu u_o \pm V\right] \sec\Theta \qquad \text{(II.2)}$$

In addition, since $\bar{v}_o$ is orthogonal to $\bar{V}$ at the cutoffs, the denominator of Equation II.1 vanishes there.

The results of this geometrical investigation can be summarized as follows. Given a well collimated ground state

beam (velocity distribution function $f(\bar{v}_o)$) which intersects a monoenergetic electron beam at right angles, the velocity distribution function $g(\bar{v})$ of the metastables will have the following properties in the plane of the incident beams:

i) it will vanish identically for all but a well defined range of values of v;

ii) within this range, metastables of any given value of v will arise from two values of v_o; each value of v_o will contribute to $g(\bar{v})$ in proportion to $v_o^2 f(\bar{v}_o)$, and will be weighted by the factor $\frac{1}{|\hat{v}_o \cdot \hat{V}|}$; since this quantity blows up at the limits of the allowed range of v, the distribution is singular there;

iii) the cutoff values of v are given by Equation II.2. The secant factor indicates that the "position" of the nonvanishing portion of $g(\bar{v})$ will be a very sensitive function of the observation angle Θ, moving off to infinite values of v as the detector moves from a direction looking into the electron beam around to a direction looking into the ground state beam.

Qualitatively, the same results are valid for beams which intersect at any angle. If the beams are considered to intersect at an angle Φ instead of at right angles, then Equation II.2 becomes

$$v_\pm = \left[\mu u_o \sin \Phi \pm V \right] \csc(\Phi - \Theta) \qquad \text{(II.3)}$$

If the detector is no longer considered to lie in the plane of the incident beams, the arguments of Cases I and II are still valid, and Case III is only complicated by the necessity for a more cumbersome generalization of Equation II.2 (see Appendix III).

APPENDIX III

SOME EXPLICIT CALCULATIONS

The purpose of this appendix is to introduce explicit polar variables into the expression for $g(\bar{v})$ (Equation 2.34). Cutoffs and integrated intensities are then discussed in terms of these variables.

III.1 The Introduction of Polar Variables into $g(\bar{v})$

The velocity distribution function $g(\bar{v})$ for the metastable atoms produced by electron impact excitation is given by (Equation 2.34)

$$g(\bar{v}) = \frac{j}{e}\frac{n_0\sigma^*}{4\pi V^2}\int_{\Omega_0} d\omega_0 \frac{v_{0+}^2 f(v_{0+}) + v_{0-}^2 f(v_{0-})}{|\hat{v}_0\cdot\hat{V}|} \qquad V<B \qquad \text{(III.1)}$$

Here

$$v_{0\pm} = B\cos\vartheta \pm \sqrt{V^2 - B^2\sin^2\vartheta} \qquad \text{(III.2)}$$

where the variables are defined in terms of the vector diagram of Figure 2.4. For purposes of calculations, the vector notation is inconvenient; the natural variables for the problem are the polar variables which are also indicated in Figure 2.4. It is therefore useful to introduce these into

Equations III.1 and III.2.

The most straightforward way to do this is to introduce the orthogonal coordinate system shown in Figure 2.4, in terms of which the important vectors are

$$\bar{v} = v\,(\sin\Theta\sin\varphi,\ \sin\Theta\cos\varphi,\ \cos\Theta) \qquad \text{(III.3)}$$

$$\mu\bar{u}_o = \mu u_o(\ 0\ ,\ 0\ ,\ 1\ ) \qquad \text{(III.4)}$$

$$v_o = v_o(\ 0\ ,\ \sin\Phi\ ,\ \cos\Phi) \qquad \text{(III.5)}$$

The absence of an azimuthal variable, ς, in the definition of $\bar{v}_o$ represents no loss of generality; the important parameter is the deviation of the vector $\bar{v}$ from the plane containing $\bar{v}_o$ and $\bar{u}_o$, which is adequately described by φ. If, however, for purposes of integration it is convenient to use the variable ς, it can be included by merely replacing φ by $\varphi-\varsigma$ in all of the expressions derived below.

From the above expressions, it is possible to write

$$\bar{B} = \bar{v} - \mu\bar{u}_o$$

$$= (v\sin\Theta\sin\varphi,\ v\sin\Theta\cos\varphi,\ v\cos\Theta - \mu u_o) \qquad \text{(III.6)}$$

Using this relation it follows that

$$B\cos\vartheta \equiv \bar{B}\cdot\hat{v}_o$$

$$= v(\sin\Theta\sin\Phi\cos\varphi + \cos\Theta\cos\Phi) - \mu u_o\cos\Phi \qquad \text{(III.7)}$$

and

$$B^2\sin^2\vartheta \equiv (\bar{B}\times\hat{v}_o)^2$$

$$= V^2 \sin^2\Theta \sin^2\varphi + \left[\mu u_o \sin\Phi + V\left(\sin\Theta\cos\Phi\cos\varphi - \cos\Theta\sin\Phi\right)\right]^2$$

(III.8)

Consequently, $g(\bar{v})$ takes the explicit form

$$g(\bar{v}) = \frac{j}{e}\frac{n_o\sigma^*}{4\pi V}\int_{\Omega_o} d\omega_o \frac{v_{o+}^2 f(v_{o+}) + v_{o-}^2 f(v_{o-})}{\sqrt{V^2 - v^2\sin^2\Theta\sin^2\varphi - \left[\mu u_o \sin\Phi + V\left(\sin\Theta\cos\Phi\cos\varphi - \cos\Theta\sin\Phi\right)\right]^2}} \qquad \text{(III.9)}$$

where

$$v_{o\pm} = V\left(\sin\Theta\sin\Phi\cos\varphi + \cos\Theta\cos\Phi\right) - \mu u_o\cos\Phi \pm \sqrt{V^2 - v^2\sin^2\Theta\sin^2\varphi - \left[\mu u_o\sin\Phi + V\left(\sin\Theta\cos\Phi\cos\varphi - \cos\Theta\sin\Phi\right)\right]^2} \qquad \text{(III.10)}$$

III.2 A General Relation for the Cutoffs

If the ground state gas enters the electron gun as a well collimated beam, then the envelope of the velocity vectors of the resulting metastables is a semi-infinite cylinder with a hemispherical cap on the end (see Appendix II). This cylinder defines the limiting metastable speeds which can be observed in a given direction (the cutoffs). Since these are important for the discussion of the metastable velocity distribution, the cylinder will now be described in terms of the variables relevant to the problem, i.e., polar coordinates.

Because the present results are to be applied to nearly orthogonal ground state and electron beams, it is legitimate to consider only the portion of the envelopes determined by the following restrictions: it is assumed that

i) $\Theta > \sin^{-1} \frac{V}{\mu u_0}$

ii) $\sin \Phi > \frac{V}{\mu u_0}$

Together, these assumptions are sufficient (though not necessary) to limit consideration to cases where the cylindrical envelope does not enclose the origin of the velocity space, and to those portions of a given envelope which are not "near the end", i.e., which are exterior to the sphere which defines the end cap (see Figure II.1).

The cylinder is most simply described in the cartesian velocity coordinate system (x,y,z) shown in Figure III.1. Here the axis of the cylinder is parallel to the y-axis, so the equation for the cylinder is

$$x^2 + (z - z_0)^2 = V^2 \qquad \text{(III.11)}$$

and y is arbitrary.

The natural variables are polar coordinates (v, Θ, φ) defined with z′ as the polar axis. The transformation between the two systems is

$$\left.\begin{aligned} x &= v \sin\Theta \sin\varphi \\ y &= v \sin\Theta \sin\Phi \cos\varphi + v \cos\Theta \cos\Phi \\ z &= -v \sin\Theta \cos\Phi \cos\varphi + v \cos\Theta \sin\Phi \end{aligned}\right\} \qquad \text{(III.12)}$$

In addition

$$z_0 = \mu u_0 \sin\Phi \qquad \text{(III.13)}$$

Consequently, the equation for the cylindrical envelope becomes

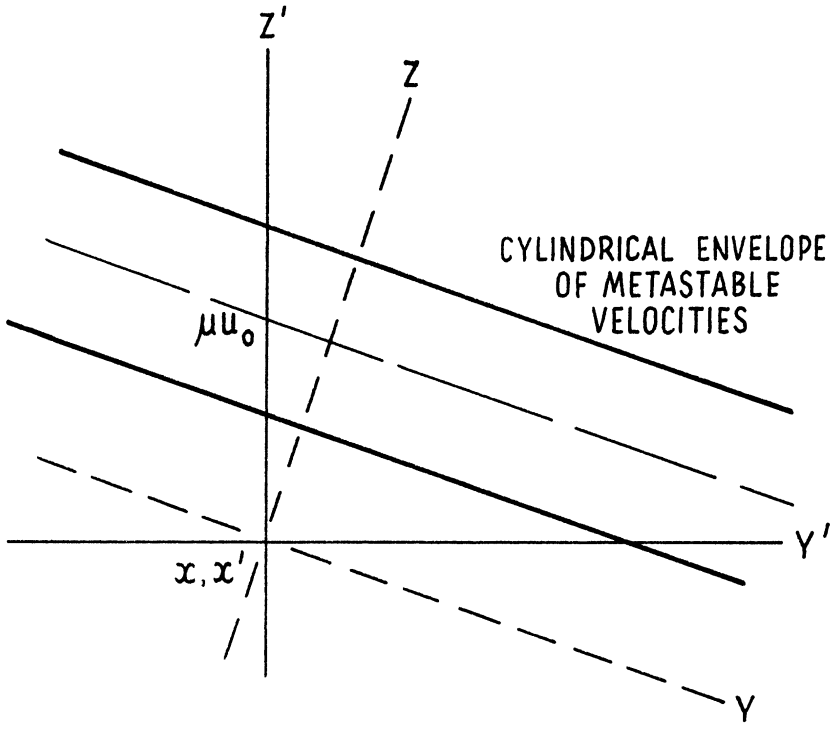

Figure III.1 Velocity space cartesian coordinate systems used in describing the cylindrical envelope of metastable velocities.

$$V^2 = v^2 \sin^2\Theta \sin^2\varphi + \left(-v\sin\Theta\cos\Phi\cos\varphi + v\cos\Theta\sin\varphi - \mu u_0 \sin\Phi\right)^2 \quad \text{(III.14)}$$

If a detector is located along a ray from the origin which is defined by the angles Θ, φ, then Equation III.14 can be solved to determine the minimum and maximum speeds V_t (cutoffs) which can be observed:

$$V_t \left\{ \sin^2\Theta\sin^2\varphi + \left(-\sin\Theta\cos\Phi\cos\varphi + \cos\Theta\sin\Phi\right)^2 \right\}$$

$$= \mu u_0 \sin\Phi\left(-\sin\Theta\cos\Phi\cos\varphi + \cos\Theta\sin\Phi\right) \pm \sqrt{\begin{array}{l} -\mu^2 u_0^2 \sin^2\Phi\sin^2\Theta\sin^2\varphi \\ + V^2\left[\sin^2\Theta\sin^2\varphi + \left(-\sin\Theta\cos\Phi\cos\varphi + \cos\Theta\sin\Phi\right)^2\right] \end{array}} \quad \text{(III.15)}$$

For a given value of Θ, these expressions are only valid for a range of azimuthal angles φ which lies symmetrically about $\varphi = 0$. The limiting value, $\varphi_{max.}$, occurs when the line to the detector just grazes the cylinder, i.e., when the two cutoffs coalesce. Thus, $\varphi_{max.}$ is the value of φ which makes the radical in Equation III.15 vanish. This condition leads to

$$\left[\left(\frac{\mu u_0}{V}\right)^2 - 1\right]\sin\Theta\sin\Phi\cdot\cos\varphi_{max.} = \cos\Theta\cos\Phi \quad \text{(III.16)}$$

$$\pm\sqrt{\begin{array}{l} \cos^2\Theta\cos^2\Phi + \left[\left(\frac{\mu u_0}{V}\right)^2 - 1\right]\cdot \\ \cdot\left\{\left[\left(\frac{\mu u_0}{V}\right)^2 - 1\right]\sin^2\Theta\sin^2\Phi - \sin^2\Theta\cos^2\Phi - \cos^2\Theta\sin^2\Phi\right\} \end{array}}$$

For values of $\varphi > \varphi_{max.}$ the distribution $g(\bar{v})$ vanishes for all v.

III.3 The Integrated Metastable Flux at Threshold

A useful quantity in an experiment is the total metastable intensity (integrated flux) in a given direction. In principle, this can be obtained by integrating the metastable velocity distribution over all velocities:

$$I(\Theta, \varphi; V) = \int_0^\infty dv\, v^2\, g(v) \qquad \text{(III.17)}$$

It would be particularly useful to evaluate this quantity for the distribution arising from a collimated ground state beam since this is the situation of present experimental interest. Unfortunately, the general integral III.17 cannot be expressed in closed form. However, it can be easily evaluated at threshold, as will be shown below.

To conform to the case of most immediate concern, the following assumptions will be made

i) the ground state gas enters the electron gun as a perfectly collimated beam

ii) the velocity distribution function in the ground state beam is Maxwellian

iii) the detector is in the plane of the incoming beams.

The intensity per unit solid angle can then be written

$$I(\Theta,\bar{\Phi},\varphi;V) = \frac{j}{e}\frac{n_0\sigma^*}{4\pi V}\frac{1}{\pi^{3/2}\alpha^3}\,J(\Theta,\bar{\Phi},\varphi,V) \qquad \text{(III.18)}$$

where

$$J(\Theta,\bar{\Phi},\varphi;V) = \int_{V_-}^{V_+} dv\, v^2\,\frac{v_{o+}^2\, e^{-v_{o+}^2/\alpha^2} + v_{o-}^2\, e^{-v_{o-}^2/\alpha^2}}{|\hat{v}_o\cdot\hat{V}|} \qquad \text{(III.19)}$$

Specializing the results of Equations III.9 and III.10 to the case $\varphi = 0$ allows this to be rewritten

$$J(\Theta,\bar{\Phi},0,V) = \int_{[\mu u_0 \sin\bar{\Phi} - V]\csc(\bar{\Phi}-\Theta)}^{[\mu u_0 \sin\bar{\Phi} + V]\csc(\bar{\Phi}-\Theta)} dv\, v^2\,\frac{v_{o+}^2\, e^{-v_{o+}^2/\alpha^2} + v_{o-}^2\, e^{-v_{o-}^2/\alpha^2}}{\sqrt{V^2 - [\mu u_0 \sin\bar{\Phi} - v\sin(\bar{\Phi}-\Theta)]^2}} \qquad \text{(III.20)}$$

where

$$v_{o\pm} = v\cos(\bar{\Phi}-\Theta) - \mu u_0 \cos\bar{\Phi} \pm \sqrt{V^2 - [\mu u_0 \sin\bar{\Phi} - v\sin(\bar{\Phi}-\Theta)]^2} \qquad \text{(III.21)}$$

Considering values of $V \ll \mu u_0$ it is observed that the radical in Equation III.21 is generally much smaller than the leading terms; in addition, the limits of integration are nearly equal. It is therefore a valid approximation to replace $v_{o\pm}$ in Equation III.20 by the single value given by the first two terms in Equation III.21. Furthermore, the terms in the numerator of Equation III.20 can be evaluated at the mean value of v, call it $\langle v\rangle$,

$$\langle v\rangle = \mu u_0 \sin\bar{\Phi}\csc(\bar{\Phi}-\Theta) \qquad \text{(III.22)}$$

and then taken outside of the integral. Equation III.20 then becomes

$$J(\Theta,\bar{\Phi},0;V) \approx 2\mu^4 u_0^4 \sin^2\Theta \sin^2\bar{\Phi} \csc^4(\bar{\Phi}-\Theta) \cdot \cdot \exp\left[-\frac{\mu^2 u_0^2}{\alpha^2}\sin^2\Theta \csc^2(\bar{\Phi}-\Theta)\right] \cdot K(\Theta,\bar{\Phi},0;V) \quad \text{(III.23)}$$

where

$$K(\Theta,\bar{\Phi},0;V) = \int_{[\mu u_0 \sin\bar{\Phi} - V]\csc(\bar{\Phi}-\Theta)}^{[\mu u_0 \sin\bar{\Phi} + V]\csc(\bar{\Phi}-\Theta)} \frac{dv}{\sqrt{V^2 - [\mu u_0 \sin\bar{\Phi} - v\sin(\bar{\Phi}-\Theta)]^2}} \quad \text{(III.24)}$$

Introducing the new variable of integration

$$u = \frac{1}{V}\left[\mu u_0 \sin\bar{\Phi} - v\sin(\bar{\Phi}-\Theta)\right] \quad \text{(III.25)}$$

leads quickly to the result

$$K(\Theta,\bar{\Phi},0;V) = \pi \csc(\bar{\Phi}-\Theta) \quad \text{(III.26)}$$

The angular dependence of the intensity very close to threshold (Equation III.18) is therefore summarized by combining Equations III.23 and III.26

$$J(\Theta,\bar{\Phi},0;V) \approx 2\pi\,\mu^4 u_0^4 \sin^2\Theta \sin^2\bar{\Phi} \csc^5(\bar{\Phi}-\Theta) \cdot \cdot \exp\left[-\frac{\mu^2 u_0^2}{\alpha^2}\sin^2\Theta \csc^2(\bar{\Phi}-\Theta)\right] \quad \text{(III.27)}$$

Since this is independent of V (the next term in the expansion for $J(\Theta,\bar{\Phi},0;V)$ is of order V) it is concluded from Equation III.18 that

$$\lim_{V\to 0} VI(\Theta,\bar{\Phi},0;V) = \frac{j}{e}\frac{n_0 \bar{\sigma}^*}{4\pi}\frac{1}{\pi^{3/2}\alpha^3} J(\Theta,\bar{\Phi},0;0) \quad \text{(III.28)}$$

i.e., that the product $VI(\Theta,\bar{\Phi},0,V)$ is non-zero but bounded.

Considering orthogonal ground state and electron beams

$\left(\Phi=\frac{\pi}{2} \Rightarrow \csc(\Phi-\Theta)=\sec\Theta\right)$, the angular behavior at threshold of the metastable intensity in the plane $\varphi=0$ is found from Equation III.27.

$$J(\Theta,\tfrac{\pi}{2},0;0)=2\pi\mu^4 u_0^4\cdot\tan^2\Theta\sec^3\Theta\exp\left[-\frac{\mu^2u_0^2}{\alpha^2}\tan^2\Theta\right] \quad \text{(III.29)}$$

In normalized form, this is the equation for the curve parametrized by $\Delta E=0$ in Figure 3.5.

APPENDIX IV

PROGRAM BY DR. E. S. FRY FOR NUMERICAL INTEGRATION OF $g(v)$ OVER FINITE DETECTOR WIDTH

The velocity distribution function for metastable atoms arising from a collimated ground state beam is discussed in Section 3.1. All calculations presented there assume that both the ground state beam and the detected portion of the metastable beam are well collimated. The program presented below integrates $g(v)$ over a detector of finite angular width $\Delta\Theta \doteq \Delta\Psi$, assuming the detector to be in the plane of the orthogonal incident beams ($\Theta = \frac{\pi}{2}$, $\varphi = 0$).

Using a Gauss-Chebychev quadrature of order n = 6, the program evaluates

$$\frac{1}{n_o}\frac{dn_o}{dU_f} = \frac{U_f^2}{\pi^{3/2} r\sqrt{\kappa}} \int_{\psi_o - \frac{\Delta\psi}{2}}^{\psi_o + \frac{\Delta\psi}{2}} d\psi \frac{\cos\psi}{\sqrt{1-\eta^2}} \left\{ T_1^2 e^{-T_1^2} + T_2^2 e^{-T_2^2} \right\} \qquad (IV.1)$$

where

$$\eta = \sqrt{\frac{\kappa+1}{\kappa}} - \frac{U_f}{r\sqrt{\kappa}} \sin\psi = \frac{1}{V}\left[\mu u_o - v\cos\Theta\right] \qquad (IV.2)$$

$$T_{1,2} = U_f \cos\psi \pm r\sqrt{\kappa}\sqrt{1-\eta^2}$$

$$= \frac{1}{\alpha}\left[v\sin\Theta \pm \sqrt{V^2 - \left[\mu u_o - v\cos\Theta\right]^2} \right] = \frac{v_{o\pm}}{\alpha} \qquad (IV.3)$$

$$r = \sqrt{\frac{mE^*}{MkT}} = \frac{\mu}{\alpha}\sqrt{\frac{2E^*}{M}} \qquad \text{(IV.4)}$$

$$\mathcal{K} = \frac{\Delta E}{E^*} \qquad \text{(IV.5)}$$

$$U_f = \frac{v}{\alpha} \qquad \text{(IV.6)}$$

and $\alpha = \sqrt{\frac{2kT}{M}}$ is the most probable atom velocity in the Maxwellian reservoir from which the ground state beam is formed.

INPUT:

The data cards must have columns 1 and 73-80 blank. A data set begins with &M and ends with &END. A run consists of as many sets as desired. The input variables and their default values are:

- - variable - -		- - default - -
E	The metastable excitation energy E^*(eV)	no default
DELE	The incident electron energy in excess of E^*(eV)	no default
PSI	The observation angle, Ψ_o (degrees)	no default
DELPSI	The spread in observation angle, $\Delta\Psi$ (degrees)	no default

- - variable - -		- - default - -
T	The atom source temperature (degrees K)	300.0
DU	The spacing between the values of U_f at which the integral is evaluated	0.005
MASS	The atom mass (at. mass units based on C^{12})	4.0026
FRAC	When the value of the integral falls to FRAC times its peak value, the integral is not evaluated at any additional points U_f.	0.001
UNCH	For plots, this is the U axis scale factor in units of U per inch. If UNCH 0.0, the axis is drawn 8.0 inches long and a "nice" scale factor is determined (U is dimensionless)	0.0
VNCH	Same as UNCH but for V (km/sec)	0.0
TOFNCH	Same as UNCH but for TOF (usec)	0.0
PATH	The machine length, used to determine the TOF spectrum (cm)	1.0

The following input variables have only two possible values T or F (true or false):

- - variable - -			- - default - -
PRNTU	T	The U spectrum is printed out	
	F	The U spectrum is not printed out	F
PRNTV		Same as PRNTU but for V	F
PRNTOF		Same as PRNTU but for TOF	F
PLTU	T	The U spectrum is plotted	
	F	The U spectrum is not plotted	F
PLTV		Same as PLTU but for V	F
PLTTOF		Same as PLTU but for TOF	F
LABEL	T	The plot is labeled	
	F	The plot is not labeled	T

There must be a comma after every input variable except the last one in a data set. There must be at least one blank space after &M and before &END. Once an input variable has been given a value, that value is retained throughout the run or until it is changed. If an input variable is not specified, the default value is used.

OUTPUT:

When PRNTU is requested, the sum of FU(U) * DU is printed out. This sum is taken over all values of U and

approximates an integral over the velocity distribution. The rest of the output is self-explanatory.

A listing of the program, written in FORTRAN IV, follows.

```
C THIS PROGRAM USES A GAUSS-CHEBYCHEV QUADRATURE TO INTEGRATE THE        FRY M001
C METASTABLE VELOCITY DISTRIBUTION OVER AN ANGLE DELPSI CENTERED         FRY M002
C AT PSI. THE ELECTRON AND INCIDENT ATOM MOMENTA ARE ASSUMED TO          FRY M003
C BE PERPENDICULAR.                                                      FRY M004
C                                                                        FRY M005
      DIMENSION U(1000),FU(1000),V(1000),FV(1000)                        FRY M006
      COMMON DIFPSI,SUMPSI,KA,RK,UF,E,DELE,T,PSI,DELPSI,MASS,LABEL       FRY M007
      NAMELIST/M/E,DELE,T,DU,PSI,DELPSI,MASS,FRAC,UNCH,VNCH,TOFNCH,PATH, FRY M008
     1LABEL,PLTU,PLTV,PLTTOF,PRNTU,PRNTV,PRNTOF                          FRY M009
      REAL K,KA,MS,MASS,MAXFU                                            FRY M010
      LOGICAL  LABEL,PLTU,PLTV,PLTTOF,PRNTU,PRNTV,PRNTOF                 FRY M011
      INTEGER H                                                          FRY M012
      PLTU=.FALSE.                                                       FRY M013
      PLTV=.FALSE.                                                       FRY M014
      PLTTOF=.FALSE.                                                     FRY M015
      PRNTU=.FALSE.                                                      FRY M016
      PRNTV=.FALSE.                                                      FRY M017
      PRNTOF=.FALSE.                                                     FRY M018
      LABEL=.TRUE.                                                       FRY M019
      UNCH=0.                                                            FRY M020
      VNCH=0.                                                            FRY M021
      TOFNCH=0.                                                          FRY M022
      PATH=1.                                                            FRY M023
      FRAC=.001                                                          FRY M024
      T=300.                                                             FRY M025
      MASS=4.00260                                                       FRY M026
      PI1=1.772454                                                       FRY M027
      DEG=.0174533                                                       FRY M028
      DU=.005                                                            FRY M029
      X1=.9659258                                                        FRY M030
      X2=.7071068                                                        FRY M031
      X3=.2588190                                                        FRY M032
    1 READ (5,M,END=500)                                                 FRY M033
      SUM=0.                                                             FRY M034
      MAXFU=0.                                                           FRY M035
```

```
      ALPHA=12996.*SQRT(T/MASS)                                        FRY M036
      R=2.5232*SQRT(E/T/MASS)                                          FRY M037
      K=DELE/E                                                         FRY M038
      KA=SQRT((K+1.)/K)                                                FRY M039
      RK=R*SQRT(K)                                                     FRY M040
      P1=(PSI-DELPSI/2.)*DEG                                           FRY M041
      P2=(PSI+DELPSI/2.)*DEG                                           FRY M042
      SP1=SIN(P1)                                                      FRY M043
      SP2=SIN(P2)                                                      FRY M044
      RKA=R*(SQRT(K+1.)-SQRT(K))                                       FRY M045
      RKB=R*(SQRT(K+1.)+SQRT(K))                                       FRY M046
      UMIN=RKA/SP2                                                     FRY M047
      A=RKB/(2.E9*DU+UMIN)                                             FRY M048
      IF(SP1.LT.A) SP1=A                                               FRY M049
      UMAX=RKB/SP1                                                     FRY M050
      WRITE (6,100) E,DELE,T,ALPHA,MASS,DELPSI,PSI                     FRY M051
      J=INT(UMIN/DU)                                                   FRY M052
      U1=FLOAT(J)*DU                                                   FRY M053
      J=INT((UMAX-UMIN)/DU)+3                                          FRY M054
      IF (J.GT.1000) J=1000                                            FRY M055
      DO 4 I=1,J                                                       FRY M056
      U(I)=U1+FLOAT(I-1)*DU                                            FRY M057
      UF=U(I)                                                          FRY M058
      LAS=I                                                            FRY M059
      IF (SP2.LT.RKA/UF) GO TO 3                                       FRY M060
```

```
      IF (SP1.GT.RKB/UF) GO TO 3                                       FRY M061
      PA=P1                                                            FRY M062
      PB=P2                                                            FRY M063
      IF (SP1.LT.RKA/UF) PA=ARSIN(RKA/UF)                              FRY M064
      IF (SP2.GT.RKB/UF) PB=ARSIN(RKB/UF)                              FRY M065
```

```
      DIFPSI=.5*(PB-PA)                                                 FRY M066
      SUMPSI=.5*(PB+PA)                                                 FRY M067
      CHEB=F(X1)+F(-X1)+F(X2)+F(-X2)+F(X3)+F(-X3)                       FRY M068
      FU(I)=CHEB*DIFPSI/PI1/RK/RK/6.*UF*UF                              FRY M069
      SUM=SUM+FU(I)                                                     FRY M070
      IF (FU(I).GT.MAXFU) MAXFU=FU(I)                                   FRY M071
      IF (FU(I).LT.FRAC*MAXFU) GO TO 5                                  FRY M072
      GO TO 4                                                           FRY M073
    3 FU(I)=0.                                                          FRY M074
    4 CONTINUE                                                          FRY M075
C READOUT OF U SPECTRUM                                                 FRY M076
    5 IF (.NOT. PRNTU) GO TO 6                                          FRY M077
      SUM=SUM*DU                                                        FRY M078
      WRITE(6,101) UMIN,UMAX,SUM                                        FRY M079
      WRITE(6,102) (U(I),FU(I),I=1,LAS)                                 FRY M080
    6 IF (.NOT. PLTU) GO TO 7                                           FRY M081
      KEY=1                                                             FRY M082
      CALL PLOTR(U,FU,UNCH,LAS,KEY)                                     FRY M083
C CALCULATION AND READOUT OF VELOCITY SPECTRUM                          FRY M084
    7 IF(.NOT.(PRNTV.OR.PLTV)) GO TO 10                                 FRY M085
      ALP=ALPHA*.00001                                                  FRY M086
      DO 8 I=1,LAS                                                      FRY M087
      FV(I)=FU(I)/ALP                                                   FRY M088
    8 V(I)=U(I)*ALP                                                     FRY M089
      IF(.NOT.PRNTV) GO TO 9                                            FRY M090
      VMIN= UMIN*ALP                                                    FRY M091
      VMAX=UMAX*ALP                                                     FRY M092
      WRITE(6,103) VMIN, VMAX                                           FRY M093
      WRITE(6,102)(V(I),FV(I),I=1,LAS)                                  FRY M094
      IF (.NOT. PLTV) GO TO 10                                          FRY M095
    9 KEY=2                                                             FRY M096
      CALL PLOTR(V,FV,VNCH,LAS,KEY)                                     FRY M097
C CALCULATION AND READOUT OF TOF SPECTRUM                               FRY M098
   10 IF(.NOT.(PRNTOF.OR.PLTTOF)) GO TO 1                               FRY M099
      ALP=ALPHA*.000001                                                 FRY M100
      DO 11 I=1,LAS                                                     FRY M101
```

```
      N=LAS+1-I                                                          FRY M102
      V(I)=PATH/U(N)/ALP                                                 FRY M103
   11 FV(I)=FU(N)*ALP*U(N)*U(N)/PATH                                     FRY M104
      IF(.NOT.PRNTOF) GO TO 12                                           FRY M105
      TMIN=PATH/UMAX/ALP                                                 FRY M106
      TMAX=PATH/UMIN/ALP                                                 FRY M107
      WRITE(6,104) TMIN,TMAX,PATH                                        FRY M108
      WRITE(6,105) (V(I),FV(I), I=1,LAS)                                 FRY M109
      IF (.NOT. PLTTOF) GO TO 1                                          FRY M110
   12 KEY= 3                                                             FRY M111
      CALL PLOTR(V,FV,TOFNCH,LAS,KEY)                                    FRY M112
      GO TO 1                                                            FRY M113
C                                                                        FRY M114
C                                                                        FRY M115
  100 FORMAT('1     THRESHOLD ENERGY(EV)='F7.3,5X,'EXCESS ENERGY(EV)=',  FRY M116
     1F7.3,5X,'SOURCE TEMPERATURE(DEG K)='F7.1                           FRY M117
     2/1H0,5X,'ALPHA(CM/SEC)='1PE11.4,8X,'ATOMIC MASS(AMU)='0PF7.4       FRY M118
     3/1H0,5X,'OBSERVATION OVER'F7.3,' DEGREES, CENTERED AT 'F7.3,       FRY M119
     4' DEGREES.')                                                       FRY M120
```

```
  101 FORMAT(1H0,10X,'MINIMUM U='F6.4,5X,'MAXIMUM U='F6.4,               FRY M121
     15X,' THE SUM OF FU(U)*DU IS ',F7.4,                                FRY M122
     2///5(6X,'U',5X,'FU(U)',6X))                                        FRY M123
  102 FORMAT(1H /5(3X,F6.3,F9.5,5X))                                     FRY M124
  103 FORMAT(1H0/6X,'ALL VALUES OF V ARE IN KILOMETERS/SEC'//20X,        FRY M125
     1'MINIMUM V='F7.4,5X,'MAXIMUM V='F7.4///5(6X,'V',5X,'FV(V)',6X))    FRY M126
  104 FORMAT(1H0/6X,'ALL VALUES OF TOF ARE IN USEC.'//10X,'MIMIMUM T=',  FRY M127
     1F6.2,5X,'MAXIMUM T='F6.2,5X,'FLIGHT PATH(CM)='F6.2//               FRY M128
     2/5(5X,'TOF',3X,'FTOF(I)',5X))                                      FRY M129
  105 FORMAT(1H /5(3X,F6.2,F10.6,4X))                                    FRY M130
  500 CALL SYSTEM                                                        FRY M131
```

```
      END                                                                FRY M132
      FUNCTION F(X)                                                      FRY F001
C THIS FUNCTION EVALUATES THE INTEGRAND OF THE CHEBYCHEV TRANSFORMED      FRY F002
C VELOCITY DISTRIBUTION INTEGRAL.                                        FRY F003
      COMMON DIFPSI,SUMPSI,KA,RK,UF                                      FRY F004
      REAL KA                                                            FRY F005
      SP=SIN(DIFPSI*X+SUMPSI)                                            FRY F006
      CP=SQRT(1.-SP*SP)                                                  FRY F007
      ETA=KA-UF*SP/RK                                                    FRY F008
      ETA1=1.-ETA*ETA                                                    FRY F009
      IF (ETA1.LE..0000001) GO TO 1                                      FRY F010
      ETA1=SQRT(ETA1)                                                    FRY F011
      T1=UF*CP+RK*ETA1                                                   FRY F012
      T12=T1*T1                                                          FRY F013
      T2=UF*CP-RK*ETA1                                                   FRY F014
      T22=T2*T2                                                          FRY F015
      X1=SQRT(1.-X*X)                                                    FRY F016
      F=(T22*EXP(-T22)+T12*EXP(-T12))*X1/ETA1*CP                         FRY F017
      RETURN                                                             FRY F018
    1 WRITE(6,100) UF,ETA                                                FRY F019
      F=(T22*EXP(-T22)+T12*EXP(-T12))*CP                                 FRY F020
  100 FORMAT(1H0/'  ERROR AT U(I)='F5.3,'  ETA='E13.7)                   FRY F021
      RETURN                                                             FRY F022
      END                                                                FRY F023
      SUBROUTINE PLOTR(X,Y,DX,L,KEY)                                     FRY P001
C THIS SUBROUTINE SPECIFIES THE PLOTTING                                 FRY P002
      COMMON DIFPSI,SUMPSI,KA,RK,UF,E,DELE,T,PSI,DELPSI,MASS,LABEL       FRY P003
      DIMENSION X(1000), Y(1000)                                         FRY P004
      LOGICAL LABEL                                                      FRY P005
      N=L                                                                FRY P006
      IF(DX .LT. .0000001) GO TO 3                                       FRY P007
      DX1=DX                                                             FRY P008
      XA=FLOAT(INT(X(1)*10.))/10.                                        FRY P009
      XB=FLOAT(INT(X(N)*10.)+1)/10.                                      FRY P010
      XLNGTH=(XB-XA)/DX                                                  FRY P011
      IF(XLNGTH .LT. 15.5) GO TO 4                                       FRY P012
```

```
      XLNGTH=15.5                                                        FRY P013
      XMAX= 15.5*DX+XA                                                   FRY P014
      DO 1 I=1,N                                                         FRY P015
      IF (X(N+1-I) .LT. XMAX) GO TO 2                                    FRY P016
    1 CONTINUE                                                           FRY P017
    2 N=N-I                                                              FRY P018
      GO TO 4                                                            FRY P019
    3 CALL PSCALE(8.,1.,XA,DX1,X(1),N,1)                                 FRY P020
      XLNGTH=8.                                                          FRY P021
    4 CALL PSCALE(6.,1.,YA,DY,Y(1),N,1)                                  FRY P022
      CALL PLTOFS(XA,DX1,YA,DY,1.,1.)                                    FRY P023
      GO TO (5,6,7),KEY                                                  FRY P024
    5 CALL PAXIS(1.,1.,1HU,-1,XLNGTH,0.,XA,DX1,.5)                       FRY P025
```



```
      GO TO 8                                                            FRY P026
    6 CALL PAXIS(1.,1.,9HV(KM/SEC),-9,XLNGTH,0.,XA,DX1,.5)               FRY P027
      GO TO 8                                                            FRY P028
    7 CALL PAXIS(1.,1.,9HTOF(USEC),-9,XLNGTH,0.,XA,DX1,.5)               FRY P029
    8 CALL PAXIS(1.,1.,1H ,1,6.,90.,YA,DY,1.)                            FRY P030
      CALL PLINE (X(1),Y(1),N,1,0,0,1)                                   FRY P031
      IF(.NOT.LABEL) GO TO 9                                             FRY P032
      CALL PENMBR(1.,8.,-.15,E,0.,'''E='',WF2.3,*')                      FRY P033
      CALL PENMBR(-0.,-0.,-.15,DELE,0.,'''    DELE='',WF2.3,*')          FRY P034
      CALL PENMBR(-0.,-0.,-.15,T,0.,'''      T='',WF4.1*')               FRY P035
      CALL PENMBR(1.,7.5,-.15,PSI,0.,'''PSI='',WF2.3*')                  FRY P036
      CALL PENMBR(-0.,-0.,-.15,DELPSI,0.,'''   DELPSI='',WF2.3*')        FRY P037
      CALL PENMBR(-0.,-0.,-.15,MASS,0.,'''     MASS='',WF1.4*')          FRY P038
    9 CALL PLTEND                                                        FRY P039
      RETURN                                                             FRY P040
      END                                                                FRY P041
                                                          196 LINES PRINTED
```

APPENDIX V

Reprinted from The Review of Scientific Instruments, Vol. 40, No. 9, 1242 (September 1969)

Detection of Metastable Atoms and Molecules with Continuous Channel Electron Multipliers*

DENIS P. DONNELLY, JOHN C. PEARL, RICHARD A. HEPPNER, AND JENS C. ZORN

Randall Laboratory of Physics, The University of Michigan, Ann Arbor, Michigan 48104

(Received 14 February 1969; and in final form, 9 May 1969)

BEAMS of metastable molecules can be rapidly and efficiently detected by allowing them to strike the cathode of a windowless electron multiplier. In this note we report on the use of a continuous channel electron multiplier[1] (Bendix "Channeltron") in this application. Compared to other multipliers, the continuous channel multiplier has the advantages of lower noise, simpler circuitry, and far smaller size for a given cathode area.

We have detected thermal beams of metastable helium, hydrogen, neon, argon, krypton, xenon, and molecular nitrogen in our experiments. Although we have not measured the yield of Auger electrons per metastable incident on the multiplier cathode, we judge that the yield is comparable to that achieved[2] on the tungsten or platinum surfaces used in the conventional Auger detectors. The detection efficiency for a given metastable species seems to remain within 10% or so of an equilibrium value in spite of the frequent exposure of the multiplier to humid air and backstreaming pump vapors.

The usual background signal, or dark current, in the Channeltron multiplier is 0.1 counts/sec or less, so it is feasible to do experiments with beam signals as low as 1 count/sec. To maintain a low background count rate it is essential to keep uv radiation (as from bare filaments) and ions (as from vacuum gauge tubes) out of the multiplier. Windows in the vacuum system need not be covered during the experiments, however, since the multiplier does not respond to visible light.

The arrangement shown in Fig. 1 is a simple, effective way to couple the output of the Channeltron to a remote pulse height analyzer.

Sometimes the Channeltrons will develop erratic gain or a very high noise level. This can come from mistreatment such as overloading due to high counting rates or from causes which are less obvious. We have usually found it possible to restore a multiplier to good operating condition by flushing it with acetone or ethyl alcohol and letting it rest on the shelf for a few days. In fact, one of our Channeltrons has been resuscitated in this manner after it had failed from a corona discharge that occurred when the system vacuum was lost with 2.5 kV still applied to the multiplier. A noisy or inoperative multiplier should not be discarded before a few of these "home remedies" have been tried.

The continuous channel multipliers are made of glass tubing which can be broken if too much strain is exerted by the mount; once the multiplier is in place, however,

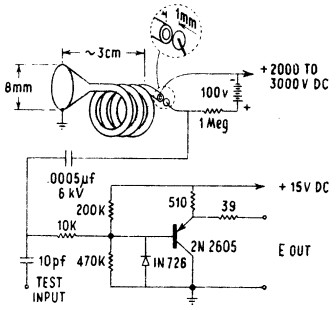

FIG. 1. The Channeltron output is picked up by a small metal button and fed to the input of an emitter follower which is mounted together with the multiplier inside the vacuum chamber. The circuit serves as an impedance transformer so that the signal pulses can be brought out through long, low impedance leads.

the assembly of multiplier plus amplifier on a single board is not overly delicate. It is useful to know that pieces of a broken Channeltron can sometimes still be used for electron multiplication, albeit with lower gain, if new electrical connections for the dc voltage are made to the resistive glass tube with conducting paint.

We are grateful to John Carrico, Christopher Tosswill, Charles Hendee, Barry Kletke, and James Svenson of the Bendix Research Laboratories for the loan of several Channeltron multipliers and for suggestions concerning their use. We thank David Crosby for his contributions to this research.

* Work supported in part by the National Aeronautics and Space Administration.

[1] M. Kaminsky, *Atomic and Ionic Impact Phenomena on Metal Surfaces* (Academic Press Inc., New York, 1965), pp. 292 ff.

[2] G. W. Goodrich and W. C. Wiley, Rev. Sci. Instrum. **33**, 761 (1962); D. S. Evans, ibid. **36**, 375 (1965).

APPENDIX VI

Reprinted from Physics Letters, Vol. 30A, No. 3, 145 (6 October 1969)

EFFECT OF RECOIL ON THE VELOCITY DISTRIBUTION OF METASTABLE ATOMS PRODUCED BY ELECTRON IMPACT *

J. C. PEARL, D. P. DONNELLY and J. C. ZORN
Randall Laboratory of Physics, University of Michigan, Ann Arbor. Michigan 48104, *USA*

Received 3 September 1969

We have shown both experimentally and by a simple kinematic argument that the velocity distribution in a beam of metastable atoms produced by electron bombardment of ground state atoms deviates strongly from the velocity distribution of the ground state atoms.

The velocity distribution of metastable atoms often enters explicitly into the analysis of resonance [1] and collision [2,3] experiments done with atomic beams. However, there have been few direct measurements and no correct theoretical description of the velocity distribution in a beam of metastable

* Research supported in part by the National Aeronautics and Space Administration.

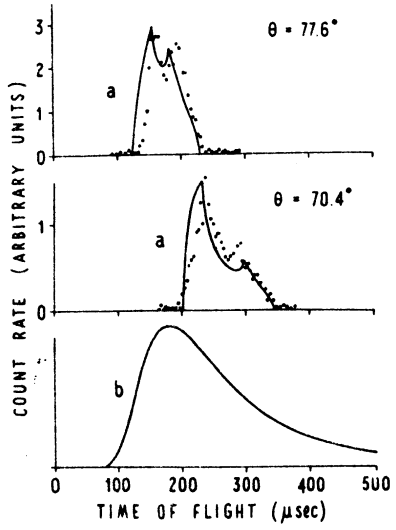

Fig. 1. Time-of-flight spectra for helium. Points represent experimental data. Curves a are theoretical accounting for the angular divergence of the incoming, ground state beam, assuming $E - E^* = 0.75$ eV. Curve b is theoretical if recoil effects are neglected.

atoms formed in the common experimental arrangement where ground state atoms in a collimated beam are excited by a transverse beam of electrons.

In our experiment a pulsed electron beam is directed at right angles ($\Phi = 90^{\circ}$) through a collimated beam of thermal energy helium atoms. The metastable atoms are detected [4] with an electron multiplier (Bendix Channeltron) which can be rotated about the interaction region in the plane defined by the incoming electron and atom beams. Samples of data taken at two different angles θ (angles measured from direction of electron beam) are plotted as points in fig. 1. Striking features of these results, when compared with what would be found if recoil effects were negligible (curve b in fig. 1) include the *narrowness* of the distributions, the *presence of two peaks*, and the *sensitivity to deflection angle* of the position of the distribution.

The principal features of these distributions can be understood from kinematic considerations. If the gas beam effuses ideally from a thermal source (most probable speed α), if the ground state beam is perfectly collimated, if the detector is small, and if the electron scattering is s-wave, then conservation of momentum and energy determine the following velocity distribution for the metastable atoms in the plane of the incident beams

$$f(v) = \frac{v^2 v_{0+}^2 \exp(-v_{0+}^2/\alpha^2) + v_{0-}^2 \exp(-v_{0-}^2/\alpha^2)}{V\,[V^2 - \{(m/M)u_0 \sin\Phi - v\sin(\Phi-\theta)\}^2]^{\frac{1}{2}}} \tag{1}$$

for $v_{\min} < v < v_{\max}$, where

$$v_{\substack{\max\\\min}} = \left[\frac{m}{M}u_0 \sin\Phi \pm V\right] \operatorname{cosec}(\Phi-\theta) \qquad \begin{cases} \theta < \Phi \\ V < (mu_0/M)\sin\Phi \end{cases} \tag{2}$$

and

$$v_{0\pm} = v\cos(\Phi-\theta) - \frac{m}{M}u_0\cos\Phi \pm \{V^2 - [\frac{m}{M}u_0\sin\Phi - v\sin(\Phi-\theta)]^2\}^{\frac{1}{2}} \tag{3}$$

Here $V = [2m(E-E^*)]^{\frac{1}{2}}/M$; m and M are the masses of the electron and atom respectively; E^* is the energy of the metastable state; and u_0 and E are the speed and kinetic energy, respectively, of the incident electron. The distribution $f(v)$, which is zero outside the limits given in eq. (2), is in disagreement with functions previously presented [7,8]. In the present experiment the detector subtends only a very small angle ($\Delta\theta \approx 0^{\circ}8'$), but the divergence of the incoming beam ($\Delta\Phi \approx 3^{\circ}$) is significant. A numerical integration of eq. (2) over the beam divergence yields curves a of fig. 1.

The present study of velocity distributions in beams of metastable atoms should facilitate the interpretation of experiments such as the fine and hyperfine structure measurements in $2^2S_{\frac{1}{2}}$ hydrogen [1,5], measurements of electron impact excitation of $n = 2$ states in helium [6], time-of-flight studies of repulsive molecular states [7], and analysis of the kinetic properties of single and multi-component gases [8].

We are indebted to R A. Heppner, E. S. Fry and W. L. Williams for their assistance and encouragement. The importance of velocity distributions to the measurement of atomic fine structure was emphasized to us by R. T. Robiscoe

References

1. W. E. Lamb Jr. and R. C. Retherford, Phys. Rev. 79 (1950) 549.
2. R. F. Stebbings, W. L. Fite, D. G. Hummer and R. T. Brackmann, Phys. Rev. 119 (1960) 1939.
3. B. Bederson, Atomic interactions, Part A, eds. B. Bederson and W. L. Fite (Academic Press, Inc., New York, 1968) pp. 89-95.
4. D. P. Donnelly, J. C. Pearl, R. A. Heppner and J. C. Zorn, Rev. Sci. Inst. (to be pubished). See also pp. 85-87 of ref. 3.
5. J. W. Heberle, H. A. Reich and P. Kusch, Phys. Rev. 101 (1956) 612;
R. T. Robiscoe, Phys. Rev. 138 (1965) A22 and Phys. Rev. 168 (1968) 4.

6. H. K. Holt and R. V. Krotkov, Phys. Rev. 144 (1966) 82;
L. Vriens, T. F. M. Bonsen and J. A. Smit, Physica 40 (1968) 229.
7. M. Leventhal, R. T. Robiscoe and K. R. Lea, Phys. Rev. 158 (1967) 49;
R. Freund and W. Klemperer, J. Chem. Phys. 47 (1967) 2897;
R. Clampitt and A. S. Newton, J. Chem. Phys. 50 (1969) 1997.
8. J. B. French and J. W. Locke in Rarefied gas dynamics, ed. C. L. Brundin (Academic Press, Inc., New York, 1967) p. 1461;
D. A. Crosby and J. C. Zorn, J. Vac. Sci. Tech. 6 (1969) 82.

* * * * *

APPENDIX VII

SIMPLE SCALING RELATIONS FOR EVALUATING EFFECTS ON DISTRIBUTIONS OF DIFFERENT MASSES AND EXCITATION ENERGIES

The relations for $g(\bar{v})$ presented in Chapters 2 and 3 apply generally to atoms of arbitrary mass and to states of arbitrary excitation energy. Nearly all of the figures presented, however, have been for 2^3S helium. The effects of using different gases (or isotopes) have not been indicated; the effects of exciting different states have only been considered briefly (Section 6.2). An informative means for simultaneously assessing the influence these factors have on metastable velocity distributions is the following.

Curve c of Figure 5.3 represents the time-of-flight spectrum for 2^3S helium if recoil effects are totally absent; the spectrum is characteristic only of the thermal distribution of velocities in the ground state gas. Scaling the time axis with the most probable velocity of the atoms in the reservoir therefore yields a curve which is representative of all gases. The same normalization, however, does not endow curves a with a similar universal character, since they are strongly dependent on recoil effects. These circumstances provide a simple method of comparing the degree to which

beams of metastables produced from various gases are distorted by recoil: relations between E^*, E, Θ and M are determined which produce fixed "shifts" (represented, for example, by those of curves a) relative to the universal curve c.

Curves a are characterized by their cutoffs. Let the cutoff velocities be normalized with respect to the most probable velocity in the ground state gas. For given shifts it is now possible to determine the angles and energy excesses which will produce the same relative shifts with respect to curve c for gases of arbitrary mass and excitation energy. Consider the incident beams and the detector to be coplanar, let Φ be fixed, and suppose that the source gases have the same temperature. Then, for a given spectrum of type a, i.e., for fixed v_+/α and v_-/α, the cutoff relations (Equation 3.5) can be inverted to give

$$\frac{\Delta E}{E^*} = \text{const.} = \frac{\Delta^2 \sin^2\Phi}{\Sigma^2 - \Delta^2 \sin^2\Phi} \qquad \text{(VII.1)}$$

and

$$\sqrt{\frac{M}{E}}\ \sin(\Phi - \Theta) = \text{const.} = \frac{2\sin\Phi}{\Sigma}\sqrt{\frac{m}{kT}} \qquad \text{(VII.2)}$$

where

$$\left.\begin{aligned} \Sigma &= \frac{v_+ + v_-}{\alpha} \\ \Delta &= \frac{v_+ - v_-}{\alpha} \end{aligned}\right\} \qquad \text{(VII.3)}$$

and E is the energy of the incident electron. Equation VII.1 says that, for states of fixed excitation energy E^*, a fixed energy excess ΔE will produce a spectrum with the same "shift" relative to curve c regardless of the mass of the atom or molecule. Equation VII.2, however, indicates that the angle at which such a spectrum is observed does depend on the mass of the excited particle. Comparing the helium cutoffs of curves a in Figure 5.3 with predictions for other gases and states yields the results shown in Table VII.I.

TABLE VII.I

Deflection angles and energy excesses which lead to the same relative structure in the time-of-flight spectra as is indicated for helium by curves a and c in Figure 5.3.

State	Atomic Mass Number	Excitation Energy E^* (eV)	Deflection Angle $(\frac{\pi}{2}-\theta)_{fast}$	$(\frac{\pi}{2}-\theta)_{slow}$	Energy Excess ΔE(eV)
$He(2^3S_1)$	4	19.82	12.4°	19.6°	0.75
$H_2(c^3\pi_u)$	2	11.86	13.6°	21.5°	0.45
$D_2(c^3\pi_u)$	4	11.86	9.6°	15.0°	0.45
$N_2(A^3\Sigma_u^+)$	28	6.16	2.6°	4.1°	0.23
$N_2(a^1\pi_g)$	28	8.54	3.1°	4.8°	0.32
$N_2(E^3\Sigma_g^+)$	28	11.87	3.6°	5.6°	0.45

ADDENDUM

TOTAL INTENSITIES IN DIRECTIONS NOT CONTAINED IN THE PLANE OF THE INCIDENT BEAMS

Normalized curves for total metastable intensities (integrals over the velocity distributions) which arise from a perfectly collimated Maxwellian ground state beam have been presented in Figure 3.5. These results, however, are calculated assuming that the detector is located in the plane of the incident beams; the "structure" in the curve for $\Delta E = 50$ eV has been explained qualitatively in terms of the non-uniform distribution of metastables along the cylindrical portion of velocity space within which all velocity vectors of the metastables must terminate.

It is of interest to investigate the intensity distribution assuming that the detector is located in a plane which does not contain the incident beams, i.e., for values of $\varphi \neq 0$. Such results are presented in Figure AD.1 for the excitation of the 2^3S metastable state of helium by electrons with energy 50 eV above the excitation threshold (note that the curves are normalized to their peak values, as in Figure 3.5). Two features are worthy of note:

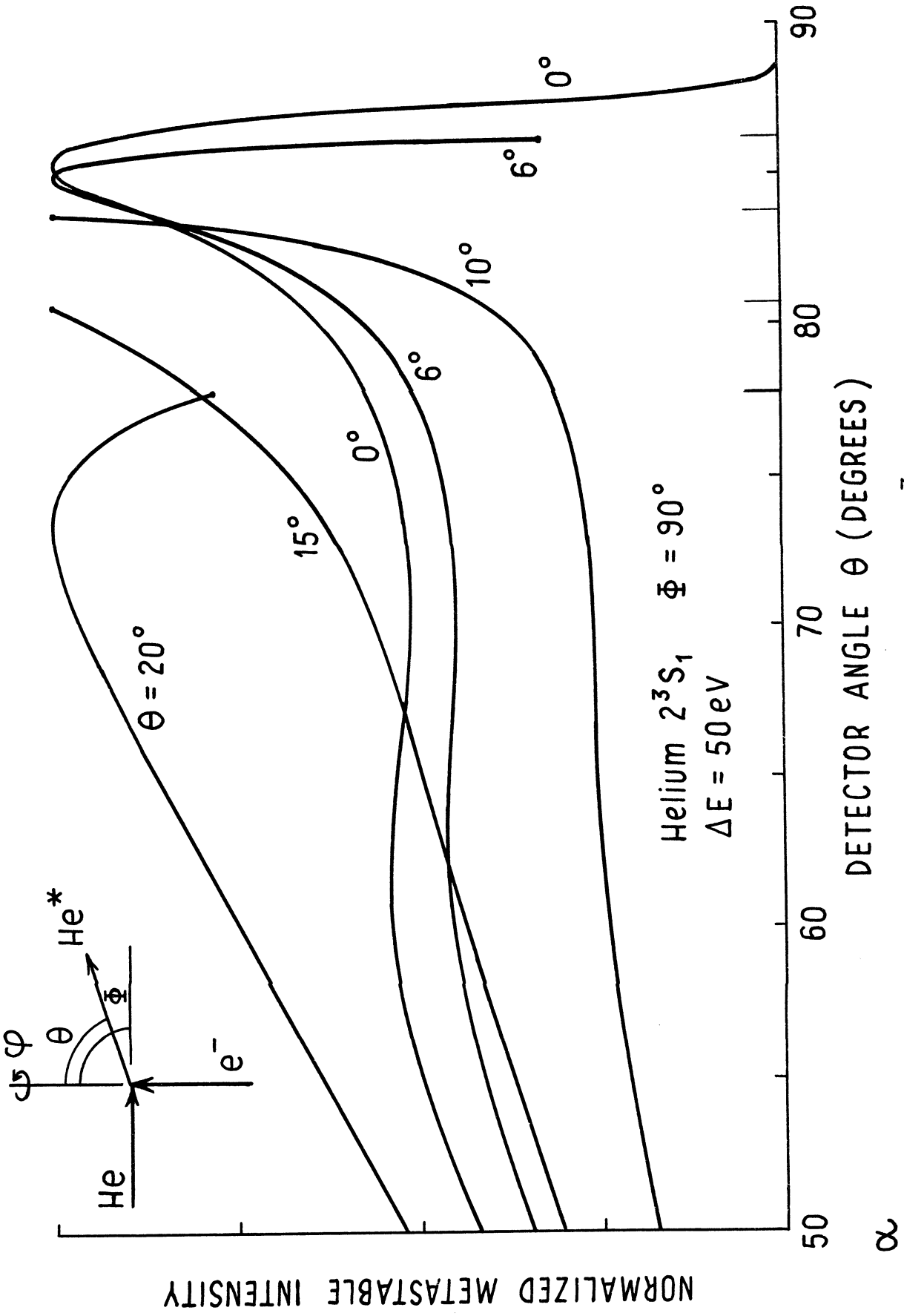

Figure AD.1 Total metastable intensity for 2^3S helium as a function of detector angle Θ. The azimuthal angle φ is the parameter; the electron energy is 69.8 eV. A perfectly collimated Maxwellian ground state beam is assumed. Electron scattering is assumed isotropic.

i) the curves for $\varphi \neq 0$ terminate abruptly. These cutoffs occur when the line of sight from the interaction region to the detector is "tangent" to the cylinder which contains the velocity vectors of the metastables;

ii) the "cutoff points" do not always occur at the peaks of the intensity curves. This is a result of the nonuniform population of metastables within the cylinder.

A different presentation of the intensities is given for electron energies of 69.8, 25 and 21 eV in Figures AD.2, AD.3 and AD.4 respectively. Here the abscissa represents the azimuthal angle φ of the detector, and the polar angle Θ is the parameter; each solid curve, therefore, corresponds to scanning the detector around a cone with its axis along the electron beam. The curves are symmetric about $\varphi = 0^{o}$. The ordinate scale differs from that of most figures in the body of the thesis by not including the factor $1/V$, which is proportional to $1/\sqrt{E-E^{*}}$ (see the discussion of pages 28 and 29). As in the previous figure, each curve terminates abruptly when the line to the detector passes outside of the populated cylinder; the dashed curves represent the loci of these "cutoff points", and reflect the velocity distribution in the ground state beam. In fact, for a ground state beam with a Maxwellian velocity distribution, the plotted quantity (essentially $VI(\Theta, \frac{\pi}{2}, \varphi_{max}, V)$ of page 28 and Section III.3 of

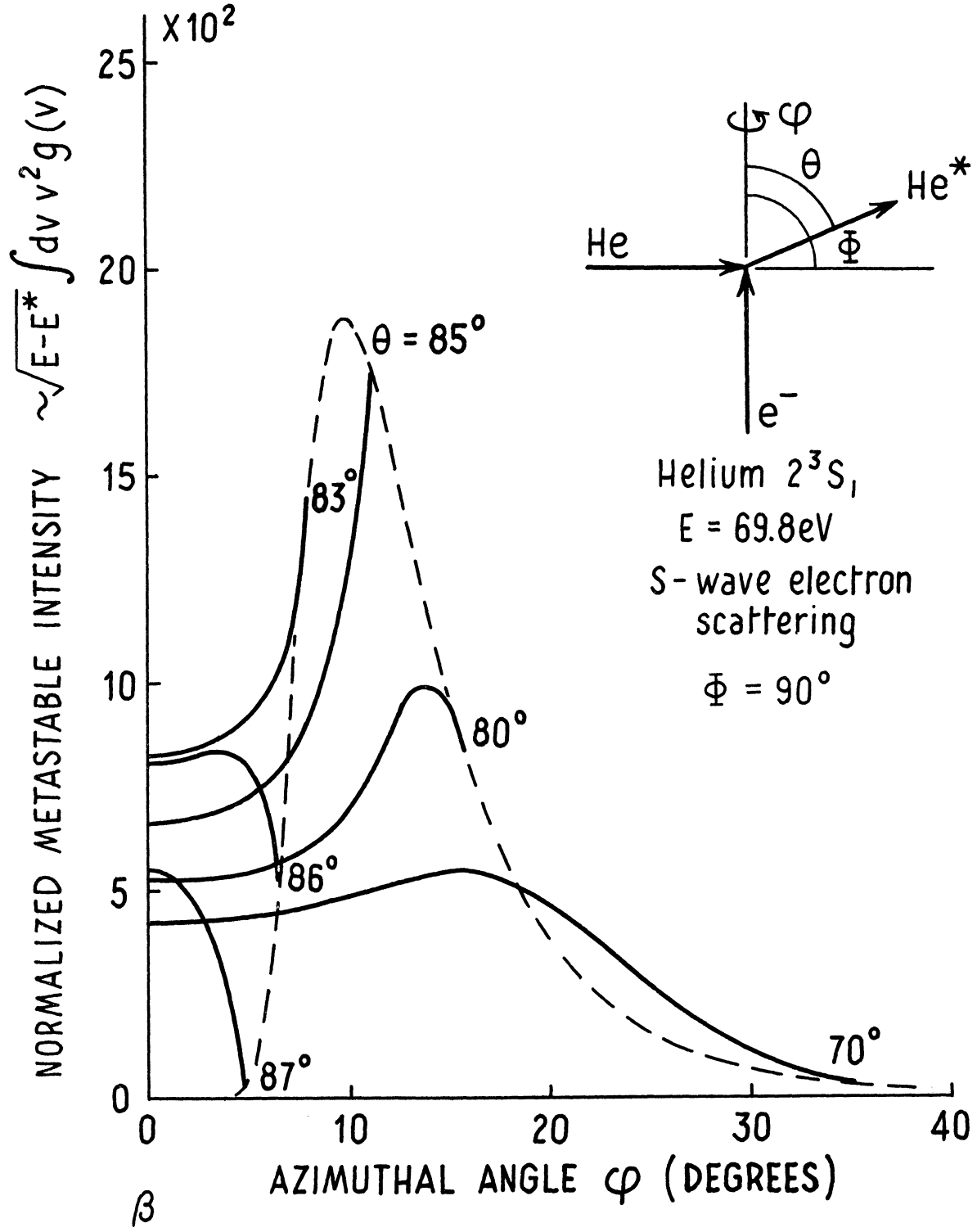

Figure AD.2 Total metastable intensity for 2^3S helium as a function of the azimuthal angle φ of the detector; the polar angle Θ is the parameter. The energy of the incident electrons is 69.8 eV. A perfectly collimated Maxwellian ground state beam is assumed; s-wave scattering of the electrons is also assumed. The dashed curve represents the locus of intensities at the cutoffs (see text).

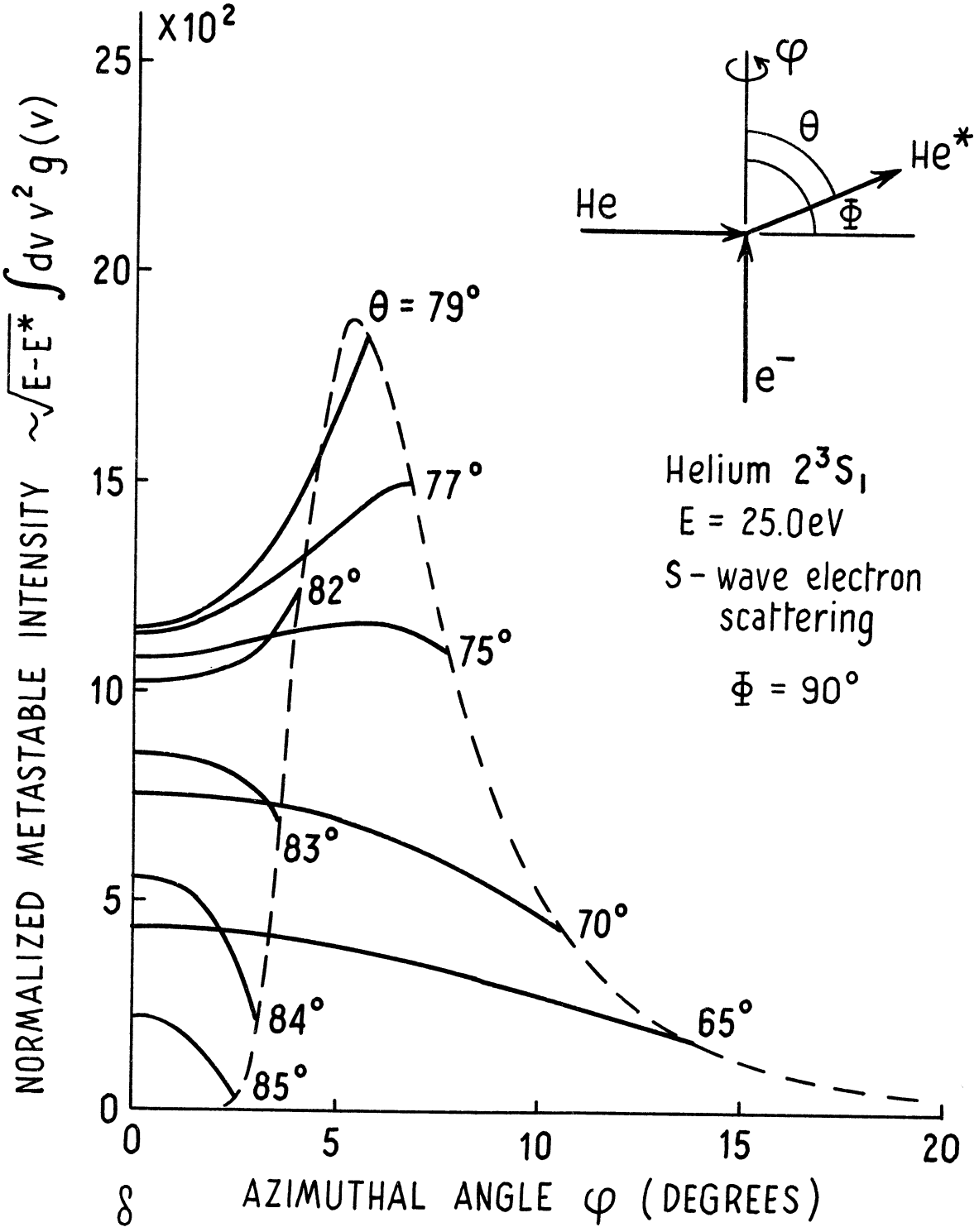

Figure AD.3 Total metastable intensity for 2^3S helium as a function of the azimuthal angle φ of the detector; the polar angle Θ is the parameter. The energy of the incident electrons is 25.0 eV. A perfectly collimated Maxwellian ground state beam is assumed; s-wave scattering of the electrons is also assumed. The dashed curve represents the locus of intensities at the cutoffs (see text).

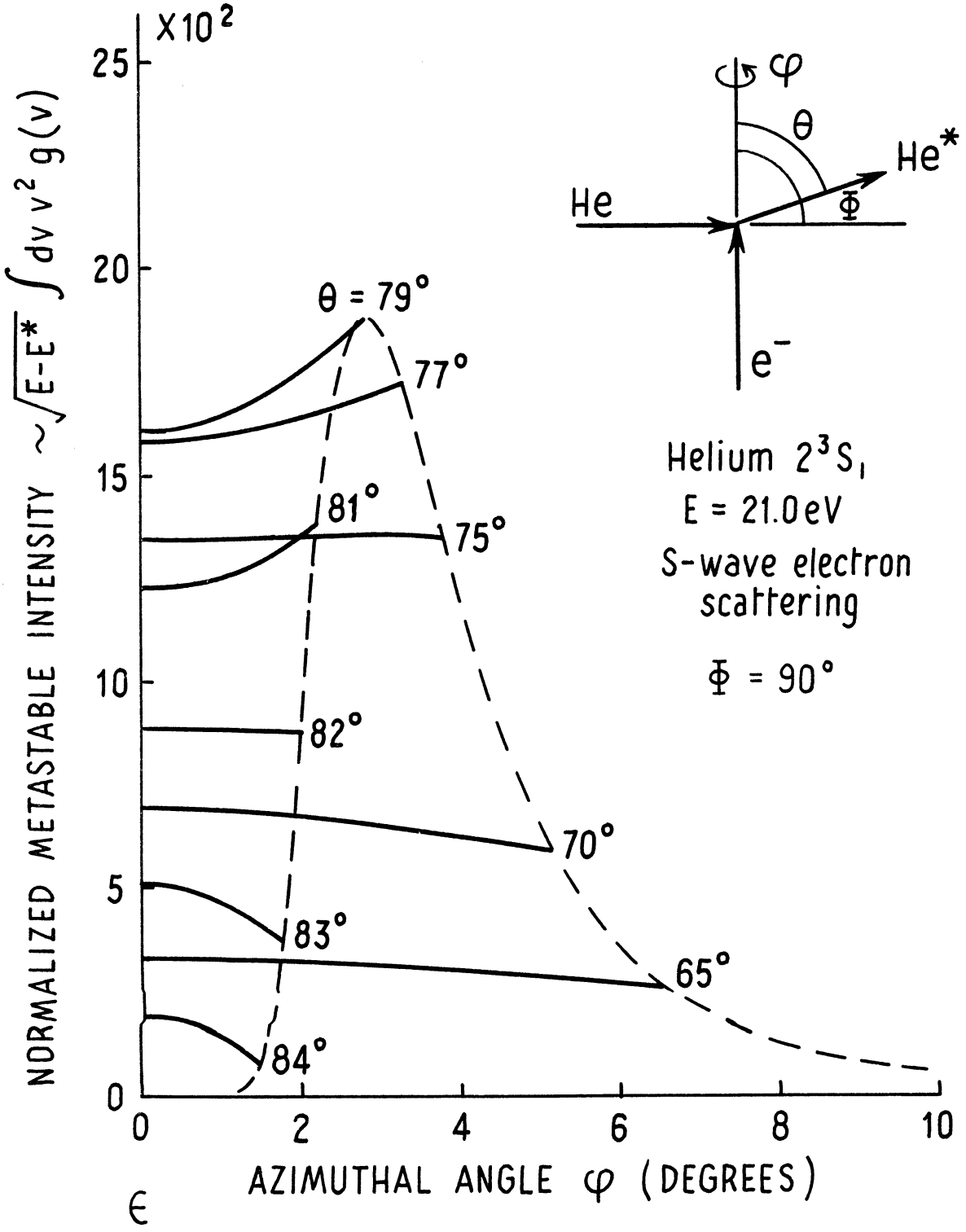

Figure AD.4 Total metastable intensity for 2^3S helium as a function of the azimuthal angle φ of the detector; the polar angle Θ is the parameter. The energy of the incident electrons is 21.0 eV. A perfectly collimated Maxwellian ground state beam is assumed; s-wave scattering of the electrons is also assumed. The dashed curve represents the locus of intensities at the cutoffs (see text).

Appendix III) takes the following form

$$VI(\Theta, \tfrac{\pi}{2}, \varphi_{max}, V) \sim \frac{V^2}{|\hat{v}_o \times \hat{v}|} v_o^2 e^{-v_o^2/\alpha^2} \qquad \text{(AD.1)}$$

where the quantities v_o and v are determined from Equations III.10 and III.15 respectively, using Equation III.16.

The above three figures show that, under the assumption of isotropic electron scattering, the total intensity may vary strongly with the azimuthal angle φ; for large energies, the intensity may be substantially greater for values of $\varphi \neq 0$ than it is in the plane of the incident beams (compare, for example the intensity at $\varphi = 10^o$ ($\Theta \approx 84^o$) with that at $\varphi = 0^o$ in Figure AD.2).

The strong effect which nonisotropic electron scattering can have on the metastable intensities is seen by comparing Figures AD.4 and AD.5. The results shown in these figures are calculated for electrons of energy 21.0 eV, corresponding to the energy of the d-wave resonance in the excitation function for the helium 2^3S state. While the intensities evaluated under the assumption of isotropic electron scattering (Figure AD.4) depend only weakly on φ, those made for d-wave scattering (Figure AD.5) show large peaks and valleys.

To summarize, it is seen from the results shown in the various figures of this addendum, that variations in the total metastable intensity which occur in the plane of the

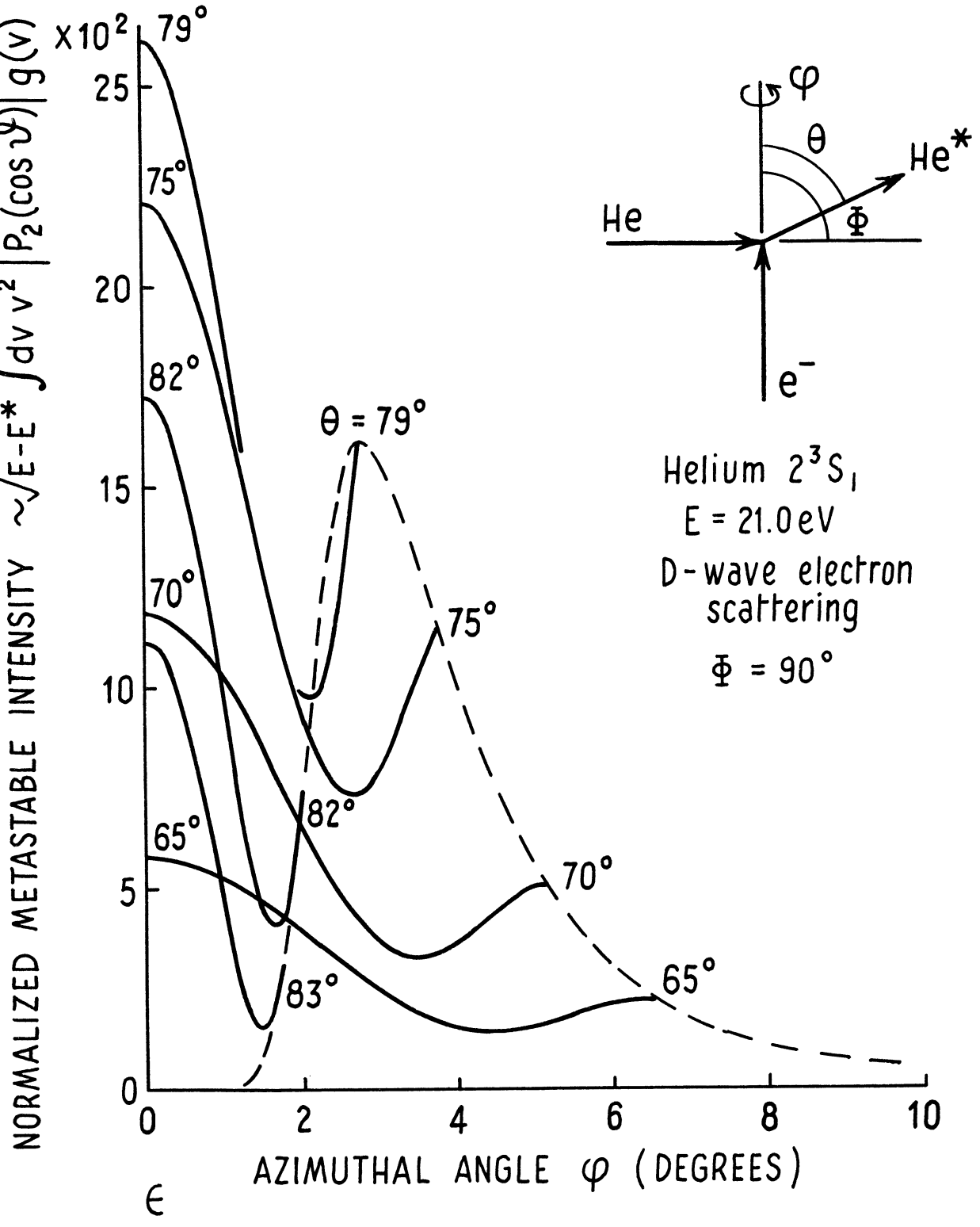

Figure AD.5 Total metastable intensity for 2^3S helium as a function of the azimuthal angle Φ of the detector; the polar angle Θ is the parameter. The energy of the incident electrons is 21.0 eV. A perfectly collimated Maxwellian ground state beam is assumed; d-wave scattering of the electrons is also assumed. The dashed curve represents the locus of intensities at the cutoffs (see text).

incident beams (cf. Figure 3.5 and the intensity variation with Θ at $\varphi = 0^{\circ}$ in Figure AD.5) are generally not representative of the variations which occur for $\varphi \neq 0$. Because of the concentration of metastables toward the "outside" of the populated cylinder in velocity space, the out-of-plane intensities can vary strongly even if the electron scattering is isotropic (Figures AD.2, AD.3 and AD.4). In addition, the inclusion of structure in the scattering cross section is seen to have a strong effect as well (Figure AD.5).

5/5/70

LIST OF REFERENCES

Alcalay, 1969 — J. A. Alcalay and E. L. Knuth, Rev. Sci. Instr., 40, 438 (1969)

Andrick, 1968 — D. Andrick, H. Ehrhardt and M. Eyb, Z. Physik, 214, 388 (1968)

Appelquist, 1970 — T. Appelquist and S. J. Brodsky, Phys. Rev. Letters, 24, 562 (1970)

Bederson, 1968 — B. Bederson in Methods of Experimental Physics, Vol. 7, Part A, B. Bederson and W. L. Fite, eds., Academic Press, New York, 1968

Clampitt, 1969 — R. Clampitt and A. S. Newton, J. Chem. Phys., 50, 1997 (1969)

Crosby, 1969 — D. A. Crosby and J. C. Zorn, J. Vac. Sci. Tech., 6, 82 (1969)

Donnelly, 1969 — D. P. Donnelly, J. C. Pearl, R. A. Heppner and J. C. Zorn, Rev. Sci. Instr., 40, 1242 (1969)

Ehrhardt, 1967 — H. Ehrhardt and K. Willmann, Z. Physik, 203, 1 (1967)

Ehrhardt, 1968 — H. Ehrhardt, L. Langhans and F. Linder, Z. Physik, 214, 179 (1968)

French, 1967 — J. B. French and J. W. Locke in Rarefied Gas Dynamics, C. L. Brundin, ed. (Academic Press, Inc., N.Y., 1967) p. 1461

Freund, 1967 — R. Freund and W. Klemperer, J. Chem. Phys., 47, 2897 (1967)

Freund, 1969 — R. Freund, J. Chem. Phys., 50, 3734 (1969)

Fry, 1969 — E. S. Fry and W. L. Williams, Rev. Sci. Instr., 40, 1141 (1969)

Heberle, 1956 — J. W. Heberle, H. A. Reich, and P. Kusch, *Phys. Rev.*, 101, 612 (1956)

Holt, 1966	H. K. Holt and R. V. Krotkov, Phys. Rev. 144, 82 (1966)
Lamb, 1950	W. E. Lamb, Jr. and R. C. Retherford, Phys. Rev., 79, 549 (1950)
Leventhal, 1967	M. Leventhal, R. T. Robiscoe and K. R. Lea, Phys. Rev., 158, 49 (1967)
Pearl, 1969	J. C. Pearl, D. P. Donnelly and J. C. Zorn, Physics Letters, 30A, 145 (1969)
Pichlik, 1970	R. Pichlik and J. C. Zorn, Bull. Am. Phys. Soc., 15, 617 (1970); J. Vac. Sci. Tech. (in press)
Rebane, 1970	T. Rebane, Ph.D. Dissertation, University of Michigan (1970)
Robiscoe, 1965	R. T. Robiscoe, Phys. Rev., 138, A22 (1965)
Robiscoe, 1968	R. T. Robiscoe, Phys. Rev., 168, 4 (1968)
Robiscoe, 1970	R. T. Robiscoe and T. W. Shyn, Phys. Rev. Letters, 24, 559 (1970)
Rubin, 1969	K. Rubin, B. Bederson, M. Goldstein and R. E. Collins, Phys. Rev., 182, 201 (1969)
Shyn, 1969	T. W. Shyn, W. L. Williams, R. T. Robiscoe and T. Rebane, Phys. Rev. Letters, 22, 1273 (1969)
Stebbings, 1960	R. F. Stebbings, W. L. Fite, D. G. Hummer and R. T. Brackmann, Phys. Rev., 119, 1939 (1960)
Toennies, 1967	J. P. Toennies, Recent Advances in Aerothermo-Chemistry, vol. 1 (AGARD Conference Proceeding, No. 12), I. Glassman, ed. (Technical Editing and Reproduction Ltd., London, 1967)
Vriens, 1968	L. Vriens, T. F. M. Bonsen and J. A. Smit, Physica, 40, 229 (1968)

Warnock, 1968 — T. T. Warnock and R. B. Bernstein, J. Chem. Phys., 49, 1878 (1968)

Zorn, 1967 — J. C. Zorn and J. C. Pearl, The University of Michigan, Space Physics Research Laboratory, Final Report 08700-1-F (1967)